

INVESTIGATION OF HIGH PERFORMANCE FIBER REINFORCED CONCRETE  
PROPERTIES: HIGH EARLY STRENGTH, TOUGHNESS, PERMEABILITY AND FIBER  
DISTRIBUTION

---

A Thesis

Presented to

the faculty of the School of Engineering and Applied Science

University of Virginia

---

in partial fulfillment

of the requirements for the degree

Master of Science

by

Evelina Khakimova

May

2016

APPROVAL SHEET

The thesis  
is submitted in partial fulfillment of the requirements  
for the degree of  
Master of Science

Evelina Khakimova

AUTHOR

The thesis has been read and approved by the examining committee:

H. Celik Ozyildirim, Ph.D., P.E.

Advisor

Devin K. Harris, Ph.D.

Advisor

Osman E. Ozbulut, Ph.D.

Accepted for the School of Engineering and Applied Science:



Craig H. Benson, Dean, School of Engineering and Applied Science

May

2016

## **ACKNOWLEDGEMENTS**

I would like to express my deep gratitude to my research advisor, Dr. H. Celik Ozyildirim, for his support and extensive contributions to this research project. Thank you for your patience, enthusiasm and vast knowledge. I have learned a great deal about materials, testing and importance of practical applications of research.

I would like to express my sincere appreciation to Dr. Devin K. Harris for acting as my academic and research advisor. Thank you for the opportunity to join your graduate research group, and providing guidance and support throughout my tenure at the University of Virginia. I appreciate your patience and understanding during this project.

Thank you to Dr. Osman E. Ozbulut for serving on my committee. Furthermore, thank you for allowing me to collaborate on projects with your graduate research group. It significantly expanded my knowledge and experiences with material properties and testing.

I would like to express my deep appreciation to the Virginia Transportation Research Council for giving me the opportunity to do my research there. Special thanks to the VTRC research and technical staff for the assistance and guidance in this research project, specifically to William Ordell, Michael Burton, Kenneth Herrick, Andrew Mills, Troy Deeds, Stephen Lane, James Copeland, Xuemeng “John” Xia, and Keith Peres. Furthermore, I would like to thank the industry for the input and assistance with this research project.

I would like to acknowledge all my fellow graduate colleagues and friends for their support and help over the many years I spent at University of Virginia. Special thanks to Muhammad

Sherif, Jonathon Tanks, Mohamad Alipour, Salman Usmani, Sherif Daghash, Mark Saliba, Mohamad Amine, Lauren Bolton, Ethan Bradshaw and the rest of the graduate group.

I would like to thank my family and friends for their unconditional love, support and understanding. I could not have done it without you.

## **ABSTRACT**

Concrete cracking, high permeability and leaking joints allow for intrusion of harmful solutions, resulting in concrete deterioration and corrosion of reinforcement. The development of durable high performance concretes with limited cracking is a potential solution for extending the service life of the structures. Furthermore, the use of high early strength durable materials will facilitate rapid and effective repairs, reducing traffic interruptions and decreasing long-term maintenance costs.

The objective of this research was to develop low permeability durable materials that can achieve high early strengths within 24 and 10 hours. Within the scope of this work, various proportions of steel and synthetic fibers were used to evaluate crack control and post-cracking performance. In addition to high early strength and crack response other characteristics, including toughness, residual strengths, permeability of cracked concrete and fiber distribution were examined. Results from the investigation provide critical evidence that the implementation of high performance high early strength fiber reinforced concrete materials will significantly improve the condition of existing and new structures, and facilitate rapid effective repairs and construction.

The study has revealed that high early strength durable concretes can be achieved with proper attention to mixture components and properties, especially the amount of portland cement, accelerating admixtures and concrete temperature. Fiber reinforced concretes with steel fibers exhibited significantly higher toughness and residual strength values compare to those with polypropylene fibers. Permeability work showed that minor increase in crack width significantly increases infiltration of solutions. Fibers can facilitate crack width control. Fiber distribution

analysis showed preferential alignment of steel fibers along the length of the beam. Proper mixing methods are essential for uniform random fiber distribution.

**Keywords:** Fiber Reinforced Concrete; High Early Strength; Very High Early Strength; Polyvinyl Alcohol Fibers; Steel Fibers; Polypropylene Fibers; Toughness; Residual Strength; Permeability of Cracked Concrete; Fiber Distribution

## TABLE OF CONTENTS

ACKNOWLEDGEMENTS .....	i
ABSTRACT .....	iii
TABLE OF CONTENTS .....	v
LIST OF FIGURES .....	vii
LIST OF TABLES .....	ix
GLOSSARY OF ACRONYMS .....	x
1.0 - INTRODUCTION .....	1
2.0 - LITERATURE REVIEW .....	4
2.1 General Review of Concrete Material and its Properties.....	4
2.2 High Performance Concrete (HPC) .....	7
2.3 High Early Strength (HES) Concrete.....	9
2.4 Very Early Strength (VES) Concrete.....	10
2.5 Fiber Reinforced Concrete .....	13
2.6 High Performance and High Early Strength Fiber Reinforced Concrete (HESFRC).....	14
2.7 Permeability .....	16
2.8 Fiber Distribution.....	18
2.8.1 Fiber Density and Distribution.....	19
2.8.2 Statistical Analysis of Spatial Fiber Distribution.....	21
3.0 - PURPOSE AND SCOPE .....	23
4.0 - METHODOLOGY .....	24
4.1 Stage I – Development of HES-FRCs .....	26
4.1.1 HES-FRC Laboratory Mixtures.....	26
4.1.2 Field HES-FRC Batches .....	28
4.2 Stage II – Development of VHES-FRCs .....	31
4.2.1 VHES Preliminary Plain Concrete Laboratory Mixtures .....	32
4.2.2 VHES-FRC Preliminary Laboratory Mixtures .....	35
4.2.3 Final VHES-FRC w/ SF and VHES-FRC w/ FA Lab Batches .....	39
4.3 Stage III – Permeability of Cracked FRC Samples .....	41
4.3.1 Crack Formation with Splitting Tensile Test.....	41
4.3.2 Permeability Analysis of Cracked Specimens .....	42
4.4 Stage IV – Fiber Distribution Analysis.....	45
4.4.1 Image Processing Analysis .....	47
4.4.2 Statistical Spatial Point Pattern Analysis .....	49
5.0 - RESULTS AND DISCUSSION.....	53
5.1 Stage I - HES-FRCs Results .....	53
5.1.1 HES-FRCs Trial Laboratory Results .....	53
5.1.2 HES-FRCs Field Results.....	55
5.2 Stage II - VHES-FRCs Results .....	63
5.2.1 VHES Exploratory Plain Concrete Lab Mixtures.....	64
5.2.2 VHES-FRC Preliminary Lab Mixtures.....	67
5.2.3 Final VHES-FRC w/ SF and VHES-FRC w/ FA Lab Batches .....	70
5.3 Stage III – Permeability of Cracked Samples .....	75

5.3.1 Splitting Tensile Testing and Crack Formation Analysis .....	76
5.3.2 Coefficient of Water Permeability .....	79
5.4 Stage IV – Fiber Distribution Analysis.....	81
5.4.1 FRC Cross-Sections with Polypropylene Fibers.....	84
6.0 - CONCLUSIONS .....	87
6.1 Stage I .....	87
6.2 Stage II.....	90
6.3 Stage III.....	93
6.4 Stage IV .....	93
7.0 - RECOMMENDATIONS AND FUTURE WORK .....	94
8.0 - REFERENCES .....	96
APPENDIX.....	99

## LIST OF FIGURES

Figure 4.1: Development of HES-FRC and VHES-FRC mixtures.....	24
Figure 4.2: (a) Polyvinyl Alcohol (PVA), (b) Polypropylene (PP), (c) Steel (S) Fibers .....	26
Figure 4.3: Curing Method and Temperature Monitoring at (a) Plant Lab and (b) Field.....	30
Figure 4.4: VHES-FRCs mixture development .....	31
Figure 4.5: (a) Slump and (b) Air Content Measurements, (c) Insulated Samples with Temperature Monitoring .....	35
Figure 4.6: Addition of Polypropylene and Steel Fibers .....	36
Figure 4.7: Elastic Modulus, Compressive and Flexural Strengths Testing.....	38
Figure 4.8: Curing of the Samples for the First 24 Hours. ....	40
Figure 4.9: (a) Splitting Tensile Test Setup, and (b) Magnifier with Scale.....	42
Figure 4.10: Unloaded Crack Widths Measured with the Magnifier.....	42
Figure 4.11: Saturation of Permeability Samples .....	43
Figure 4.12: Permeameter Testing Setup.....	44
Figure 4.13: Schematic of the Flexural Test Setup, and Two Slicing Methods (a) HTH and (b) THTHT .....	46
Figure 4.14: Two slicing methods: HTH and THTHT .....	46
Figure 4.15: Fiber cross-sections at different angles .....	47
Figure 4.16: Image Analysis Process: (a) Inverse; (b) Binary; (c) Pixel Removal; (d) Final.....	48
Figure 4.17: (a) Clustered; (b) Regular (Ordered); (c) Random Distributions (Figure adapted from Diggle (2003)).....	49
Figure 4.18: (a) K-function (b) F-function (Figure adapted from Akkaya et al. (2000b)) .....	50
Figure 4.19: Graphic Representations of (a) $K[s]\pi^{1/2}$ function and (b) F-function.....	51
Figure 5.1: HES-FRCs Flexural Results at 24 hours (a) and 7 days (b).....	55
Figure 5.2: Temperature developments vs Age for the HES-ECC.....	57
Figure 5.3: 28-Day HES-ECC Flexural Results .....	57
Figure 5.4: Temperature development of HES-FRCs w/ (a) PP and (b) S fibers.....	58
Figure 5.5: HES-FRCs w/ PP fibers (Plant Lab Cured) (a) Batch w/ 15 lb/yd <sup>3</sup> (b) Batch w/ 18 lb/yd <sup>3</sup> .....	59
Figure 5.6: HES-FRC w/ S fibers (Plant Lab Cured) (a) Batch w/ FA (b) Batch w/ SF .....	60
Figure 5.7: HES-FRCs Drying Shrinkage Results.....	63
Figure 5.8: Temperature Development for preliminary VHES w/ SF mixtures.....	65
Figure 5.9: VHES w/ SF (800 and 850) temperature developments .....	68
Figure 5.10: Flexural test results for VHES w/ SF plain and FR concretes .....	69
Figure 5.11: Temperature developments of the final lab VHES-FRCs with PP and S fibers .....	72
Figure 5.12: VHES-FRCs w/ SF (a) w/ PP Fibers (b) w/ S fibers.....	73
Figure 5.13: VHES-FRCs w/ FA (a) w/ PP Fibers (b) w/ S fibers .....	74
Figure 5.14: Final Lab VHES-FRCs Drying Shrinkage Results .....	75
Figure 5.15: Load versus Laser Displacement Plots for Various Crack Widths (Example) .....	76
Figure 5.16: Laser Crack Width versus Magnifier Crack Width Under Load.....	78
Figure 5.17: Average Crack Width Recovery After Unloading (a) HES-FRCs (b) VHES-FRCs	78
Figure 5.18: Coefficient of Water Permeability versus Crack Width (a) HES-FRCs (b) VHES- FRCs .....	79

Figure 5.19: Steel Fiber Cross-Section Image Analysis .....	81
Figure 5.20: Steel Fiber Density per Cross-Section Side (a) HTH (b) THTHT .....	82
Figure 5.21: Spatial Steel Fiber Distribution Analysis (a) $(K[s]/\pi)^{1/2}$ (b) F - function.....	83
Figure 5.22: PP Fiber Cross-Section Image Analysis Processing .....	84
Figure 5.23: PP Fiber Density per Cross-Section Side (HTH) .....	85
Figure 5.24: Spatial PP Fiber Distribution Analysis (a) $(K[s]/\pi)^{1/2}$ (b) F – function.....	85
Figure 5.25: F-function comparison between S and PP fiber cross-sections.....	86

## LIST OF TABLES

Table 4.1: Used Fresh and Hardened Concrete Test Methods.....	25
Table 4.2: Characteristics of Fibers (provided by the manufacturer) .....	25
Table 4.3: Final Trial lab HES-FRC Mixture Designs .....	27
Table 4.4: Field HES-FRC Mixture Designs .....	28
Table 4.5: Mixture Designs for VHES with Silica Fume and Fly ash SCMs.....	33
Table 4.6: VHES-FRCs Preliminary Lab Mixture Designs.....	36
Table 4.7: Final VHES-FRC w/ SF and VHES-FRC w/ FA Mixture Designs .....	39
Table 5.1: Fresh Lab HES-FRCs Properties .....	54
Table 5.2: Hardened Lab HES-FRC Properties .....	54
Table 5.3: Fresh Field HES-FRC Properties.....	56
Table 5.4: HES-ECC Hardened Properties .....	56
Table 5.5: HES-FRCs w/PP Fibers Hardened Properties .....	58
Table 5.6: HES-FRCs w/ S Fibers Hardened Properties .....	60
Table 5.7: 28-Day HES-FRC Flexural Test Results (Plant Lab Cured).....	61
Table 5.8: 28-Day HES-FRC Flexural Test Results (Field Cured) .....	61
Table 5.9: VHES-800 w/ SF and VHES-850 w/ SF fresh concrete properties.....	64
Table 5.10: Compressive strength results for exploratory VHES w/ SF mixtures .....	66
Table 5.11: VHES-882 w/ FA fresh concrete properties .....	66
Table 5.12: VHES-882 w/ FA Compressive Strength Results .....	67
Table 5.13: Fresh concrete properties of VHES-800 w/ SF and fibers .....	67
Table 5.14: Fresh concrete properties of VHES-850 w/ SF and fibers .....	67
Table 5.15: Compressive strength results for VHES-FRC w/ SF.....	68
Table 5.16: 28-Day Trial VHES-800 w/ SF Hardened Properties.....	70
Table 5.17: 28-Day Trial VHES-850 w/ SF Hardened Properties.....	70
Table 5.18: Final Lab VHES-FRCs Fresh Concrete Properties .....	71
Table 5.19: Final Lab VHES-FRCs Compressive Strength Results.....	73
Table 5.20: Final Lab VHES-FRCs Flexural Results versus Age .....	73
Table 5.21: Final Lab VHES-FRCs 28-day Flexural Results.....	74
Table 6.1: Advantages and Disadvantages of the SCMs addition .....	91
Table 6.2: Advantages and Disadvantages of the HES-FRCs and VHES-FRCs .....	92

## **GLOSSARY OF ACRONYMS**

**AASHTO** - American Association of State Highway and Transportation Officials Bridge Specifications

**ACI** - American Concrete Institute

**AEA** – *Air-Entraining Admixture*

**ASCE** – *American Society of Civil Engineers*

**ASTM** – *American Society for Testing and Materials*

**CSR** – Complete Spatial Randomness

**CWP** - Coefficient of Water Permeability

**ECC** - Engineered Cementitious Composite

**FA** – Fly Ash

**FHWA** - Federal Highway Administration

**FRC** – Fiber Reinforced Concrete

**H** – Horizontal

**HES** – High Early Strength

**HES-ECC** - High Early Strength Engineered Cementitious Composite

**HES-FRC** - High Early Strength Fiber Reinforced Concrete

**HES-FRC w/ S Fibers** - High Early Strength Fiber Reinforced Concrete with Steel Fibers

**HES-FRC w/ PP Fibers** - High Early Strength Fiber Reinforced Concrete with Polypropylene Fibers

**HES-FRC w/ FA** - High Early Strength Fiber Reinforced Concrete with Fly Ash

**HES-FRC w/ SF** - High Early Strength Fiber Reinforced Concrete with Silica Fume

**HESFRC** - High Early Strength Fiber Reinforced Concrete

**HPC** – High Performance Concrete

**HRWRA** - High-Range Water-Reducing Admixture

**LMC** - Latex Modified Concrete

**LMC-VE** - Latex Modified Concrete with very early strength

**LVDT** - Linear Variable Differential Transducers

**NCHRP** - National Cooperative Highway Research Program

**NISS** - National Institute of Statistical Sciences

**NJDOT** – New Jersey Department of Transportation

**NSC** – Normal Strength Concrete

**PC** – Plain Concrete without fibers

**PCA** – Portland Cement Association

**PP** – Polypropylene (Fibers)

**PVA** – Polyvinyl Alcohol (Fibers)

**S** – Steel (Fibers)

**SCM** – Supplementary Cementitious Material

**SF** – Silica Fume

**SHRP** - Strategic Highway Research Program

**SRA** – Shrinkage Reducing Admixture

**T** – Transverse

**VDOT** – Virginia Department of Transportation

**VES** – Very Early Strength

**VHES** - Very High Early Strength

**VHES w/ SF** - Very High Early Strength Concrete with Silica Fume

**VHES w/ FA** - Very High Early Strength Concrete with Fly Ash

**VHES-800 w/ SF** - VHES-800 with Silica Fume

**VHES-850 w/ SF** - VHES-850 with Silica Fume

**VHES-882 w/ FA** - VHES-882 with Fly Ash

**VHES-FRC** - Very High Early Strength Fiber Reinforced Concrete

**VHES-FRC w/ SF** - Very High Early Strength Fiber Reinforced Concrete with Silica Fume

**VHES-FRC w/ FA** - Very High Early Strength Fiber Reinforced Concrete with Fly Ash

**VHS** – Very High Strength

**VTM** – Virginia Test Method

**VTRC** - Virginia Transportation Research Center

**w/cm** – Water-Cementitious Materials Ratio

## 1.0 - INTRODUCTION

New construction and rehabilitation of existing structures are in need of high performance durable materials that facilitate extension of service life of structures with minimal maintenance. According to the American Society of Civil Engineers (ASCE) 2015 report card for Virginia's infrastructure, Virginia's bridges and culverts are estimated to be in poor condition, with a grade of "C" (ASCE 2015). Over 20% of Virginia's transportation structures are classified as structurally deficient or functionally obsolete, and require major rehabilitation procedures. According to the latest 2015 National Bridge Inventory (NBI) database, about 50% of highway bridges in Virginia used concrete as the superstructure material (NBI 2015). Therefore, the use of durable concretes that facilitate extension of service life of transportation structures is essential.

The durability of concrete greatly depends on its strength, resistance to cracking and permeability (Shah and Wang 1997). Volumetric changes due to moisture and temperature, chemical reactions, and excessive loading are often the primary cause of concrete cracking. The intrusion of water and harmful solutions through these cracks or high permeability concrete results in corrosion of internal primary steel reinforcement and deterioration of concrete through sulfate attacks, alkali-silica reactions and freeze-thaw damage. Hence, the use of durable concrete mixtures with high resistance to cracking and low permeability is expected to increase the service life of structures. The addition of supplementary cementitious materials (SCMs) has been shown to improve concrete durability and also reduce its permeability; furthermore, the addition of fibers helps limit concrete deterioration by minimizing crack occurrence by producing tighter cracks. Consequently, concretes reinforced with fibers have lower permeability than unreinforced concretes (Rapoport et al. 2001). The addition of large volumes of fibers (0.5% to 2.0% by volume)

is expected to significantly improve post-cracking performance of the concrete, increasing its durability, residual strengths and toughness. However, the challenges associated with making high fiber volume concretes must be overcome.

In addition to the use of durable materials, the repair time is also of great importance. The strength of concrete at early ages strongly influences the construction and repair methods. Rapid concrete placement and repairs would allow for accelerated construction, and reduction of traffic interruptions and commuter costs (Sprinkel 2006). Therefore, high performance high early strength fiber reinforced concrete mixtures are a promising technology that may satisfy the rapid construction and durability requirements.

The purpose of this research was to develop durable concrete mixtures that exhibit:

1. high early strength,
2. low permeability,
3. resistance to cracking.

The desired mixtures were expected to reach the compressive strength of 3,000 psi within 24 and 10 hours, for high and very high early strength requirements, respectively. The investigation also evaluated the influence of the addition of supplementary cementitious materials (SCMs) on durability enhancement; and the effects of fiber type and volume fraction on crack resistance. According to the VDOT (2007) Road and Bridge Specifications, it is desired for the permeability values to stay below the 1500 Coulomb (C) limit. Whereas, the VDOT (2009) Guide Manual for Causes and Repair of Cracks in Bridge Decks states that crack widths that are less than 0.2 mm do not need to be filled with the sealing agent or epoxy. The performance of the mixtures was determined based on durability tests, including compressive and flexural strengths, toughness,

drying shrinkage, and permeability. Other characteristics such as residual strengths, permeability of cracked concrete and fiber distribution were also examined.

The project was divided into four main stages. The first stage focused on the development of high early strength fiber reinforced concrete (HES-FRC) mixtures that can reach 3,000 psi compressive strength within 24 hours. The transition into the second stage included further modification of the HES-FRC mixtures. The very high early strength fiber reinforced concretes (VHES-FRCs) developed 3,000 psi compressive strength within 10 hours. The third stage focused on testing of the permeability of cracked FRCs. Crack widths of 0.1 mm to 0.5 mm were formed in FRC, and falling head permeability was performed. The objective of the fourth, final stage of the project was to examine the fiber distribution within the concrete mixtures. Spatial fiber dispersion was studied at the cross-sections of the crack location.

The first chapter of this thesis covers review of literature on high performance, high early strength and fiber reinforced concretes. The last two literature review sections discuss the studies on permeability of cracked concrete and fiber distribution. The next chapter covers the project methods for each of the stages described previously. The results chapter is followed by the conclusion and recommendations chapters.

## **2.0 - LITERATURE REVIEW**

The first section of the literature review covers the development of high performance concrete (HPC), which is characterized as concrete with enhanced mechanical and durability properties. The next section discusses high early strength (HES) and very early strength (VES) or very high early strength (VHES) concretes. In this project the concrete is considered HES if it achieves the required strength within one to three days; whereas, VES or VHES concretes achieve the required strength within a matter of hours. The next two parts review studies on fiber reinforced concrete (FRC) and high-performance FRCs, including a review of the influence of fiber addition to concrete for performance enhancement and cracking control. Finally, the last two sections discuss the effect of crack widths on concrete permeability, and the importance of fiber dispersion and alignment in concrete.

### ***2.1 General Review of Concrete Material and its Properties***

Concrete is the most widely used building material in the world (Kosmatka and Wilson 2011). The main concrete components include cement (7-15%), coarse and fine aggregates (up to 75%), water (up to 20%) and air. Often supplementary cementitious materials and chemical admixtures are added to concrete mixtures to further improve fresh and hardened concrete properties.

Hydraulic portland cement and water undergo chemical hydration reactions to set and harden with time, forming *paste* as a final product. In the US, portland cement is categorized by the American Society for Testing and Materials (ASTM) C150 test method into several types. Type I cement is general purpose cement used for wide range of applications, from bridges and buildings to pipes and tanks. Type II and Type V cements due to lower contents of  $C_3A$  (tricalcium aluminate) provide moderate and high sulfate resistance, respectively. Type III cement is similar

to Type I cement with finer ground particles, and it is used when a higher early strength is required. Type IV cement facilitates the reduction of heat of hydration.

Supplementary cementitious materials (SCMs) such as fly ash, silica fume, and slag cement are often used to improve durability of concrete. In this project fly ash and silica fume were used. *Fly ash (FA)* has two classes – C and F, with Class F having a lower calcium amount than Class C. Class F fly ash can constitute from 15% to 25% of total cementitious material in concrete mixtures, and it facilitates the reduction of water demand, increase of workability, and reduction of bleeding and segregation. Fly ash increases concrete setting time due to pozzolanic reactions, and lowers heat of hydration. *Silica fume (SF)* is a very fine material, and can make up from 5% to 10% of total cementitious material in concrete mixtures. Lower permeability and increased early-age strength could result from the use of silica fume (Kosmatka and Wilson 2011). However, it also increases water demand, especially in higher replacement rates, and decreases workability and air content. Furthermore, silica fume is more expensive than fly ash. Both SCMs generally enhance overall concrete strength, reduce concrete permeability and alkali-silica reactivity, improving resistance to corrosion and sulfate reactions.

Chemical admixtures are often used to help achieve required fresh and hardened concrete properties. *Air-Entraining* admixture (AEA) is used to improve durability of concrete by stabilizing entrained air bubbles. The addition of the AEA improves workability of fresh concrete, reduces bleeding, and increases resistance to freezing and thawing. *High-Range Water-Reducing* admixture (HRWRA) enhances workability of concrete without the need for increasing water content, and consequently, allows for lower water to cementitious materials (w/cm) ratio, lower permeability and higher strength. Accelerating admixtures accelerate the early age strength gain

by reducing the setting time and increasing the strength gain after the set. *Shrinkage reducing admixture (SRA)* reduces the effects of capillary pore surface tension formed during concrete drying, and it consequently helps reduce shrinkage of concrete mixtures.

Other ways to achieve certain concrete properties is through controlling concrete temperature. Strength at early stages is especially affected by the initial fresh concrete mixture and curing temperatures. Higher temperatures increase strength development at early ages and decrease setting time. According to Kosmatka and Wilson (2011), the setting time of concrete decreases by 33% for every 10°F increase in temperature. High temperatures decrease concrete air content, thus amount of air-entraining admixture needs to be adjusted accordingly. Additionally, there may be a loss in workability due to high concrete temperatures.

Concrete cracking is one of the main reasons for reduction in concrete durability. Shrinkage, thermal contractions, chemical reactions, and excessive loads are some of the causes of crack formation. Hydration process of cement results in volume reduction causing *chemical shrinkage* or *autogenous shrinkage* to occur, which is significant at low water-cementitious material ratios. *Plastic shrinkage* occurs due to changes in volume of fresh concrete due to water loss, the bleeding rate falls behind the moisture evaporation rate causing plastic shrinkage cracking of fresh concrete. Generally, it is characterized by irregular, short cracks up to 3 ft. in length. Some of the main reasons plastic shrinkage occurs are high air and concrete temperatures, high cementitious content, low w/cm ratios and wind during placement (Kosmatka and Wilson 2011). *Drying shrinkage* occurs due to moisture changes in hardened concrete. Shrinkage cracks develop when the tensile strength of concrete is exceeded. Lower water content reduces drying shrinkage. To prevent shrinkage cracking, the drying shrinkage values need to stay below 0.07% in 4 months (Babaei

and Fouladgar 1997). Furthermore, bridge deck cracking is significantly influenced by the water, cement and paste contents (Darwin et al. 2004). Higher crack density is observed for greater water and cement contents. Limiting the concrete paste content to below 0.27 significantly decreases crack density. According to the ACI (2013), the paste content represents an amount of cement paste in concrete or mortar, expressed as percent volume of the whole mixture.

## ***2.2 High Performance Concrete (HPC)***

High performance concrete is often defined as concrete with significantly enhanced short-term and long-term properties. High strength, high toughness, low-permeability, long-term durability, good workability and other parameters often represent high-performance concretes (Nawy 2001).

According to the National Cooperative Highway Research Program (NCHRP) 441 report on High Performance Concrete Specification and Practices for Bridges, there is a number of HPC definitions.

- The Federal Highway Administration (FHWA) and American Concrete Institute (ACI) define HPC in early work mainly based on strength and durability characteristics. Typically, a substantial number of standard tests need to be performed to evaluate the HPC performance (NCHRP 2013).
- The American Association of State Highway and Transportation Officials Bridge Specifications (AASHTO) defines two HPC classes, P(HPC) for prestressed concrete members with strength requirements greater than 6,000 psi; and A(HPC) for cast-in-place (CIP) construction with strength requirements less than 6,000 psi (NCHRP 2013).

FHWA started the implementation of HPC in 1991. And by year 2005, the majority of the states implemented low permeability HPCs in state specifications (Vanikar and Triandafilou

2005). In Virginia, about 76 bridge structures were implemented in the HPC program by the year 1999. For these structures HPC was tested for strength and permeability, with the required 28-day compressive strength ranging from 7,000 to 10,000 psi. For beams and deck concrete maximum permeability requirements were limited to 1500 C and 2500 C, respectively. The outcome of the implementation program demonstrated that the HPC mixtures were more workable, had lower permeability, and had greater strength when compared to conventional concretes (Ozyildirim 2005).

In the transportation industry early HPC developments were commonly described as concretes with low permeability and high strength (Ozyildirim 1993). The use of SCMs and low w/cm ratios enabled the reduction of concrete permeability and increase of ultimate strength. The introduction of self-consolidating concretes resulted in the production of mixtures with high workability.

The Strategic Highway Research Program (SHRP) completed a 5-year study, starting in 1987, on the mechanical behavior of HPC. It investigated high early strength (HES), very early strength (VES), very high strength (VHS) and high early strength fiber reinforced (HESFRC) concretes (Zia et al. 1993). Researchers developed VES concrete mixtures that reached 2,000 psi within 6 hours, with 2,000 psi compressive strength being enough to carry regular traffic loads. HES concrete mixtures reached 5,000 psi within 24 hours. Concrete mixture designs for VES and HES types included Type III cement, and a maximum w/cm ratio of 0.40 and 0.35, respectively. A freeze-thaw durability factor (ASTM C666) of 80% after 300 cycles was required for all three types of concretes. The 6<sup>th</sup> volume of the SHRP study investigated the HESFRC performance. The review of that part of the study will be discussed in the later sections.

### ***2.3 High Early Strength (HES) Concrete***

The development of HES concrete and study of its performance have been investigated by a number of researchers, and it remains as a topic of continued study as the properties are constantly being enhanced. HES concrete mixtures are instrumental in accelerated construction, fast repairs, construction in cold weather and other applications (Kosmatka & Wilson, 2011). The development of HES depends on the cement type, amount of paste, w/cm ratio, fresh concrete and curing temperatures, addition of SCMs and chemical admixtures (Kosmatka & Wilson, 2011). Type III or HES cements, low w/cm ratio, high temperature curing and accelerating admixtures are common ways of achieving high concrete strength at early ages.

Maik and Ramme investigated the properties of HES concrete with large dosages of high calcium Class C fly ash. In their project, Type I cement was replaced by fly ash from 0 to 30% in 5% increments. The compressive strength results showed that the increase in Class C fly ash amount leads to an increase in early age strength. Two production plants achieved 3,000 to over 4,000 psi in 22 hours; and 3,000 psi in 11 hours and over 5,000 psi in 26 hours, respectively (Naik and Ramme 1990).

Another study by Cangiano et al. (2009) considered using over 1000 lb/yd<sup>3</sup> of Type I CEM 52.5R cement or Type II/A-LL CEM 42.5R with no addition of SCMs or accelerating admixtures for development of rapid hardening concretes (RHC). European Standard EN 197-1 classifies Type I CEM as portland cement that consists of 95-100 % of clinker, whereas Type II/A-LL CEM is portland-composite cement that includes 80-94% of clinker and 6-20% of limestone. Notation R stands for high early strength class, with 42.5R and 52.5R designations conforming to strengths of over 2,900 psi and 4,300 psi in 2 days, respectively. The temperature gain of RHC was much faster

and higher than of the control mixtures, with temperature rising from around 80° F to over 150° F in less than 10 hours. The RHC with 1<sup>st</sup> cement type reached over 11,000 psi in 24 hours, and the mix with the 2<sup>nd</sup> cement type reached over 7,000 psi in one day.

A study by Sounthararajan and Sivakumar (2012) explored HES concrete with steel fibers, and investigated the dependence of concrete mixture ingredients and proportions. Grade 53 ordinary portland cement was used in the HES mixtures, which satisfies the requirements of Indian Standard, IS 12269-1987, with a strength requirement of over 3,900 psi in 3 days. Steel fiber volume fractions of 0.5% and 1.5%, and 1.0% of accelerating admixture by cement weight were added to the mix. The compressive strength results at 7 days varied from 4,000 psi to over 7,500 psi for different mixture proportions. The authors concluded that the lower w/cm ratio of 0.3, higher fine-to-coarse aggregate ratio of 0.8, and 1.5% of steel fibers by volume produced the highest early-age strength.

Nevertheless, according to ACI 544 Report on Fiber Reinforced Concrete, there is no consensus on the effect of fibers on compressive strength of FRC. In some studies the addition of fibers resulted in decrease of compressive strength (ACI 2009).

#### ***2.4 Very Early Strength (VES) Concrete***

There are no minimum strength criteria described in available standards or research work for the VES concrete mixtures. From the literature review, it can be concluded that concretes that can achieve compressive strengths of 2,000 psi and higher in a matter of several hours are considered VES. According to Parker and Shoemaker (1991) study of concrete pavement patching materials, a compressive strength of 2,000 psi is sufficient to open the patches to traffic. The New Jersey Department of Transportation (NJDOT) conducted a study on VES concrete (Punurai et al. 2007).

The VES concrete mixture reached over 2,250 psi in compressive strength and over 350 psi in flexural strength in about 6.5 hours. Type I cement was used in the study, with a cement content ranging from 611 lb/yd<sup>3</sup> to 705 lb/yd<sup>3</sup>. The accelerating admixture at a dosage of 32 - 45 fl. oz/cement weight was used to increase the early strength gain. It was concluded that the fresh concrete mixture temperature played a key role in strength gain. The researchers noted that the temperature of fresh concrete mixture needs to stay above 82 °F to achieve the required early strength. At the same time, it is desirable to keep the curing temperature below the 140 °F, to minimize cracking due to temperature effects. Temperatures above 149 °F detrimentally affect concrete surfaces, leading to high moisture loss after removal of curing blankets. Wetting the concrete surface under the curing blankets was recommended (Punurai et al. 2007). The application of curing compounds can also help retain moisture in concrete. Proper concrete curing for an appropriate period before service is crucial for the development of desired strength and durability. In addition, Maryland State Highway Administration (MSHA) also conducted a study on VES concrete mixtures with Type III cement, with compressive strength reaching over 2500 psi in 4 hours.

VES concrete with fibers was investigated by Soroushian and Ravanbakhsh (1999). The study considered the use of accelerating admixtures and fibers to achieve early-age strength. Type I cement was used for normal strength concrete (NSC), and for VES and VES with polypropylene or cellulose fibers concretes. All mixtures included a calcium chloride accelerating admixture at 27 lb/yd<sup>3</sup>. The cast samples were insulated inside styrofoam containers for the first 24 hours. Compressive strengths of over 3,000 psi were reached for VES concrete samples without fibers within 8 hours, whereas VES concrete samples with fibers reached over 4,000 psi. The mixtures

with cellulose fibers performed better than the mixtures with polypropylene fibers. Thus, the HES concrete with cellulose fibers was modified by reducing the cement content from 840 lb/yd<sup>3</sup> to 700 lb/yd<sup>3</sup>, and by reducing accelerator amount to 22 lb/yd<sup>3</sup>. This reduction facilitated the decrease of shrinkage due to drying and thermal effects, but at the same time still allowed for the development of the required early-age strength (Soroushian and Ravanbakhsh 1999).

VDOT has successfully used Rapid Set cement concrete mixtures with latex in concrete overlays to obtain VES strength and low permeability mixtures. Sprinkel (2006) from the Virginia Transportation Research Center (VTRC) has extensively investigated the properties of Latex Modified Concrete (LMC), and specifically its application for bridge overlays. LMC with very early strength (LMC-VE) can achieve a compressive strength of over 2,500 psi in 3 hours, which allows for rapid repairs and early lane opening to traffic. Other benefits of LMC-VE include low permeability and very low shrinkage. Hence, the LMC-VE overlay system effectively protects bridge decks at “a minimum of inconvenience to the traveling public” (Sprinkel 2006).

Some of the main drawbacks of HES and VES concretes are increase in thermal and autogenous shrinkage, as well as an increase in elastic modulus. The use of high early strength cements, high fresh concrete temperatures and low w/cm ratios causes greater heat generation at early ages (Mehta and Burrows 2001). Hence, there is a high risk of significant cracking, potentially leading to a decrease in concrete durability. The long-term strength is also negatively impacted by the high temperatures at early ages (Klieger 1958; Nawy 2001). The increase in fresh concrete temperature also causes a decrease in slump and an increase in water demand (Klieger 1958). Furthermore, the cost of HES and VES concretes is usually high compared to the normal strength concretes due to addition of accelerating admixtures and use of special cements.

## ***2.5 Fiber Reinforced Concrete***

The addition of various types of fibers for enhancement of concrete properties has been in practice since the 1960s (ACI 2009). There are several types of fibers that are commonly used in the industry: steel, synthetic and natural. This project focuses on steel and synthetic fibers only, as they are the preferred materials for transportation structures.

Microcracks in concrete form under load due to the low tensile capacity of concrete. With further loading, the microcracks develop into macrocracks leading to concrete failure (Nawy 2001). With the addition of fibers, microcrack formation is more controlled, and concrete failure becomes ductile with the ability to sustain further stresses. Fibers significantly improve concrete tensile and flexural strengths, toughness, post-cracking behavior and cracking control. Low amounts of fibers (about 0.1-0.3% by volume) help with control of plastic shrinkage and bleeding; while high fiber amounts (0.6% - 2.0% by volume) improve concrete strength and toughness, and assist with cracking control, reducing crack widths (Kosmatka and Wilson 2011).

Steel FRC (SFRC) is often used in cast-in-place construction, highway and overlay rehabilitations and other applications. The main advantages of SFRC are significantly enhanced tensile, flexural and fatigue strengths, increased toughness, and impact and energy absorption properties. Bond strength between the concrete and steel fibers is increased with the increase in fiber length; however, it is preferable to keep the aspect ratio of fibers below 100 for better dispersion and workability (PCA 1991). Furthermore, the addition of steel fibers does not affect freeze-thaw durability of concrete (PCA 1991). Steel fibers in sound durable concrete due to fiber discontinuity corrode only on the surface. For cracked concrete with crack widths less than 0.1 mm, the harmful solutions cannot penetrate easily to corrode the reinforcement (ACI 2009).

There are several types of synthetic fibers: acrylic, carbon, polyvinyl alcohol (PVA), nylon, polypropylene (PP) and others. In this project only PVA and PP fibers were considered. The addition of PP fibers does not influence concrete compressive strength, but it increases impact and flexural fatigue strengths, as well as toughness of the composite material. The bond strength between PP fibers and concrete matrix is mechanical, and thus greatly depends on the shape of the PP fibers (PCA 1991).

VTRC has been studying properties of FRC for a number of years. Between 1993 and 1997, Ozyildirim, Moen and Hladky studied applications of FRC for the use in transportation industry. Steel and synthetic (polypropylene and polyolefin) fibers were considered during the investigation. The addition of fibers affected workability of concrete, thus proper mixing and the addition of HRWRA were essential for achieving effective results. The study concluded that with increases in fiber content the FRC impact resistance and toughness considerably improve, with the steel fibers performing better than the synthetic fibers. The optimal FRC mixtures were implemented in as a series of Virginia bridge overlay projects. Visual surveys showed expected results, with FRC sections having tighter cracks than the control sections without fibers (Ozyildirim et al. 1997).

In another VTRC study, Brown et al. (2010) investigated the performance of self-consolidating concrete (SCC) with the inclusion of synthetic or steel fibers. The study concluded that the addition of synthetic fibers at a volume fraction of 0.3% or steel fibers at a volume fraction of 0.5% increases concrete residual strength and toughness, with no detriment to SCC workability.

## ***2.6 High Performance and High Early Strength Fiber Reinforced Concrete (HESFRC)***

The 6th volume of the SHRP study investigated the properties of HESFRC (Naaman et al. 1993). The compressive strength requirement was 5,000 psi in 24 hours. The researchers looked

at two types of fibers, steel and polypropylene, at 1.0% and 2.0% of fibers by volume. Samples with steel or polypropylene fibers alone, as well the hybrid mixtures, with two types of steel fibers or steel and polypropylene fibers together were investigated. Furthermore, the effects of the addition of silica fume and latex on HESFRC were examined. A maximum w/cm ratio of 0.34 was used for the HESFRC mixtures without silica fume, whereas the HESFRC with silica fume maintained 0.32 w/cm ratio. Flexural, splitting tensile and flexural fatigue tests were conducted. One of the objectives was to achieve a post-cracking bending strength (modulus of rupture) higher than the first cracking strength. The results showed a significant increase in compressive, flexural and splitting tensile strengths, as well as a bending toughness index for 1.0% and 2.0% by volume of 30/50 steel fibers. On the contrary, the addition of polypropylene fibers at 1.0% and 2.0% by volume was not as effective, and did not perform as well as the steel fiber HESFRC mixtures. According to the study, silica fume improved long-term concrete properties, but had no influence on the early-age characteristics. The addition of latex also did not improve the early-age concrete properties.

High early strength and enhanced energy absorption and impact capacity of HESFRC allow for a wide range of potential applications in highway-related construction. HESFRCs can be effectively implemented in maintenance work that involves repair of concrete bridge decks, overlays, connections, joints and piers; and new construction of bridge decks and piers, pavements, and median barriers. In addition, the authors propose the use of HESFRC in reinforced and prestressed concrete members (Naaman et al. 1993).

High early strength Engineered Cementitious Composite (HES-ECC) has been also previously investigated by a number of researchers (Li and Li 2011; Wang and Li 2006). ECC is a high

performance fiber reinforced mortar material that exhibits high ductility and strain hardening behavior. The conventional ECC mixture uses Type I cement and Class F fly ash with a total of over 2000 lb/yd<sup>3</sup> of cementitious material, and 2.00% of polyvinyl alcohol (PVA) fibers by volume. In the studies by Li, Li and Wang, the developed HES-ECC used rapid-hardening blended portland cement or Type III cement with accelerating admixture. Over 3,500 psi compressive strength and 1,000 psi ultimate flexural strength were reached in 3 to 4 hours.

### ***2.7 Permeability***

Permeability represents concrete's resistance to penetration by water and solutions. Concrete permeability is one of the most important durability characteristics of concrete. Intrusion of harmful solutions through sound high permeability concrete or through cracked concrete can significantly deteriorate the material and lead to corrosion of reinforcing steel. High continuity of pores and voids inside the concrete significantly increase permeability (Kosmatka and Wilson 2011). The lower the permeability of concrete, the better it resists freezing and thawing cycles, penetration of chlorides, corrosion of reinforcement, sulfate attacks, alkali-silica and other harmful reactions (Shah and Wang 1997).

ASTM methods are used to determine the permeability of sound concrete. The *ASTM C1202* and *ASTM C1760* involve the passage of electrical current through samples to obtain permeability and conductivity of the concrete. *ASTM C1585* standard is used to determine concrete's rate of absorption. Furthermore, a number of studies were conducted to investigate permeability of cracked concrete. In their project Wang et al. (1997) investigated the relationship between the permeability of concrete and crack characteristics, such as crack width, length and growth pattern. Feedback-controlled splitting tensile tests were performed on 1 in. thick cylindrical samples to

generate cracks of various widths (from 25 micron ( $\mu\text{m}$ ) up to 550  $\mu\text{m}$ ). Linear variable differential transducers (LVDTs) were attached on both sides of the sample perpendicular to the direction of applied load to monitor the crack growth. The average value of the two LVDTs was used as the sample crack width. The cracked samples were then vacuumed, saturated and soaked in water for at least 12 hours prior to water permeability testing. The permeability test consisted of monitoring the water flow through the cracked sample secured between the two plexiglas plates.

Laminar axial water flow was assumed, and Darcy's law and continuity of flow were used to determine the water permeability coefficient,  $k$  (Equation 2.1).

$$k = \frac{a \cdot l}{A \cdot t} \cdot \ln \left( \frac{h_1}{h_2} \right) \quad \text{Equation 2.1}$$

where  $k$  – permeability coefficient,  $a$  – area of the pipette,  $A$  – area of the concrete sample,  $l$  – sample thickness,  $t$  – flow time,  $h_1$  – initial head of water reading,  $h_2$  – final head of water reading.

It was concluded that the crack widths of less than 50  $\mu\text{m}$  did not affect the concrete permeability; however, it rapidly increased for the cracks widths from 50  $\mu\text{m}$  up to 200  $\mu\text{m}$ .

In another study, Aldea et al. (1999) considered the effects of sample thickness, average crack width and material constituents. Again, the feedback-controlled splitting tensile and water permeability testing procedures were conducted. Thicknesses of 1 in. and 2 in., crack widths from 50  $\mu\text{m}$  up to 350  $\mu\text{m}$ , and samples with paste, mortar, normal strength or high strength concretes were studied. The results of the study indicated that crack widths less than 100  $\mu\text{m}$  do not have an effect on the permeability of concrete. Whereas, a rapid permeability increase is observed for concrete with cracks wider than 100  $\mu\text{m}$ .

Additional studies were conducted on the permeability of cracked concrete under load, in order to more closely match the performance of structures in the field. The same splitting tensile test method was used to form cracks, however brackets were used to keep the load on the specimen and preserve the original crack width. Water permeability test setup identical to the previous study was used for this project. The same trend of rapid permeability increase with growth in crack width was observed. The results also revealed that the loaded samples displayed higher permeability coefficients than the unloaded samples (Aldea et al. 2000).

National Institute of Statistical Sciences (NISS) studied permeability of cracked fiber reinforced concrete (Rapoport et al. 2001). Effects of steel fiber addition on concrete permeability were investigated. The same procedures as in previous studies for crack formation and water permeability testing were utilized. It was proven again that the crack widths of 100  $\mu\text{m}$  or less do not affect concrete permeability. Thus, the permeability of those cracks was not influenced by fiber addition. For the crack widths greater than 100  $\mu\text{m}$  the results showed that the width is still limited due to fibers preventing wide cracks from forming; thus higher amount of fibers in concrete leads to decrease in permeability. The effects of stitching and multiple cracking due to high fiber dosages restrict widening of cracks and reduce the crack length and area. Distribution of stresses due to fibers tended to cause multiple tight cracks instead of single large crack, hence reducing the ability of water to get through the sample.

## ***2.8 Fiber Distribution***

Distribution of fibers in concrete mixtures can significantly influence the performance of concrete. Potential clumping of fibers during mixing, as well as internal and external vibrations of the FRC mixtures during placement can impact fiber distribution. Workability of concrete and

placing techniques can influence fiber alignment, and potentially lead to fiber settlement. Uniformly dispersed fibers spread the induced stresses more effectively throughout structural elements, leading to better crack control and post-cracking performance. Fiber clumping leaves some areas of concrete without fibers. At such areas less energy is required to form cracks, and acting as defects they detrimentally affect mechanical performance of FRC (Akkaya et al. 2000a; b, 2001).

However, due to random fiber distribution, only a certain amount of fibers is properly oriented and aligned to efficiently resist tensile and flexural stresses (PCA 1991). For randomly spaced fibers, only about 40% of fiber length is considered to be effective in resisting applied forces. The effectiveness of fibers is reduced with the increase of the angle between the direction of fibers and applied forces (Nawy 2001). Nevertheless, the performance of FRC is considerably enhanced compared to plain concrete without fibers. In structural elements where placement of conventional reinforcement is complicated, the usage of FRC is most suitable (PCA 1991).

### 2.8.1 Fiber Density and Distribution

Soroushian and Lee investigated steel fiber distribution and orientation in concrete (Soroushian & Lee, 1990). The number of fibers per unit cross-sectional area is often determined by using Equation 2.2 below:

$$N_f = \alpha \cdot \frac{V_f}{A_f} \quad \text{Equation 2.2}$$

where  $N_f$  – fiber number per unit area,  $\alpha$  – orientation factor,  $V_f$  – fiber volume fraction in concrete,  $A_f$  – fiber cross-sectional area.

According to previous studies, the orientation factor  $\alpha$  ranges from 0.41 to 0.82. It represents an average ratio of fiber length in all possible fiber orientations to an original fiber length. In a true three-dimensional (3-D) space, the  $\alpha$  was calculated to be 0.41 (Soroushian and Lee 1990). However, due to boundary restrictions because of the mold size, casting flow and FRC placement procedures the factor increases, and boundary effects of 2-D and 3-D orientations need to be considered. According to Xia and Mackie (2014), simplified fiber orientation factors in 2-D and 3-D cases are  $2/\pi$  and  $1/2$ , respectively. Soroushian and Lee (1990) studied top, middle and bottom portions of 6 in. x 6 in. FRC cross-sections with different fiber types and dosage percentages. The study concluded the orientation factor is not influenced by the specific portions of beam cross-section cuts or fiber type. Whereas, the vibration of FRC impacts the fiber orientation, and fibers tend to 2-D orient in horizontal planes.

Ozyurt et al. (2006) investigated the use of AC-impedance spectroscopy (AC-IS) and image analysis techniques to study fiber distribution and orientation. An orientation factor was derived from Equation 2.2 above from experimentally determined number of fibers ( $N_f$ ) per beam cross-section cut. The higher the orientation factor the more fibers are oriented normal to the cut plane.

The relationship between the fiber distribution and orientation and tensile and flexural strengths of ultra-high strength FRC was also investigated (Kang and Kim 2011, 2012; Kang et al. 2011). Two different fresh concrete placing directions, longitudinal and transverse, were considered during the casting of flexural beams. The beams were sliced in the horizontal, vertical and transverse directions, and the image analysis of cross-sections was performed. It was concluded that the fiber distribution depends on the casting direction, and, in its turn, significantly affects post-cracking flexural and tensile strengths. The fibers tend to align parallel to the

longitudinal direction of the beam in case of the longitudinal casting method; and perpendicular in case of the transverse method. It was concluded, that the longitudinal fiber alignment was beneficial to the post-cracking flexural and tensile capacities.

### 2.8.2 Statistical Analysis of Spatial Fiber Distribution

Statistical spatial point pattern analysis can be used to examine the fiber dispersion. Some of the statistical methods used for the spatial analysis are the nearest *neighbor distances*, *point-to-nearest-event distances* (F-function) and *second-order spatial point process* (K-function) (Diggle 2003). The K-function can be used to quantify the tendency of fiber clumping, whereas the F-function describes the areas without fibers. The value of K-function under a complete spatial randomness (CSR) condition would be  $\pi s^2$ . If the K-function value is higher than the value under the CSR condition, clumping is observed. The CSR condition for the F-function is represented by  $1 - e^{-\pi\lambda s^2}$ . Higher values of F-function compared to the values under CSR condition represent the decrease in fiber-free zones.

Spatial dispersion of fibers in cement composites has been investigated. A study by Akkaya et al. (2001) investigated cement and silica fume composite system with 3.0% of PVA fibers by volume. For the analyzed specimens multiple cracking was observed. The locations of the first several cracks were related to a higher fiber clumping and higher K-function values; whereas later cracks coincided with more of a random dispersion and lower K-function values. The first crack location also exhibited lower values of F-function, meaning higher number of areas without fibers.

Another study examined the spatial distribution of fibers of different lengths (Akkaya et al. 2000b). It was concluded that the use of longer fibers leads to smaller values of F-function,

meaning higher number of areas without fibers. Whereas a distribution similar to the dispersion under CSR condition was observed for samples with shorter fibers.

### **3.0 - PURPOSE AND SCOPE**

Concrete cracking and high permeability allow for intrusion of harmful solutions, resulting in concrete deterioration and corrosion of reinforcement. The use of durable, low permeability, high performance concretes with controlled cracking for repairs and new construction would improve the service life of the structures. Furthermore, the use of high early strength durable materials would facilitate rapid and effective repairs, reducing traffic interruptions and decreasing long-term maintenance costs.

The purpose of this project was to develop durable concrete mixtures that exhibit high early strength, low permeability and resistance to cracking. The proposed mixtures were expected to reach compressive strengths of 3,000 psi within 24 and 10 hours, for high and very high early strength requirements, respectively. The main factors considered during the development of the concrete mixtures with early strength were the use of: high cement contents, low w/cm ratios, high fresh concrete and curing temperatures, accelerating admixtures and insulated curing. The use of SCMs, fly ash and silica fume, and large volumes of steel and synthetic fibers was investigated for improvement of concrete durability and cracking control.

Performance of the mixtures was determined based on durability tests, including compressive and flexural strengths, toughness, residual strengths, drying shrinkage, and permeability. Other characteristics, including permeability of cracked FRC specimens, fiber density and spatial distribution were also examined.

## 4.0 - METHODOLOGY

The project was split into two main stages regarding the strength requirement. The first stage was conducted in the laboratory and the field. Initially, the development of high early strength fiber reinforced concrete (HES-FRC) mixtures that can achieve 3,000 psi compressive strength in 24 hours was investigated in the laboratory. These mixtures were also designed for improved durability. The laboratory batches led to the selection of optimal HES-FRC mixtures for a bridge rehabilitation project. Then, field testing was performed. The second stage included the development of very high early strength fiber reinforced concretes (VHES-FRCs) that could achieve 3,000 psi compressive strength in 6 to 10 hours. This stage of work was conducted in the laboratory. The investigation was focused on mixture ingredients and admixture proportioning, fiber amounts, variation of w/cm ratios, as well as the variation of fresh concrete temperature and curing temperature. Preliminary batches were prepared and tested for strength to attain the very high early strengths. When satisfactory strengths were obtained, larger batches were prepared to determine characteristics other than compressive strength, such as flexural strength, toughness and residual strength, drying shrinkage, permeability of cracked samples and fiber distribution. The diagram in Figure 4.1 shows the breakdown of the HES-FRC and VHES-FRC mixtures.

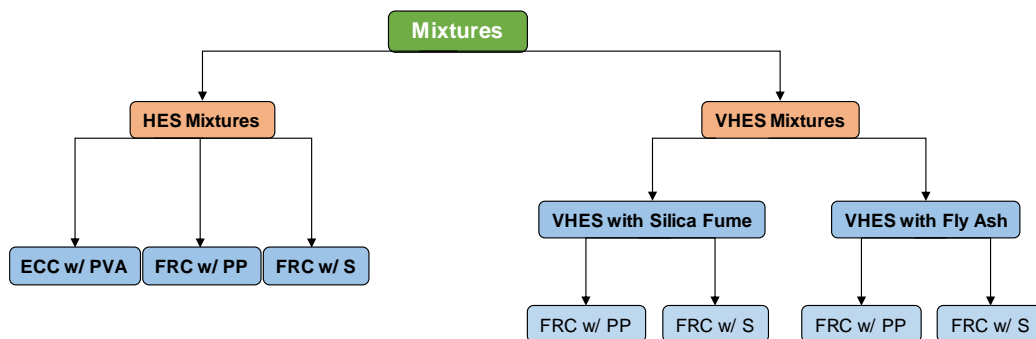


Figure 4.1: Development of HES-FRC and VHES-FRC mixtures

The last two stages of the project focused on the analysis of permeability of cracked concrete samples and fiber distribution for both, HES-FRC and VHES-FRC samples. All of the testing was completed at the Virginia Transportation Research Council (VTRC). Table 4.1 shows the ASTM and other test methods and specimen sizes used during this research project.

**Table 4.1: Used Fresh and Hardened Concrete Test Methods**

<i>Fresh Concrete Properties</i>	<b>Test Method</b>	
Air Content	ASTM C231	-
Slump	ASTM C143	-
Unit Weight	ASTM C138	-
Temperature	ASTM C1064	-
<i>Hardened Concrete Properties</i>	<b>Test Method</b>	<b>Specimen Size</b>
Compressive strength	ASTM C39	4 by 8 in. cylinder
Elastic modulus	ASTM C469	4 by 8 in. cylinder
Flexural strength	ASTM C1609	4 by 4 by 14 in. beam
Shrinkage (length change)	ASTM C157	3 by 3 by 11 in. beam
Splitting tensile strength	ASTM C496	6 by 2 in. cylinder
Permeability (Chloride Ion Penetrability)	ASTM C1202	4 by 2 in. cylinder
Permeability (Falling Head)	VDOT Virginia Test Method -120	6 by 2 in. cylinder
Maturity Test Method 1	ASTM C1074	-
Maturity Test Method 2	ASTM C918	-

Three different fiber types were considered for this study: polyvinyl alcohol (PVA), polypropylene (PP) and steel (S) fibers. Table 4.2 and Figure 4.2 show the characteristics of the fibers and their properties.

**Table 4.2: Characteristics of Fibers (provided by the manufacturer)**

<b>Material</b>	<b>Polyvinyl Alcohol (Nycon 2013)</b>	<b>Polypropylene (Grace 2016)</b>	<b>Steel (Bekaert 2016)</b>
Form	Straight, Monofilament	Monofilament, Crimped	Straight, Hooked Ends
Diameter [microns]	38	-	900
Length [in.]	0.375	2	2.36
Aspect Ratio	-	75	65
Specific Gravity	1.3	0.91	7.85
Tensile Strength [ksi]	240	80	335
Flexural strength [ksi]	5,700	-	-
Young's Modulus [ksi]	-	1,000	30,460
Wire Ductility	-	-	6%

- No values were provided by the manufacturer

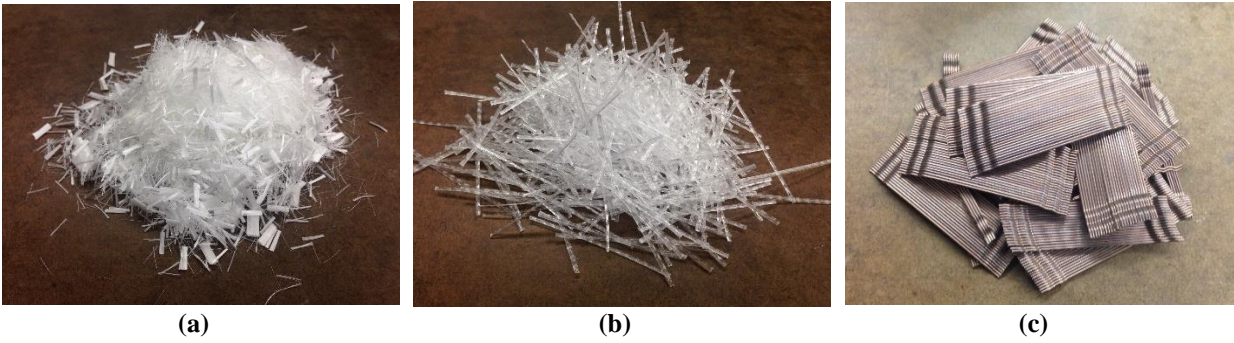


**Figure 4.2: (a) Polyvinyl Alcohol (PVA), (b) Polypropylene (PP), (c) Steel (S) Fibers**

#### ***4.1 Stage I – Development of HES-FRCs***

##### **4.1.1 HES-FRC Laboratory Mixtures**

HES-FRC mixtures that can achieve 3,000 psi compressive strength in 24 hours were developed in the laboratory. High cement contents and accelerating admixtures were used for the HES gain. Fly ash was added to all the mixtures for improvement of overall durability, reduction of permeability and increased resistance to chemical distress.

Two HES-FRCs with either PP or S fibers were developed. Based on the manufacturers recommended dosages, 15 (1.00%) and 18 lb/yd<sup>3</sup> (1.20%) of PP fibers, or 66 (0.50%) and 80 (0.60%) lb/yd<sup>3</sup> of S fibers were added to the FRC mixtures. In addition, a modified HES Engineered Cementitious Composite (ECC) mixture was considered in this research project. ECC is a mortar mixture developed by Victor Li (Li, 2003). In this work the conventional ECC mixture was modified to obtain HES. Standard volume dosage of PVA fibers at 44 lb/yd<sup>3</sup> (2.00% by vol.) was used.

The laboratory work included proportioning of concrete ingredients and amount of fibers, adjustment of w/cm ratios, and dosages of accelerating admixtures. The used Type C accelerating admixtures, Type F high-range water reducing admixture (HRWRA) and Type S shrinkage

reducing admixture (SRA) were in conformance with ASTM C494, and the air-entraining admixture (AEA) – with ASTM C260. An accelerating admixture was added to all three mixtures at the dosage of 60-75 oz/cwt. In addition, SRA was added to the HES-ECC at a dosage of 1.5 gal/yd<sup>3</sup> to help control shrinkage of the mortar mixture due to high amount of cementitious materials. The final proposed mixtures are presented in Table 4.3. To improve the post-cracking performance of HES-FRC with S fibers, the final dosage of fibers by volume was increased to 0.60%. Whereas, the dosage of PP fibers was limited to 1.20% to facilitate mixing procedures and to reduce clumping of fibers. Commercially available AEA and HRWRA were used to achieve the specified air content and workability.

**Table 4.3: Final Trial lab HES-FRC Mixture Designs**

<b>Components [lb/yd<sup>3</sup>]</b>	<b>HES-ECC</b>	<b>HES-FRC w/ PP</b>	<b>HES-FRC w/ S</b>
Type I/II Cement	961	720	560
Class F Fly Ash	1,153	180	140
Water	656	360	280
Mortar Sand	767	-	-
Natural Sand	-	1,084	1,394
Coarse Aggregate	-	1,350	1,431
Total Cementitious Material	2,114	900	700
<i>w/cm</i>	<i>0.31</i>	<i>0.40</i>	<i>0.40</i>
PVA (%)	44 (2.00%)	-	-
PP (%)	-	18.4 (1.20%)	-
S (%)	-	-	80 (0.60%)
SRA [gal/yd <sup>3</sup> ]	1.5	-	-
AA [oz/cwt]	60	75	60
Mixture Temperature [°F]	75	74	75

The main objective of the exploratory trial batching was to obtain the required 24-hour compressive strength. Consequently, only the 4 in. by 8 in. cylinders were made to test the compressive strength at 24 hours, 7 and 28 days. In addition, flexural beams were tested at 24 hours and 7 days. The mixing procedure for all laboratory HES-FRCs batches followed the ASTM C192 procedure, and consisted of mixing all the concrete ingredients and admixtures first, then

adding fibers, and performing additional mixing until composite material homogeneity was achieved. The specimens were covered with wet burlap and plastic, and kept in a laboratory room temperature (72°F) for the first 24 hours. After the 24-hour testing, the specimens were demolded and moved to the moisture room until further testing. The moisture room relative humidity was set to be above 95% and air temperature was about  $73 \pm 3$  °F.

#### 4.1.2 Field HES-FRC Batches

Two HES-FRC mixtures and modified HES-ECC mixture were implemented in a bridge rehabilitation project in Virginia. Table 4.4 shows the mixture designs used for field batches.

**Table 4.4: Field HES-FRC Mixture Designs**

Components [lb/yd <sup>3</sup> ]	HES-ECC	HES-FRC w/ PP		HES-FRC w/ S	
		15 lb/yd <sup>3</sup>	18 lb/yd <sup>3</sup>	w/ FA	w/ SF
Type I/II Cement	961	698	723	542	628
Class F Fly Ash	1,153	183	177	140	-
Silica Fume	-	-	-	-	50
Water	570	333	328	233	264
Mortar Sand	725	-	-	-	-
Natural Sand	-	1,197	1,193	1,463	1,613
Coarse Aggregate	-	1,340	1,337	1,493	1,493
Total Cementitious Material	2,114	881	900	682	678
<i>w/cm</i>	0.27	0.38	0.36	0.34	0.39
PVA (%)	44 (2.00%)	-	-	-	-
PP (%)	-	15 (1.00%)	18 (1.2%)	-	-
S (%)	-	-	-	80 (0.60%)	66 (0.50%)
SRA [gal/yd <sup>3</sup> ]	1.5	-	-	-	-
Accelerating Admixture [oz/cwt]	15	16.5	24	25	0
Mixture Temperature [°F]	79	90	91	80	95
Air Temperature [°F]	86	85	84	79	96

##### 4.1.2.1 HES-ECC

The HES-ECC was mixed according to the VDOT Special Provision for the conventional ECC (VDOT 2015). The mixing procedure included mixing all the ingredients and admixtures until homogeneity and proper flow of the material were achieved. PVA fibers were added last, and the

mixture was mixed at 12 – 15 high revolutions per minute (RPM) for additional time until the composite material appeared homogeneous.

The HES-ECC w/cm ratio was reduced to 0.27 to facilitate early strength gain. Accelerating admixture amount was decreased to 15 oz/cwt due to high fresh concrete and air temperatures.

#### *4.1.2.2 HES-FRCs with Polypropylene Fibers*

Two batches of HES-FRCs with PP fibers were made. For the first batch, all concrete ingredients and admixtures were added first until a workable mixture was achieved, and the PP fibers were added last. Mixing issues were encountered due to balling of fibers; hence only 1.00% of fibers by volume was added in 2-pound dissolvable bags. Due to the mixing issues with the first batch, for the second batch the 1.00% of PP fibers by volume was added in 2-pound dissolvable bags first with the water and admixtures. Then, the rest of the concrete mixture components were mixed in. As a result, significantly less balling was observed for this batch. It was decided to add the rest of 0.20% of PP fibers by volume directly, manually at the end of mixing, with a total of 1.20% of PP fibers by volume in the mix. Despite the balling of fibers in both batches, the rest of the fibers were well dispersed, and the mixtures achieved a homogeneous state.

The w/cm ratios were reduced for both batches to help with strength development at early ages. Less accelerating admixture amounts compared to the preliminary laboratory work were used due to high fresh concrete and air temperatures.

#### *4.1.2.3 HES-FRC with Steel Fibers*

Two batches of HES-FRC with S fibers were made. The mixing procedure for both batches consisted of mixing all of the concrete components first, then adding S fibers last, and mixing for additional time until material homogeneity was achieved. The first batch included 20% fly ash and

0.60% S fibers by volume. The w/cm ratio was reduced to 0.34 to help with early strength gain, and the amount of accelerating admixture was reduced due to high fresh concrete and air temperatures. For the second batch, silica fume at about 7% and S fibers at 0.50% by volume were used. The 0.50% was a recommended dosage by the manufacturer. Because of the addition of silica fume and a higher Portland cement content, accelerating admixture was not used.

For all three systems, six compressive strength cylinders and two flexural beams were left in the field beside the bridge repair area under burlap and plastic coverings and cured at field air temperature, ranging from 80 - 95°F (Table 4.4). The rest of the samples were taken to the plant laboratory and cured at plant lab room temperature of 75°F. The specimens taken to the plant lab included another set of compressive strength cylinders, flexural beams, length change (drying shrinkage) beams, and small (chloride ion penetrability test) and large (falling head permeability test) cylinders. Figure 4.3 shows the curing method and temperature monitoring setup. Temperature developments in the field and in the plant lab were recorded.

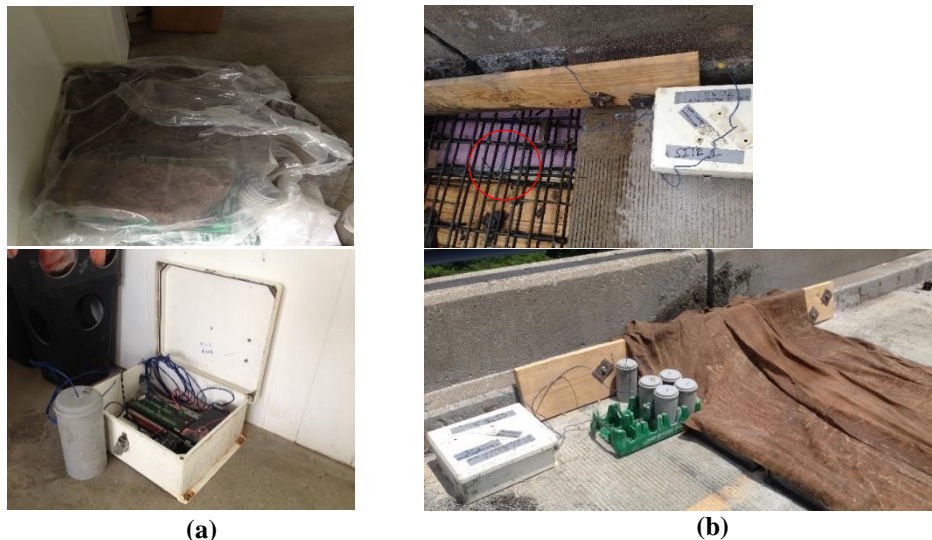


**Figure 4.3: Curing Method and Temperature Monitoring at (a) Plant Lab and (b) Field**

The compressive strength cylinders from the field and plant lab were tested at 24-30 hours after casting, and then at 7 and 28 days. The flexural beams were tested at 1, 7 and 28 days. For the first seven days the drying shrinkage samples were subjected to moist curing. The small permeability samples were moist cured for the first seven days, followed by the accelerated moist curing at 100 °F for the next three weeks, and tested at 28 days. The permeability testing of the mixes with S fibers was not performed due to the presence of conductive steel fibers that would have affected the test results.

#### 4.2 Stage II – Development of VHES-FRCs

The successful outcome of the first stage of the project allowed for a transition to the second stage. The objective of this stage of the study was to develop VHES-FRC mixtures that can achieve compressive strength of 3,000 psi in 6 to 10 hours. For this project, a number of mixtures was considered. Figure 4.4 shows the breakdown of VHES-FRC mixture development process.

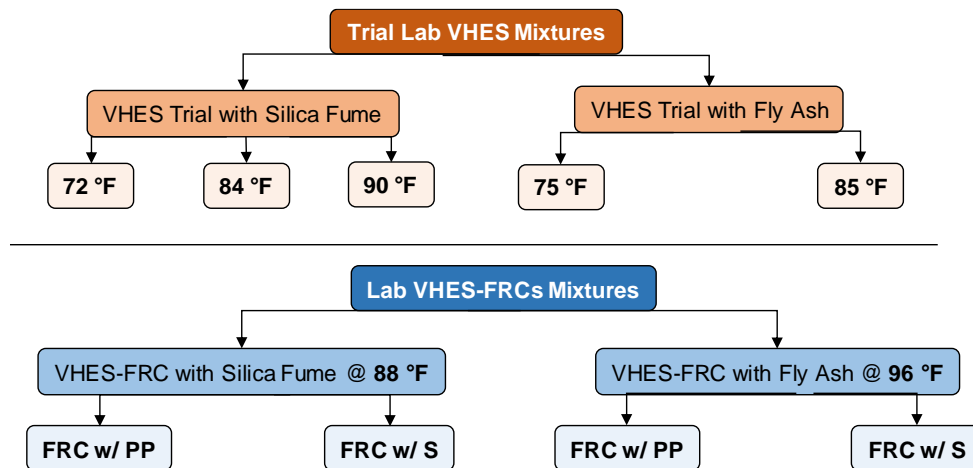


Figure 4.4: VHES-FRCs mixture development

The development of VHES concretes mixtures mainly focused on the use of:

- increased cement contents;
- reduced w/cm ratios;
- increased fresh concrete temperature;
- higher amounts of accelerating admixtures to reduce concrete setting time and increase early strength gain;
- insulated curing until the required strength was reached.

#### 4.2.1 VHES Preliminary Plain Concrete Laboratory Mixtures

The first step for this stage was to develop the plain concrete mixtures without fibers that could achieve the required compressive strength of 3,000 psi within the required time. Table 4.5 shows the selected VHES mixture proportions. The preliminary *VHES w/ SF* concrete mixture designs were developed by consulting with the industry. Whereas, the mixture design of *VHES w/ FA* was adopted from the existing VDOT patching mixtures for pavement repairs, which require 2,000 psi compressive strength within 6 hours. Hence, the trial batches were tested for strength requirement of 2,000 psi. The successful results lead to the implementation of *VHES w/ FA* patching mixtures in this project, with the compressive strength requirement of 3,000 psi within 10 hours.

The VHES mixtures were mixed and kept at different temperatures in order to determine the importance of mix and curing temperatures on the strength development. Exploratory batches with the *VHES-800 w/ SF* were made at three different temperatures: 72, 84 and 90 °F. One batch with *VHES-850 w/ SF* at 75 °F was made for comparison. Two trial batches with *VHES-882 w/ FA* were made with fresh concrete temperatures at 75 °F and 85 °F.

**Table 4.5: Mixture Designs for VHES with Silica Fume and Fly ash SCMs**

<b>Components [lb/yd<sup>3</sup>]</b>	<b>VHES - 800 w/ SF</b>	<b>VHES - 850 w/ SF</b>	<b>VHES - 882 w/ FA</b>
Type I/II Cement	750	800	750
Class F Fly Ash	-	-	132
Silica Fume	50	50	-
Water	288	280.5	265
Fine Aggregate	1005	984	1061
Coarse Aggregate	1823	1823	1676
Total cementitious material	800	850	882
w/cm	0.36	0.33	0.30
<b>Admixtures [oz/cwt]</b>			
Set Accelerating	24	24	24
Hardening Accelerating	30	30	20

In order to obtain the desired fresh concrete temperature Equation 4.1 below was used. It determines the temperature of fresh concrete,  $T$  (shown in blue), by using the temperature and mass of concrete components: coarse and fine aggregates, cement, water temperature and free moisture (Kosmatka and Wilson 2011). Generally, mixing water temperature,  $T_w$  (shown in red), is adjusted to achieve certain fresh concrete temperature.

$$T = \frac{0.22(T_a M_a + T_s M_s + T_c M_c) + T_w M_w + T_{ws} M_{ws} + T_{wa} M_{wa}}{0.22(M_a + M_s + M_c) + M_w + M_{ws} + M_{wa}} \quad \text{Equation 4.1}$$

where  $T_i$  is the temperature in degrees Fahrenheit of the fresh concrete ingredients and  $M_i$  is the mass of ingredients in pounds (where  $i$  is  $a$ ,  $s$ ,  $c$ ,  $w$ ,  $ws$ , and  $wa$  – concrete components).

The aggregates and cementitious materials were kept at room laboratory temperature of 73°F. Based on the literature review, the fresh concrete temperature,  $T$ , was increased to 80 - 90 °F. To obtain the recommended fresh concrete temperatures, the water temperature,  $T_w$ , was increased to 120 – 130 °F (shown in red, in example calculation below). An example calculation of the fresh concrete temperature is shown below:

$$\frac{0.22 \left( 73^{\circ}\text{F} \times 1823 \frac{\text{lb}}{\text{yd}^3} + 73^{\circ}\text{F} \times 1094 \frac{\text{lb}}{\text{yd}^3} + 73^{\circ}\text{F} \times 750 \frac{\text{lb}}{\text{yd}^3} + 73^{\circ}\text{F} \times 50 \frac{\text{lb}}{\text{yd}^3} \right) + 130^{\circ}\text{F} \times 288 \frac{\text{lb}}{\text{yd}^3} + 73^{\circ}\text{F} \times 20 \frac{\text{lb}}{\text{yd}^3} + 73^{\circ}\text{F} \times 0 \frac{\text{lb}}{\text{yd}^3}}{0.22 \left( 1823 \frac{\text{lb}}{\text{yd}^3} + 1094 \frac{\text{lb}}{\text{yd}^3} + 750 \frac{\text{lb}}{\text{yd}^3} + 50 \frac{\text{lb}}{\text{yd}^3} \right) + 270 \frac{\text{lb}}{\text{yd}^3} + 20 \frac{\text{lb}}{\text{yd}^3} + 0 \frac{\text{lb}}{\text{yd}^3}}$$

$$= 87^{\circ}\text{F}$$

In addition, a temperature loss after about one hour of mixing for revolving drum mixers was calculated using Equation 4.2 below. A sample calculation of temperature loss is demonstrated below:

$$T = 0.25(t_r - t_a) = 0.25(87^{\circ}\text{F} - 73^{\circ}\text{F}) = 3.5^{\circ}\text{F} \quad \text{Equation 4.2}$$

where  $t_r$  is the final required temperature, and  $t_a$  is the air temperature.

A standard mixing procedure for VHES plain concrete was followed and included:

- addition of coarse and fine aggregates,
- addition of 50% of water with the AEA admixture,
- followed by cementitious materials and the remainder of water,
- addition of set and hardening accelerating admixtures,
- and addition of HRWRA.

The total mixing time was 5 minutes. The mixtures were consolidated with a small vibrating table. For each batch, slump and air content values were measured (Figure 4.5 (a) and (b)). If the values were unsatisfactory, additional AEA and HRWRA were added to the concrete mixture to reach the values within the required VDOT specifications (VDOT 2007). For each batch, eight 4 in. x 8 in. cylinders were made to test the compressive strength of concrete, and one cylinder was used to monitor the temperature of concrete with a thermocouple. All samples were covered with plastic and insulating material and kept inside the styrofoam containers for the first 24 hours

(Figure 4.5 (c)). Then the samples were demolded and moved to the moisture room for 28 days. The moisture room relative humidity was above 95% and air temperature was about  $73 \pm 3$  °F.

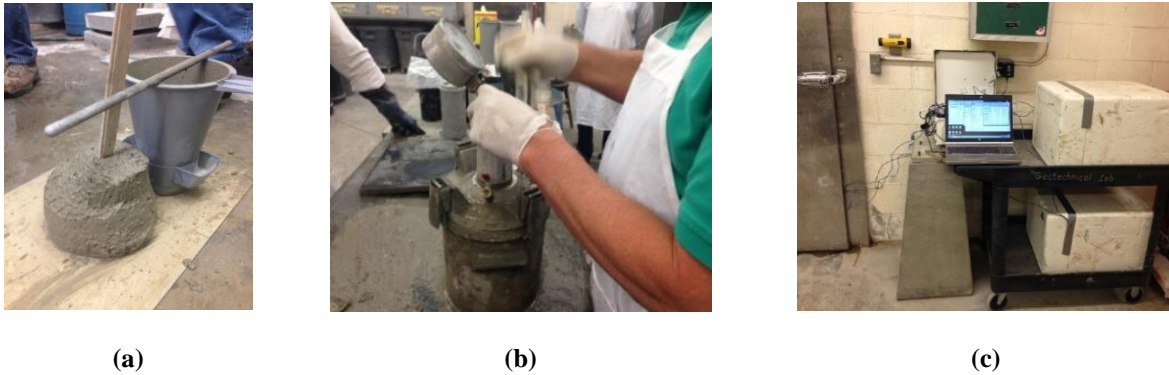


**Figure 4.5: (a) Slump and (b) Air Content Measurements, (c) Insulated Samples with Temperature Monitoring**

#### 4.2.2 VHES-FRC Preliminary Laboratory Mixtures

The next stage of the project was the addition of fibers to the VHES plain concrete mixtures. Two types of fibers were considered in this case: PP and S fibers. Three batches for each *VHES w/ SF* concrete were made: plain concrete control mixture with no fibers, mixture with 15 lb/yd<sup>3</sup> of PP fibers (1.00% by volume) and the mixture with 66 lb/yd<sup>3</sup> of S fibers (0.50% by volume). Table 4.6 shows the VHES-FRCs preliminary lab mixture designs. To improve the early strength gain, the w/cm ratios were reduced to 0.34 and 0.32 for the *VHES-800 w/ SF* and *VHES-850 w/ SF*, respectively.

Available natural sand fine aggregate and 0.5 in. (#78) crushed coarse aggregate were used. Smaller size crushed coarse aggregate is recommended for the use in HSC (ACI 2015). Ultimate strength is increased and bond strength improved due to greater surface area of smaller aggregates. In addition, smaller aggregates facilitate workability, which reduces with the addition of fibers.

**Table 4.6: VHES-FRCs Preliminary Lab Mixture Designs**

<b>Component [lb/yd<sup>3</sup>]</b>	<b>VHES-800 w/ SF</b>			<b>VHES-850 w/ SF</b>		
Type I/II Cement	750			800		
Silica Fume	50			50		
Water	272			272		
Fine Aggregate	1368			1327		
Coarse Aggregate	1481			1481		
Total cementitious material	800			850		
<i>w/cm</i>	0.34			0.32		
PP	-	15	-	-	15	-
S	-	-	66	-	-	66
<b>Total Fiber Content (%)</b>	<b>0%</b>	<b>1.00%</b>	<b>0.50%</b>	<b>0%</b>	<b>1.00%</b>	<b>0.50%</b>
<b>Admixtures [oz/cwt]</b>						
Set Accelerating	24			24		
Hardening Accelerating	30			30		
<i>Paste Content</i>	0.32			0.33		

The same mixing procedure as for plain concrete was followed, except for the addition of fibers. Fibers required additional mixing to achieve homogeneity. They were manually spread into the mixer to facilitate more uniform fiber distribution in the mix (Figure 4.6). Some balling was observed for mixtures with PP fibers; hence the balls were removed or broken apart manually during mixing. No mixing issues were observed for mixtures with S fibers.



**Figure 4.6: Addition of Polypropylene and Steel Fibers**

For each batch the following specimens were made:

- Eight 4 in. by 8 in. cylinders were made to test the compressive strength starting from 6 hours after casting and about every hour until the compressive strength of 3,000 psi was reached. Then the rest of the cylinders were tested at 1, 7 and 28 days.
- Three 4 in. by 4 in. by 14 in. flexural beams were made to test at the time the 3,000 psi compressive strength was reached, and then later tested at 7 and 28 days.
- Two length change beams were made to determine the drying shrinkage development. The samples were subjected to moist curing for the first seven days.
- Two 2 in. by 4 in. cylinders were cast to test for permeability, according to ASTM C1202. The samples were subjected to moist curing for the first seven days, followed by accelerated curing at 100 °F for three weeks. The permeability testing of the mixes with S fibers was not performed due to the presence of conductive steel fibers that would have affected the test results.

Figure 4.7 displays the elastic modulus, compressive strength, and flexural strength testing. The cylinder specimens were loaded in force control at a rate of 26,400 lbs/min. The flexural beams were loaded according to the ASTM C1609 procedure in four-point bending in displacement control at a rate of 0.010 in/min. The values were recorded every 30 lbf of applied force. From the flexural test results, first-peak and peak flexural strengths, residual strengths, toughness and equivalent flexural strength ratio were determined.



**Figure 4.7: Elastic Modulus, Compressive and Flexural Strengths Testing**

According to the ASTM C1609, the first-peak strength, and the residual strengths,  $f_{150}^D$  and  $f_{600}^D$  at net deflections of  $\frac{L}{150}$  and  $\frac{L}{600}$ , are calculated by using Equation 4.3 below:

$$f = \frac{P \cdot L}{b \cdot d^2} \quad \text{Equation 4.3}$$

where  $P$  – first-peak load,  $L$  – specimen span length,  $b$  – sample width, and  $d$  – sample depth.

Toughness value,  $T_{150}^D$ , is calculated as an area under the load-deflection curve from 0 to  $\frac{L}{150}$  net deflection value. Furthermore, the equivalent flexural strength ratio,  $R_{T,150}^D$ , is calculated by using the determined  $f_1$  – first-peak strength and Equation 4.4 below:

$$R_{T,150}^D = \frac{150 \cdot T_{150}^D}{f_1 \cdot b \cdot d^2} \cdot 100\% \quad \text{Equation 4.4}$$

ASTM C1018 was withdrawn in the year 2006, due to lack of interest and support; however, the methods used for calculation of toughness indices,  $I_5$ ,  $I_{10}$ ,  $I_{20}$  and residual strength factors  $R_{5,10}$  and  $R_{10,20}$  are still often used by researchers. The indices represent a ratio of the area under the

load-deflection curve up to 3.0, 5.5 and 10.5 times the first-crack deflection to the area up to first-crack. The residual strength factors are calculated using Equation 4.5 below:

$$R_{5,10} = 20 \cdot (I_{10} - I_5) \quad \text{and} \quad R_{10,20} = 10 \cdot (I_{20} - I_{10}) \quad \text{Equation 4.5}$$

#### 4.2.3 Final VHES-FRC w/ SF and VHES-FRC w/ FA Lab Batches

For the last step of this stage, two batches with PP or S fibers were made for each *VHES-FRC with silica fume* and *VHES-FRC with fly ash* mixtures. VHES-FRC with silica fume at 800 lb/yd<sup>3</sup> of total cementitious material was selected due to the lower cement content. It was decided to increase the steel fiber content to 0.60% by volume to improve the post-cracking flexural performance. In addition, the amount of hardening accelerating admixture was reduced from 30 oz/cwt to 20 oz/cwt to save on the total mixture cost. Table 4.7 shows the final mixture designs.

**Table 4.7: Final VHES-FRC w/ SF and VHES-FRC w/ FA Mixture Designs**

<b>Components [lb/yd3]</b>	<b>VHES-FRC w/ SF</b>		<b>VHES-FRC w/ FA</b>	
Cement Type I/II	750		750	
Silica Fume (6%)	50		-	
Boral Fly Ash (15%)	-		132	
Water	272		265	
Fine Aggregate	1437		1364	
Coarse Aggregate	1407		1407	
Total cementitious material	800		882	
<i>w/cm</i>	0.34		0.30	
PP (%)	15 (1.00 %)	-	15 (1.00 %)	-
S (%)	-	80 (0.60 %)	-	80 (0.60 %)
<b>Admixtures [oz/cwt]</b>				
Set Accelerating	24		24	
Hardening Accelerating	20		20	
<i>Paste Content</i>	0.32		0.33	
Mix Temperature [°F]	88		96	

The mixing procedure for VHES-FRCs with PP fibers was modified to reduce balling. The PP fibers were added at the beginning of mixing with coarse and fine aggregates. Consequently, less

balling was observed. The same mixing procedure as in trial batching was followed for the VHES-FRCs with S fibers. An AEA and HRWRA were used to achieve specified air content and workability.

For each batch the same type and number of specimens as in the preliminary VHES-FRC batches were made. In addition, two 6 in. by 12 in. large cylinders for the cracked concrete permeability testing were made. The methods for the testing of permeability of cracked concrete will be discussed in the following section. All specimens were covered with plastic and insulating material, and kept inside the styrofoam containers for the first 24 hours. Furthermore, flexural beams and large cylinders were kept inside the insulated containers as well (see Figure 4.8).



**Figure 4.8: Curing of the Samples for the First 24 Hours.**

The temperatures of cylinders, and environment inside the containers and the lab were recorded using multiple thermocouples with a data logger. The same testing equipment and procedures as in trial testing were performed. From the flexural test results, first-peak and peak flexural strengths, residual strengths, toughness and equivalent flexural strength ratio were determined.

### ***4.3 Stage III – Permeability of Cracked FRC Samples***

Two 6 in. by 12 in. cylinders were cast for the HES-FRCs and VHES-FRCs with PP and S fibers. The cylinders were sliced into 6 in. by 2 in. cylinders for the permeability testing several months after casting and being kept in the moisture room. For each batch, eight to ten 6 in. by 2 in. cylinders were tested.

#### **4.3.1 Crack Formation with Splitting Tensile Test**

Based on the literature review, the crack widths of 100, 200, 300, 400 and 500  $\mu\text{m}$  were formed by using the splitting tensile testing procedure (ASTM C496). The cylinders were loaded in displacement control at a rate of 0.026 in/min. The values were recorded every 100 ms. The MTS laser extensometer LX500 was used to capture the horizontal displacement between the two reflective tapes in the center on one side of the specimen. The laser extensometer has a resolution of 0.0001 in. In addition, the 9X transparent base magnifier with a 20 mm scale was used to observe the cracks with and without the applied load. Figure 4.9 shows the splitting tensile test setup (a) and the magnifier (b).

Based on the several trial tests, it was determined that in order to achieve the desired crack width after unloading and crack relaxation, the samples needed to be loaded about 0.1-0.2 mm of additional crack width displacement. The laser extensometer values were monitored, and the test was stopped manually when the required crack width was observed.

The cracks were measured along the sample with the magnifier. As expected, the crack width was not uniform along the crack length. Crack widths at the top, middle and bottom of the sample, as well as the maximum crack width were recorded.

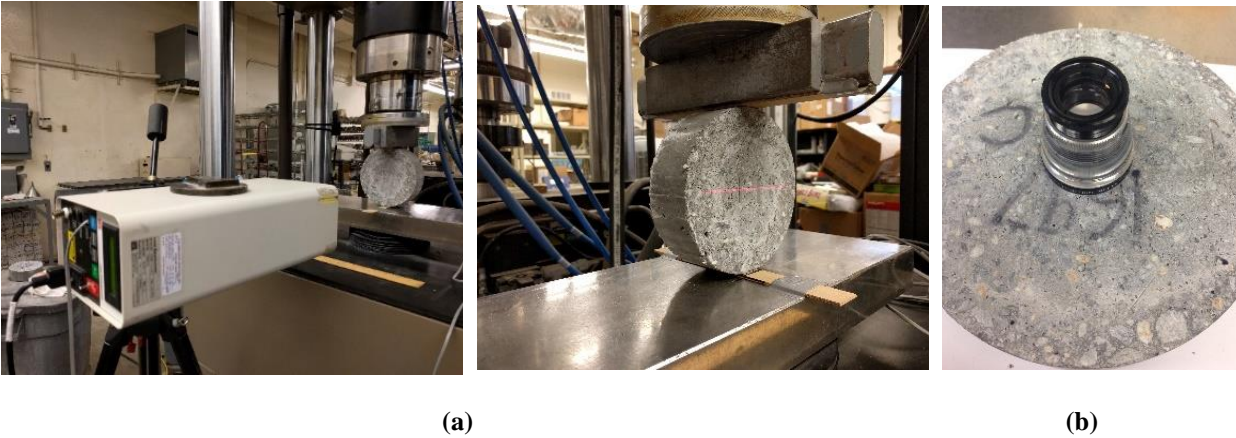


**Figure 4.9: (a) Splitting Tensile Test Setup, and (b) Magnifier with Scale**

The crack width was measured under load and after the load was removed, and the relaxation of the cracks was determined. Furthermore, the crack widths were measured again after the permeability testing to ensure the correct width was used. The comparison between the recorded laser extensometer and observed magnifier values under load was performed. Figure 4.10 shows the crack width measurements by the magnifier for selected example specimens.

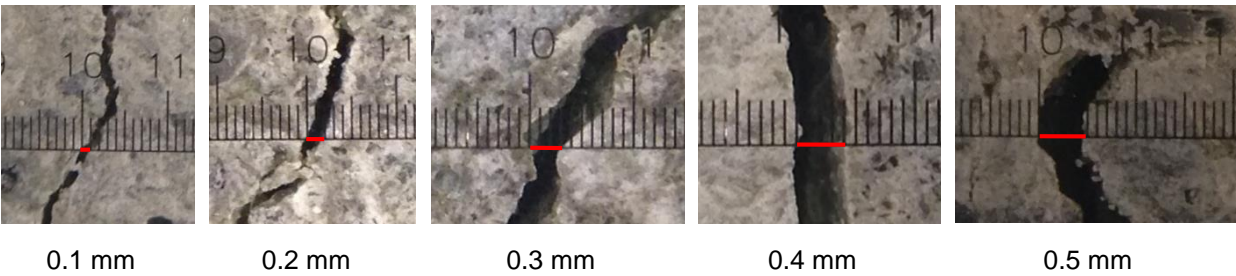


**Figure 4.10: Unloaded Crack Widths Measured with the Magnifier**

#### 4.3.2 Permeability Analysis of Cracked Specimens

ASTM C1202 was followed to saturate the cracked specimens for the permeability testing. Distilled water was used to saturate the samples. The specimens were vacuumed for three hours to remove trapped air, and then the distilled water was pumped into the container, with the pump

running for one more hour. The specimens were then soaked for at least another 16 hours (see Figure 4.11).



**Figure 4.11: Saturation of Permeability Samples**

The VDOT Virginia Test Method (VTM) – 120, method for the measurement of permeability of bituminous paving mixtures using a flexible wall permeameter, was followed to perform the testing of the cracked concrete samples. VTM – 120 is a falling head permeability test, and is used to measure a coefficient of water permeability, i.e. the laminar water flow rate through the saturated sample. The time for the water to travel and the change in head level were recorded.

The permeameter setup included: a graduated 500 ml. cylinder with the inner diameter of 1.25 in., a sealing tube with a flexible latex membrane that can fit samples with 6 in. diameter and 3.15 in. height, a cap assembly, a pedestal plate, a frame and clamp assembly, an air pump with pressure gauge capable of applying 15 psi pressure and vacuum to evacuate air from the sealing tube, and an outlet pipe of 2 in. long and 0.7 in. in diameter. See Figure 4.12 for the permeameter setup used in this project.

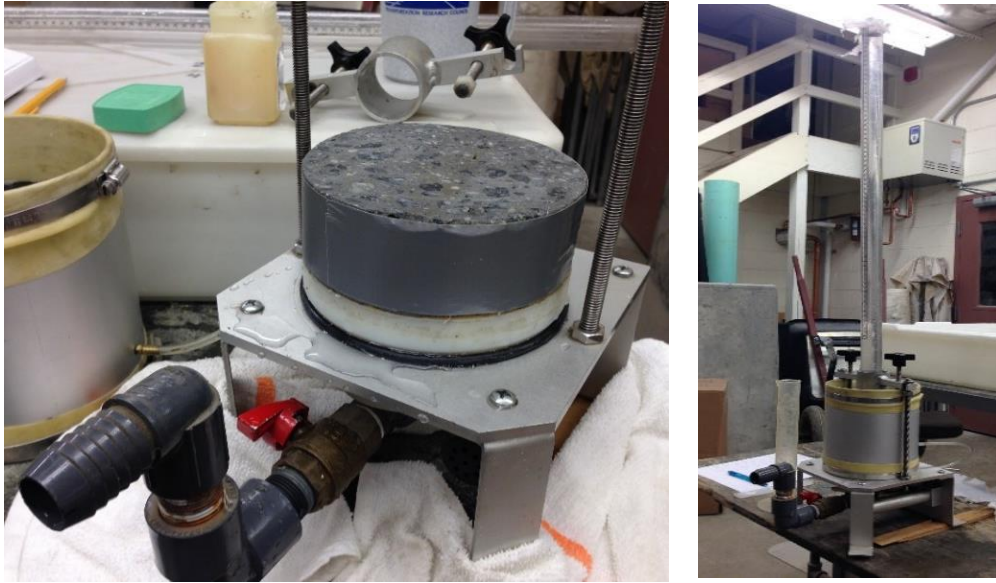


**Figure 4.12: Permeameter Testing Setup**

Prior to saturation, the samples were taped along the sides to make sure the rough edges and steel fibers would not puncture the sealing tube membrane, and to also ensure a better seal between the samples and the membrane. The permeability test procedure included positioning of the sample in the center of the permeameter pedestal, placing the sealing tube over the sample, tightening all connections and clamps, and applying the confining pressure of about 15 psi. Then the graduated cylinder was filled above the initial timing mark. The flow control valve was opened, and the time for the water to flow from the initial to final timing marks was recorded. The water travel time for the 100, 200, 300, 400 and 500  $\mu\text{m}$  cracks was approximately 30 minutes, 10 minutes, 2 minutes, 1.5 minutes and 45 seconds, respectively. For the 100  $\mu\text{m}$  width cracks and smaller the test procedure was stopped at 30 minutes, and the water level was recorded at the corresponding *cm*. In addition, several solid uncracked samples were tested to make sure there was no water leakage between the specimens and the sealing tube. The water level did not move for several

hours, confirming that no leakage was taking place, and the water flowed through the formed cracks.

The test was performed three times for each sample, and the average coefficient of water permeability was determined. Equation 4.6 below was used to determine the coefficient of water permeability,  $k$  (VTM-120).

$$k = \frac{a \cdot l}{A \cdot t} \cdot \ln \left( \frac{h_1}{h_2} \right) \quad \text{Equation 4.6}$$

where  $k$  – permeability coefficient,  $a$  – area of the standpipe,  $A$  – average area of the concrete test specimen,  $l$  – average sample thickness,  $t$  – average flow time,  $h_1$  – initial hydraulic head, and  $h_2$  – final hydraulic head.

The temperature of the water was measured and corrected to 68 °F, by using Equation 4.7 below (VTM-120):

$$k_{20} = R_T \cdot k, \quad \text{Equation 4.7}$$

where  $k_{20}$  – corrected coefficient of water permeability, and  $R_T$  - a ratio of the viscosity of water at the test temperature to the temperature of water at 68 °F.

#### ***4.4 Stage IV – Fiber Distribution Analysis***

The last stage of this project was focused on investigation of the fiber distribution. The tested flexural beams were sliced in the transverse (T) and the horizontal (H) directions into 1 in. deep sections. Only samples with S and PP fibers were analyzed. Two beams with S fibers from each batch and one beam with PP fibers from each batch were used for the analysis. Figure 4.13 below shows the schematic of the ASTM C1609 with third-point flexural loading, and the transverse and

horizontal cutting orientations for two slicing methods. The transverse cross-sections were 4 in. by 4 in., whereas horizontal cross-sections were 3.25 – 3.5 in. by 4 in. Figure 4.14 shows the T and H cutting orientations for the actual beams after the flexural testing was performed.

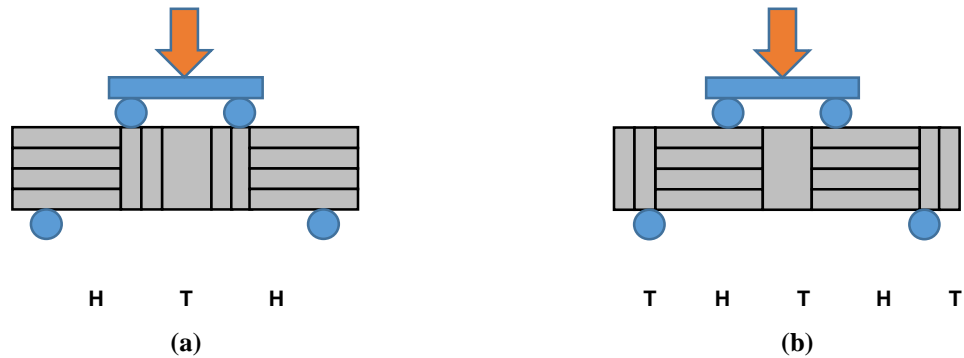


**Figure 4.13: Schematic of the Flexural Test Setup, and Two Slicing Methods (a) HTH and (b) THTHT**

Each S fiber cross-section was treated with a dark color dye to create a high contrast between the steel fibers and concrete. Then the digital images of the cross-sections were taken and analyzed in MATLAB through image processing analysis.

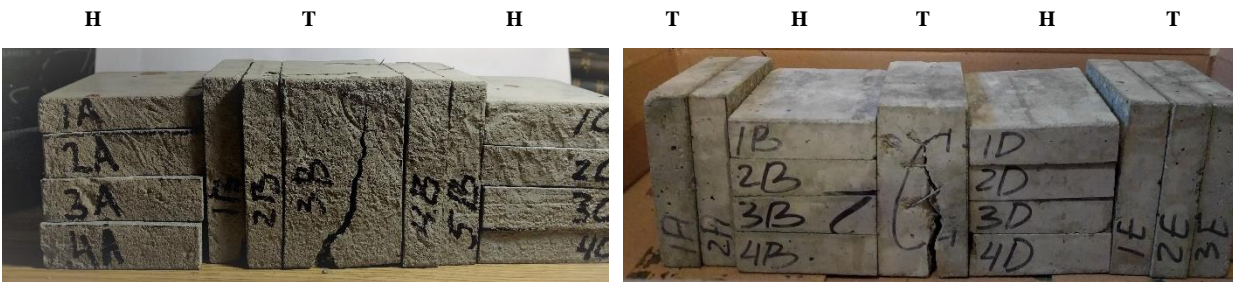


**Figure 4.14: Two slicing methods: HTH and THTHT**

However, the same approach was not applicable for the cross-sections with PP fibers. The individual fibers had to be marked with a sharpie to create the contrast between the fibers the rest of the concrete components. Thus, due to a more complicated analysis of the cross-sections with PP fibers only several sections from each beam and each batch were analyzed.

Due to a random fiber orientation, it was decided to split the fiber cross-section sizes into two categories: cross-sections with the angles below the  $45^\circ$  and fiber cross-sections with the angles above  $45^\circ$ . Figure 4.15 shows fiber cross-sections at various angles.

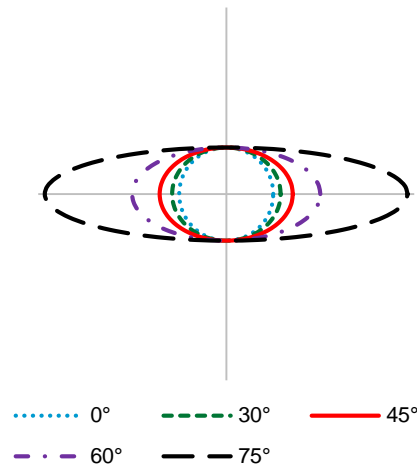


**Figure 4.15: Fiber cross-sections at different angles**

The effectiveness of fibers to resist the applied stresses gets reduced with the increase of the orientation angle between the direction of fibers and applied forces (Nawy 2001). Hence, fibers that are perpendicular to the cross-section face are the most effective in resisting applied bending stresses during flexural testing. Therefore, fibers oriented at the  $45^\circ$  angle or less were included in the fiber count, whereas fibers at the angles higher than  $45^\circ$  were removed by the MATLAB code procedure or manually.

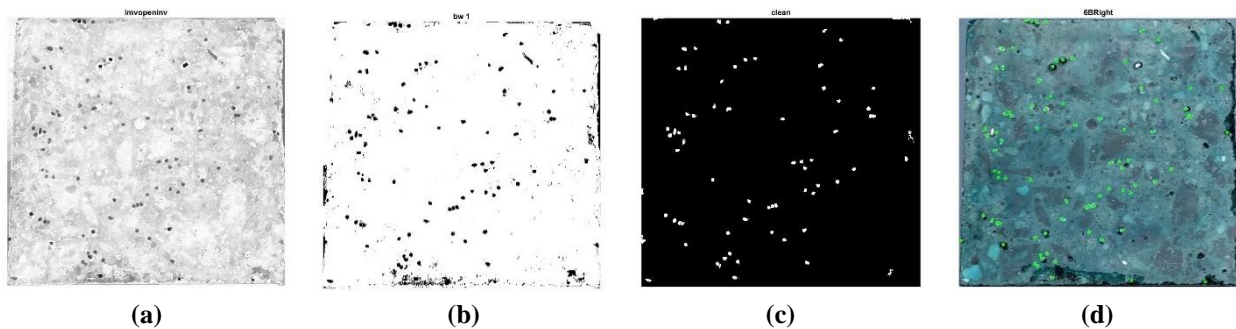
#### 4.4.1 Image Processing Analysis

Image processing analysis was used to study the cross-sections. The digital images of the cross-sections were analyzed in MATLAB software, using built-in image processing functions. The MATLAB code is attached in the Appendix. The brief step-by-step code summary and functions

are described below with the image references for the cross-section with S fibers. A similar procedure was followed for the analysis of the cross-sections with polypropylene fibers.

1. First function *rgb2hsv* converts the red, blue and green (RGB) colors of the image to hue, saturation and value layers (HSV). The *value* or *hue* layers of the image were used for the analysis.
2. Function *imopen* morphologically opens the image on the grayscale. Then the result image is subtracted from the value image to remove the difference in the lighting in the background.

Figure 4.16 (a) shows the inverse of this step's final image.



**Figure 4.16: Image Analysis Process: (a) Inverse; (b) Binary; (c) Pixel Removal; (d) Final**

3. Function *im2bw* is used to convert the image to binary by thresholding. The thresholding level was modified manually depending on the image. All values greater than a set thresholding level turned white (1s) and the values less than thresholding level turned black (0s). See Figure 4.16 (b) for the result image.
4. Functions *xor* and *bwareopen* in combination removed all the pixels that are less and greater than set limits. The result image was cleared from the small noise pixels and pixels larger than the desired fiber size. See Figure 4.16 (c) for the result image. Some of the points had to be removed manually for a proper fiber count.

5. The last image, Figure 4.16 (d), shows the final result image with centroids of the fibers plotted over the original image.

#### 4.4.2 Statistical Spatial Point Pattern Analysis

Finally, the spatial point pattern statistical analysis was performed to evaluate fiber dispersion. The point pattern analysis is used to determine the trend of the spatial dependence of the pattern. Figure 4.17 shows the representations of the (a) clustered (b) regular or (c) random point patterns.

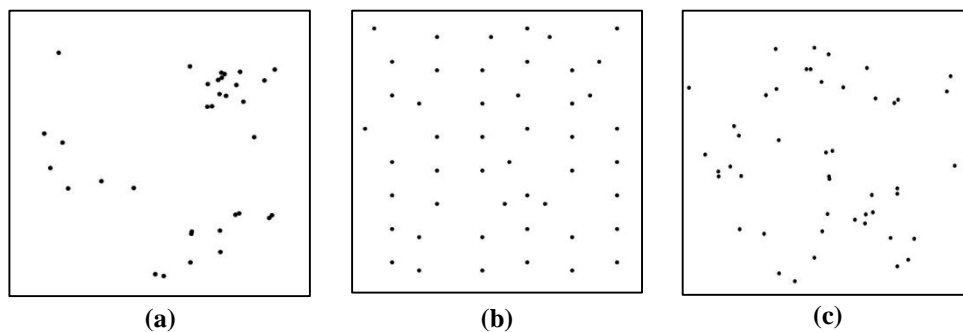


**Figure 4.17: (a) Clustered; (b) Regular (Ordered); (c) Random Distributions (Figure adapted from Diggle (2003))**

Fiber coordinates were determined from the image processing and analyzed through K-function and F-function. The methods used to determine the two functions are represented graphically in Figure 4.18 (a) and (b), respectively. The K-function represents the tendency of fiber clumping and measures the distance between fibers. The function considers a number of fibers within distance  $s$  of an arbitrary fiber in the cross-section. Distance  $s$  was varied from 0 to the half of the width of the specimen (1.5-2 in.).

The F-function can be used to measure the empty spaces between the fibers. It determines the distribution of distances  $s$  from a random sample point in the cross-section or from a generated grid point to its nearest fiber. In this research work, the grid point method was utilized. Diggle (2003) recommends using a  $k \times k$  grid to represent the sample points, where  $k \approx$

$\sqrt{\text{number of fibers}}$ . A value twice of that was used for the grid dimensions. The size of  $k$  does not improve the statistical precision, but facilitates the smoothness of the curve. Similarly, distance  $s$  was varied from 0 to the half of the sample width.

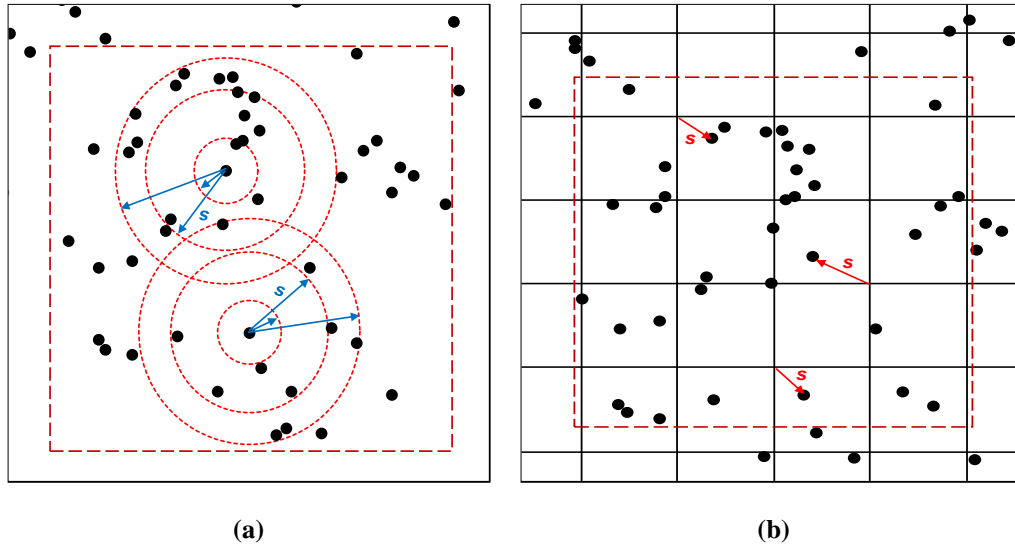


Figure 4.18: (a) K-function (b) F-function (Figure adapted from Akkaya et al. (2000b))

Random point pattern distribution can be described as a distribution under the complete spatial randomness (CSR). The calculated K-function and F-function values can be compared to the values obtained under CSR conditions to evaluate fiber dispersion patterns. In practice, the CSR condition is not attainable, and represents an idealized condition. But it is a convenient tool to aid the classification of point patterns. For the K-function the clustering is observed for values greater than CSR, and regularity for values less than CSR. Whereas, the F- function values that drift below the CSR curve indicate a more aggregated pattern, with more fiber-free areas. If the function values drift above the CSR curve, it would indicate a more regular, uniform pattern. Graphic representations of the  $\left(\frac{K[s]}{\pi}\right)^{1/2}$  and F-function are represented in the Figure 4.19 (a) and (b) for

clustered, regular and random point pattern distributions. The value of  $\left(\frac{K[s]}{\pi}\right)^{1/2}$  equals to the distance  $s$  (see Equation 4.11 (a) for reference).

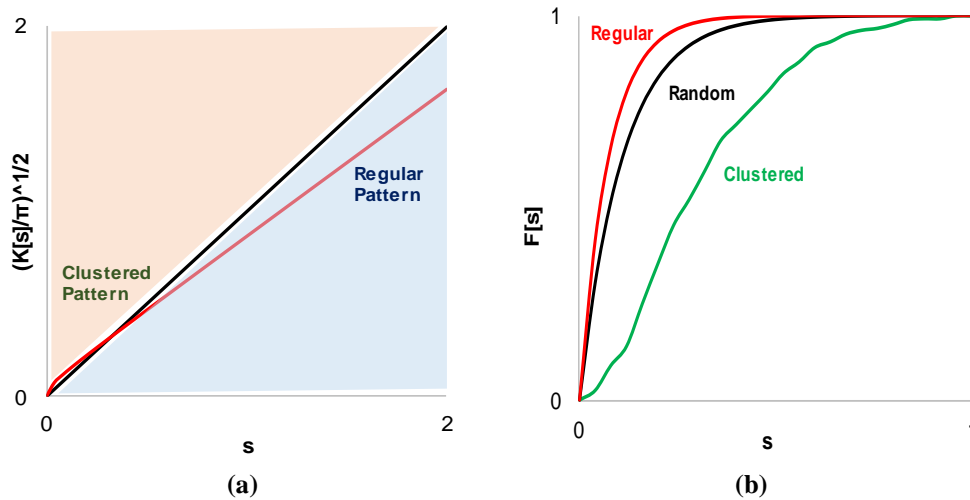


Figure 4.19: Graphic Representations of (a)  $\left(\frac{K[s]}{\pi}\right)^{1/2}$  function and (b) F-function

The K-function is calculated by using the Equation 4.8:

$$K(s) = \frac{\text{Number of fibers within distance } s \text{ of an arbitrary fiber}}{(\text{Total Number of such fibers}) \cdot \lambda} \quad \text{Equation 4.8}$$

where  $\lambda$  is a fiber density, and is represented by Equation 4.9:

$$\lambda = \frac{\text{Expected number of fibers}}{\text{Unit Study Area}} \quad \text{Equation 4.9}$$

F-Function can be calculated by using the Equation 4.10:

$$F(s) = \frac{\text{Number of sample points in the study area with nearest fiber within distance } s}{\text{Total number of sample points in the study area}} \quad \text{Equation 4.10}$$

Under a complete spatial randomness (CSR) for a homogeneous Poisson process the K-function and F-function are calculated using Equation 4.11 and Equation 4.12, respectively.

$$K(s) = \pi s^2 \quad \text{Equation 4.11}$$

$$F(s) = 1 - e^{(-\lambda\pi s^2)} \quad \text{Equation 4.12}$$

In addition, the edge effects were considered through a buffer zone (red, dotted box in Figure 4.18 (a) and (b)). A study area of observation inside the beam cross-section area a certain distance away from the edges was selected to account for edge effects. The calculated values are more precise for the smaller  $s$  distances, because they are less likely to be affected by the edge effects. The MATLAB K-function and F-function calculation codes are attached in the Appendix section.

## **5.0 - RESULTS AND DISCUSSION**

This chapter is divided into four main sections discussing the results of the lab and field HES-FRCs mixtures, the exploratory and final lab VHES-FRCs mixtures, permeability of the cracked FRC samples with PP and S fibers, and the fiber dispersion analysis in FRC specimens with PP and S fibers.

### ***5.1 Stage I - HES-FRCs Results***

This stage discusses the results of the final trial laboratory and the field implemented HES mixtures, including HES-ECC, HES-FRC w/ PP fibers, and HES-FRC w/ S fibers. The compressive strength requirement for the mixtures was 3,000 psi in 24 hours. The fresh and hardened concrete properties are presented. Toughness and residual strengths were determined for both plant lab and field 28-day cured specimens. Temperature developments of the field closure pours, field and plant lab cylinders were recorded. In addition, drying shrinkage data is presented.

#### **5.1.1 HES-FRCs Trial Laboratory Results**

As it was indicated in the methods chapter, the trial laboratory HES-FRC mixtures were focused on testing the compressive and flexural strengths. Table 5.1 shows the fresh properties of the trial lab HES-FRCs. The air content of FRC mixtures with S and PP fibers was within the VDOT standards (VDOT 2007). The HES-ECC was not air entrained; however, earlier work has shown that ECC provides satisfactory resistance to freezing and thawing without an air entrainment (Ozyildirim and Viera 2008). The ECC is a self-consolidating mixture, therefore the slump flow of 22 in. was measured; whereas FRCs with PP and S fibers are not as workable, resulting in lower slump values. Furthermore, the addition of fibers can substantially decrease workability of the mixtures.

**Table 5.1: Fresh Lab HES-FRCs Properties**

<b>Fresh Properties</b>	<b>HES-ECC</b>	<b>HES-FRC w/ S Fibers</b>	<b>HES-FRC w/ PP Fibers</b>
Air Content [%]	-	7	7
Unit Weight [lbs/ft <sup>3</sup> ]	-	146	138
Slump Flow [in.]	22	-	-
Slump [in.]	-	3	4
Temperature [°F]	75	74	75

Table 5.2 shows the hardened HES-FRC properties. The HES-FRCs reached over 3,000 psi compressive strength within 24 hours. The modified HES-ECC mixture reached about 2,800 psi compressive strength in 24 hours due to high fly ash amount. However, when the temperatures in the field are high, they would facilitate the strength development due to faster hydration reaction. Whereas, in the cold environment to facilitate the strength development fresh concrete temperature can be increased and external heat can be applied during curing. Hence, in the field it was expected for HES-ECC to achieve the required strength within 24 hours. The samples displayed low permeability and elastic modulus values within the standards (VDOT 2007).

**Table 5.2: Hardened Lab HES-FRC Properties**

<b>Compressive Strength [psi]</b>	<b>HES-ECC</b>	<b>HES-FRC w/ S Fibers</b>	<b>HES-FRC w/ PP Fibers</b>
1 Day	2,830	3,490	3,640
7 Days	5,510	5,860	5,730
28 Days	-	7,620	6,740
<b>First-Peak / Peak Flexural Strength [psi]</b>			
1 Day	450 / 1,005	535 / 845	575 / 740
7 Days	660 / 1,360	795 / 895	770
Elastic Modulus [10 <sup>6</sup> psi]	-	4.1	3.71
Permeability [C]	217	-	508

All HES-FRC mixtures exhibited deflection hardening behavior and high residual strengths (Figure 5.1). The residual strength can be defined as a remaining concrete strength in the post-peak load region (ACI 2013); whereas the deflection hardening behavior is characterized by an increase in load carrying capacity with further deformation after the first crack (Naaman 2007). The HES-

ECC exhibited the best post-cracking performance. The load carrying capacity kept increasing, and the test had to be stopped manually due to the LVDT limitations. The HES-FRC with S fibers displayed deflection hardening followed by deflection softening. The HES-FRC with PP fibers exhibited some degree of deflection hardening with high residual strengths after the first-peak. On average the increase of 43% in first-peak flexural strength from day 1 to day 7 can be observed for all samples.

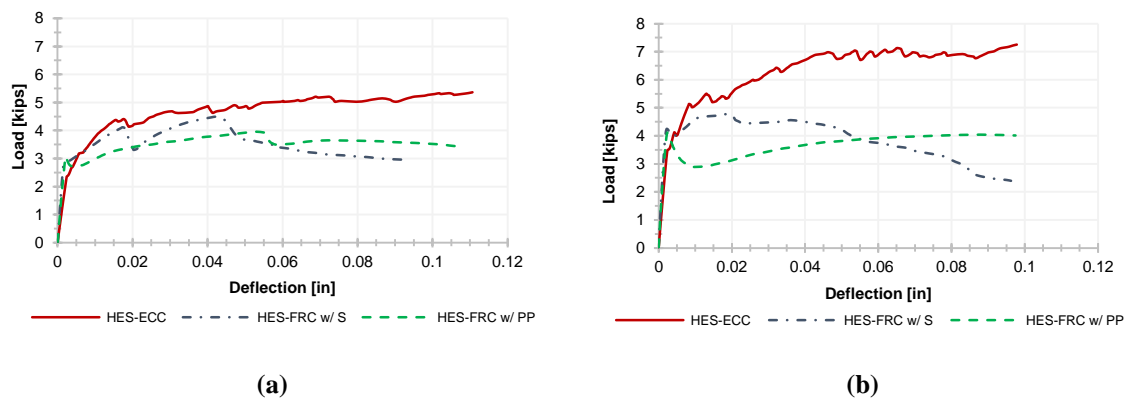


**Figure 5.1: HES-FRCs Flexural Results at 24 hours (a) and 7 days (b)**

### 5.1.2 HES-FRCs Field Results

The optimal laboratory mixtures were implemented in the field rehabilitation project. This section will discuss the results of the field batches. Table 5.3 displays fresh HES-FRCs properties of the field batches. The air content of the FRC mixtures was within the VDOT standards (VDOT 2007). The fresh concrete temperatures were elevated due to high air temperatures, which helped with the early strength gain.

**Table 5.3: Fresh Field HES-FRC Properties**

Fresh Properties	HES-ECC	HES-FRC w/ PP		HES-FRC w/ S	
		15 lb/yd <sup>3</sup>	18 lb/yd <sup>3</sup>	w/ FA	w/ SF
Air Content [%]	2.5	5.3	5.3	5.5	5.2
Unit Weight [lbs/ft <sup>3</sup> ]	122	-	138	146	146
Slump Flow [in.]	20	-	-	-	-
Slump [in.]	-	8.5	4.8	7.5	4.0
Mix Temperature [°F]	79	90	91	80	95
Air Temperature [°F]	86	85	84	79	96
Relative Humidity [%]	-	49	48	64	51

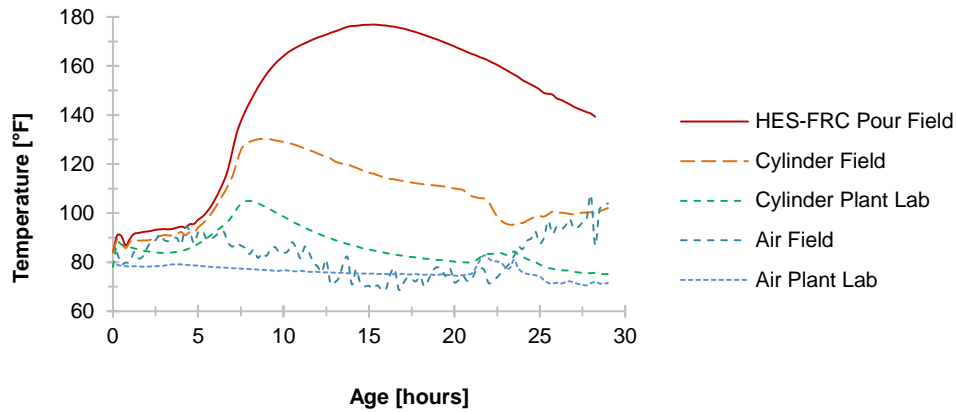
### 5.1.2.1 HES-ECC

Table 5.4 displays HES-ECC hardened properties. The plant lab cured specimens did not reach 3,000 psi in 24 hours. However, the field cured samples, kept on top of the closure pour at the bridge reached the required strength within 24 hours.

**Table 5.4: HES-ECC Hardened Properties**

Test	Age	Plant Lab	Field
Compressive Strength [psi]	24 hours	2,770	3,440
	7 Days	4,380	5,300
	28 Days	6,520	6,730
First-Peak / Peak flexural strength [psi]	28 Days	695 / 1,245	750 / 1,060
Elastic Modulus [10 <sup>6</sup> psi]	28 Days	2.43	2.59
Permeability [C]	28 Days	169	129

The temperature developments in the field and in the plant lab were monitored and displayed in Figure 5.2. As expected, the higher temperatures facilitated the early strength gain. The temperature gain in the closure pour was significantly higher compared to the cylinders; thus it was concluded that the HES-ECC pour reached the required strength sooner than 24 hours. Furthermore, HES-ECC exhibited low elastic modulus values, which are beneficial to cracking control; and the permeability values were significantly below the 1500C specified standard.



**Figure 5.2: Temperature developments vs Age for the HES-ECC**

The HES-ECC deflection hardening behavior was typical for the material, with an increase in flexural strength of over 60% on average from the first-peak (Figure 5.3). The test samples exhibited multiple tight cracking, with crack widths less than 0.1 mm.

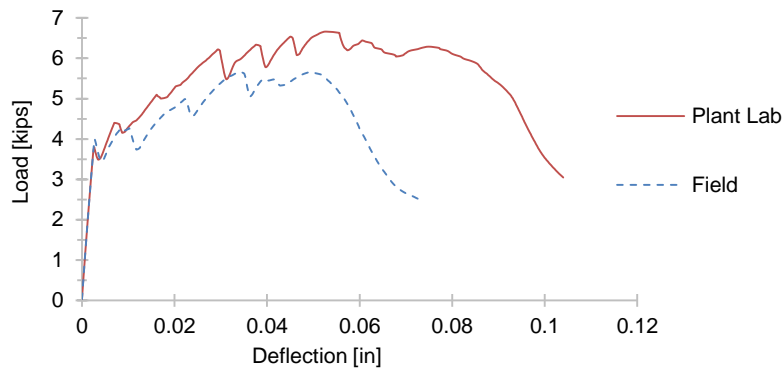


**Figure 5.3: 28-Day HES-ECC Flexural Results**

Similar to the HES-ECC system, the temperature developments of HES-FRCs with PP and S fibers were monitored (Figure 5.4 (a) and (b)). The temperature gain in the PP and S closure pours was significantly higher compared to the field and plant lab cured cylinders; thus it was concluded that the closure pours reached the required strength before 24 hours.

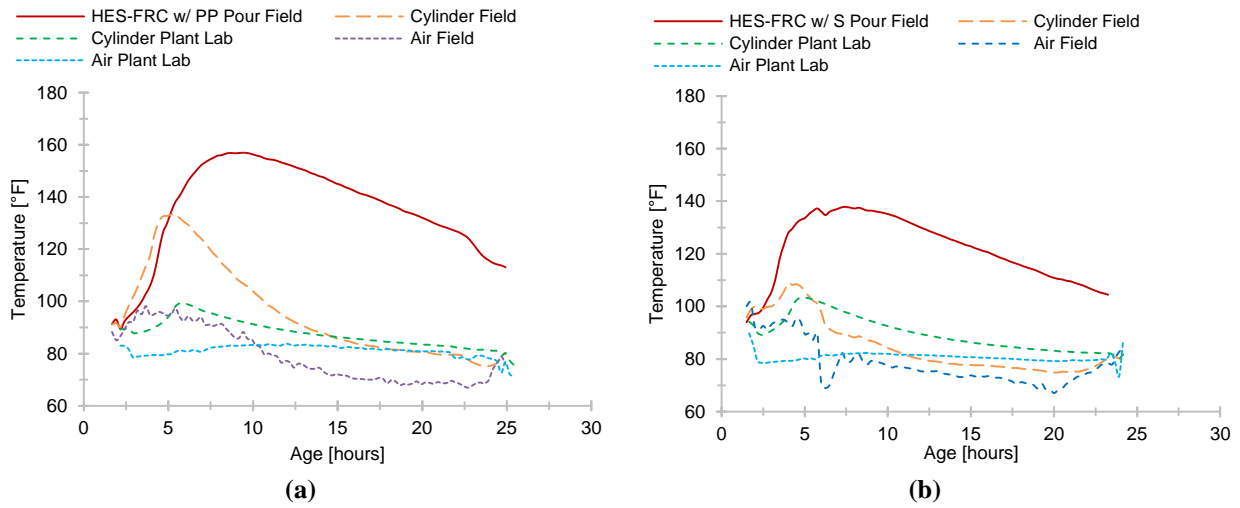


**Figure 5.4: Temperature development of HES-FRCs w/ (a) PP and (b) S fibers**

#### 5.1.2.2 HES-FRCs with Polypropylene Fibers

Table 5.5 shows the hardened properties for the two batches of HES-FRC with 15 lb/yd<sup>3</sup> and 18 lb/yd<sup>3</sup> of PP fibers. Both batches reached 3,000 psi compressive strength in about 24 hours. The permeability values were satisfactory and below the specification limit of 1500 C.

**Table 5.5: HES-FRCs w/PP Fibers Hardened Properties**

Test	15 lb/yd <sup>3</sup>			18 lb/yd <sup>3</sup>		
	Age	Field	Plant Lab	Age	Field	Plant Lab
Compressive Strength [psi]	21 hours	-	3,100	27 hours	-	3,170
	24 - 27 hours	3,020	3,090	31 hours	3,010	3,280
	7 Days	-	4,650	7 Days	4,090	4,400
	28 Days	5,640	6,140	28 Days	5,130	5,390
First Peak / Peak flexural strength [psi]	1 Day	490	620	1 Day	390	480
	7 Days	-	720	7 Days	-	670
	28 Days	720	810	28 Days	700	795
Elastic Modulus [10 <sup>6</sup> psi]	28 Days	3.31	3.39	28 Days	2.94	3.10
Permeability [C]	28 Days	976	643	28 Days	1,293	933

The HES-FRCs with PP fibers exhibited high residual strengths, but no deflection hardening behavior (Figure 5.5). No significant difference in residual strengths was observed between the

batches with 15 lb/yd<sup>3</sup> or 18 lb/yd<sup>3</sup> of PP fibers. The first-peak flexural strength values were comparable to the HES-ECC first-peak values. According to the NCHRP 540 Report on guidelines for early-opening to traffic for concrete pavement repairs, flexural strength values ranging from 260 to 400 psi were most common among the state highway agencies for the 6-8 hour concrete repair materials, whereas values of 300 to 600 psi were observed for the 20-24 hour repair materials (Van Dam et al. 2005). Hence, the obtained flexural strength values are within the reported range.

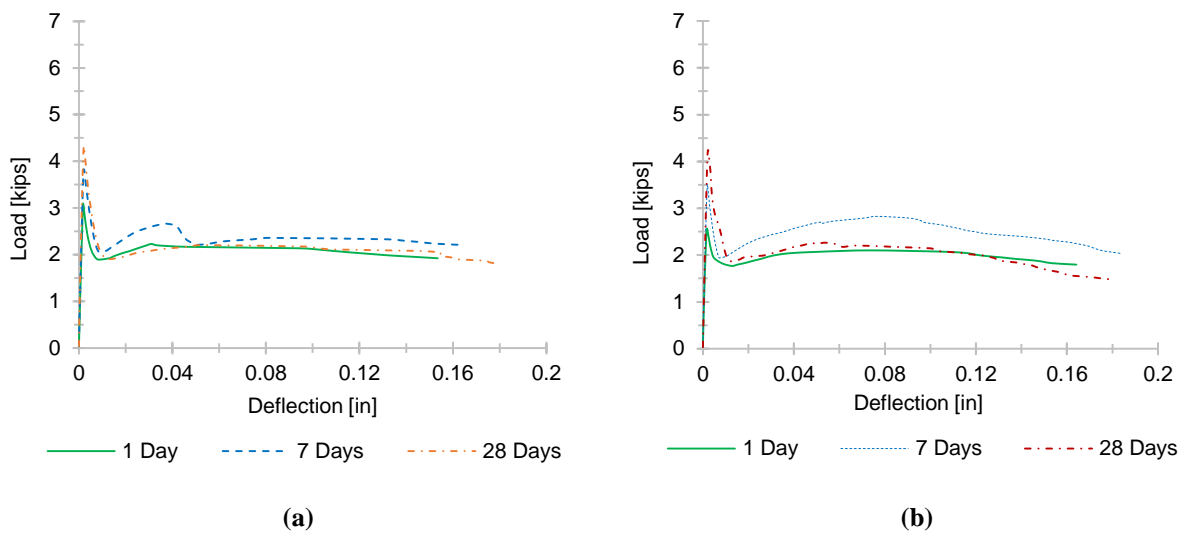


**Figure 5.5: HES-FRCs w/ PP fibers (Plant Lab Cured) (a) Batch w/ 15 lb/yd<sup>3</sup> (b) Batch w/ 18 lb/yd<sup>3</sup>**

### 5.1.2.3 HES-FRCs with Steel Fibers

Table 5.6 displays the hardened properties of HES-FRC with S fibers. All batches reached 3,000 psi compressive strength within 24 hours. Chloride ion penetrability test was not conducted due to the presence of conductive steel fibers, which affect the test results. The HES-FRC w/ FA and 0.60% of S fibers by volume displayed deflection hardening behavior followed by deflection softening (Figure 5.6 (a)). Whereas the HES-FRC w/ SF and 0.50% of S fibers by volume did not display deflection hardening, but exhibited high residual strengths (Figure 5.6 (b)).

**Table 5.6: HES-FRCs w/ S Fibers Hardened Properties**

Test	w/ FA and 0.60% S Fibers by Vol.			w/ SF and 0.50% of S Fibers by Vol.		
	Age	Field	Plant Lab	Age	Field	Plant Lab
Compressive Strength [psi]	24 hours	-	3,440	21 hours	3,430	-
	31 hours	3,930	3,330	29 hours	4,020	4,080
	7 Days	5,160	5,520	7 Days	5,380	5,610
	28 Days	6,440	6,790	28 Days	6,600	7,100
First-Peak / Peak flexural strength [psi]	1 Day	570 / 600	585 / 640	1 Day	685 / 815	640
	7 Days	-	835 / 925	7 Days	-	840 / 910
	28 Days	895 / 940	980 / 1,270	28 Days	1,090	1,000
Elastic Modulus [ $10^6$ psi]	28 Days	3.63	3.85	28 Days	4.32	4.42

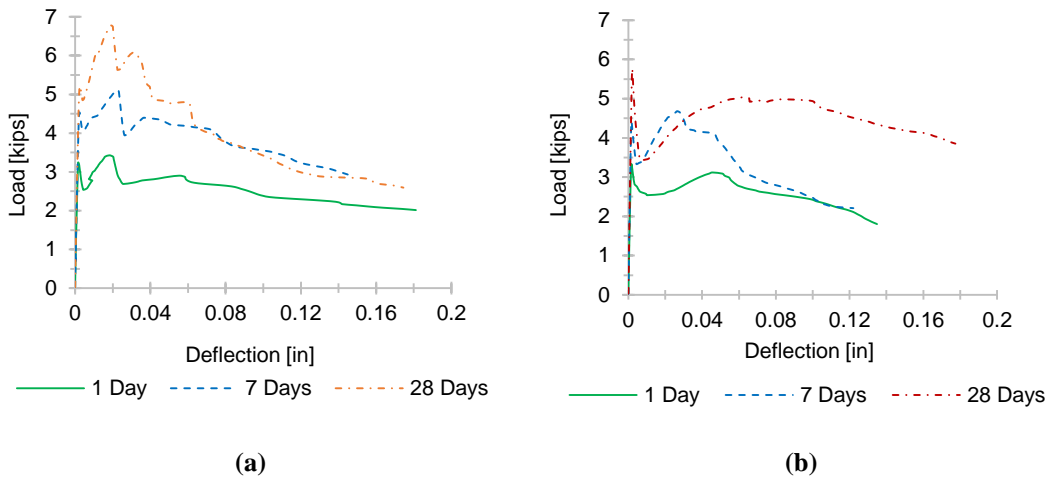


**Figure 5.6: HES-FRC w/ S fibers (Plant Lab Cured) (a) Batch w/ FA (b) Batch w/ SF**

The obtained flexural strength values meet the requirements of the NCHRP reported range of 300 to 600 psi for 20-24 hour concrete repair materials (Van Dam et al. 2005). The S fiber system performed significantly better than the HES-FRC w/ PP fibers, with overall higher first-peak and ultimate flexural strengths. The first-peak flexural strength was on average 24% higher compared to PP fiber systems.

Table 5.7 and Table 5.8 show the 28-day toughness and residual strengths values obtained from the plant laboratory and field cured specimens, respectively. There was some difference between the field and lab results, but it could be attributed to the variability between the specimens.

**Table 5.7: 28-Day HES-FRC Flexural Test Results (Plant Lab Cured)**

Test	HES-ECC	HES-FRC w/ PP		HES-FRC w/ S	
		15 lb/yd <sup>3</sup>	18 lb/yd <sup>3</sup>	w/ FA	w/ SF
First-Peak / Peak flexural strength [psi]	695 / 1,245	810	795	890 / 1270	1,000
Toughness, $T_{150}^D$ [in.-lb]	450	210	190	400	350
Residual Strength, $f_{600}^D / f_{150}^D$ [psi]	990 / 1145	370 / 410	370 / 410	1265 / 710	745 / 930
Equivalent Flexural Strength Ratio, $R_{T, 150}^D$ [%]	149	62	55	97	75
I <sub>5</sub>	5	4	4	4	4
I <sub>10</sub>	10	6	6	9	7
I <sub>20</sub>	23	10	11	18	13
R <sub>5,10</sub>	106	42	40	92	56
R <sub>10,20</sub>	130	39	50	96	60

**Table 5.8: 28-Day HES-FRC Flexural Test Results (Field Cured)**

Test	HES-ECC	HES-FRC w/ PP		HES-FRC w/ S	
		15 lb/yd <sup>3</sup>	18 lb/yd <sup>3</sup>	w/ FA	w/ SF
First-Peak / Peak flexural strength [psi]	750 / 1,060	720	700	895 / 940	1,090
Toughness, $T_{150}^D$ [in.-lb]	340	180	210	350	340
Residual Strength, $f_{600}^D / f_{150}^D$ [psi]	895 / 425	380 / 500	400 / 535	740 / 820	730 / 925
Equivalent Flexural Strength Ratio, $R_{T, 150}^D$ [%]	105	60	71	93	83
I <sub>5</sub>	5	4	4	4	5
I <sub>10</sub>	9	6	6	7	8
I <sub>20</sub>	21	11	11	14	14
R <sub>5,10</sub>	94	40	38	65	65
R <sub>10,20</sub>	111	50	50	70	60

The results for HES-ECC and HES-FRC w/ S fibers specimens were comparable. The two systems exhibited significantly higher toughness values compared to the HES-FRCs w/ PP fibers. Hence, the ductility of these systems is considerably higher. Similar trends were observed for the residual strengths at L/600 and L/150 deflection values.

The increased flexural and ultimate load capacity after the first crack is characterized by the equivalent flexural strength ratio. The flexural strength capacity of HES-ECC after the first crack was the highest at 149%, followed by HES-FRC w/ S fibers at about 86% on average, and HES-FRC w/ PP fibers at 59% on average. The toughness indices represent the amount of the energy it takes to bend the beam to a certain deflection. As expected, the values increased with the increase in deflection. Again, the HES-ECC samples exhibited the best performance, followed by HES-FRC w/ S fiber specimens. No significant difference in flexural performance between the two batches with HES-FRC w/ PP fibers was observed. However, a substantial difference between the batches with *HES-FRC w/ FA* and 0.60% of S fibers by volume and *HES-FRC w/ SF* and 0.50% of S fibers by volume was determined. No deflection hardening behavior was exhibited by the second batch, and the decrease in toughness values of about 14% and reduction in  $R_T^D$ , 150 values of 30% was determined.

Figure 5.7 displays the drying shrinkage test results for the three HES-FRC systems. All systems displayed substantial length change due to high paste, cement and water contents. The HES-ECC had the greatest shrinkage with the paste content of 0.83. The system displayed a length change value of over 0.16% in 4 months. The paste content for the HES-FRC with PP fibers mix was 0.38 and the length change values of about 0.09% at 4 months. The HES-FRC w/ S fibers had the lowest paste content of 0.29. The mix with silica fume exhibited 0.06% length change in 4 months.

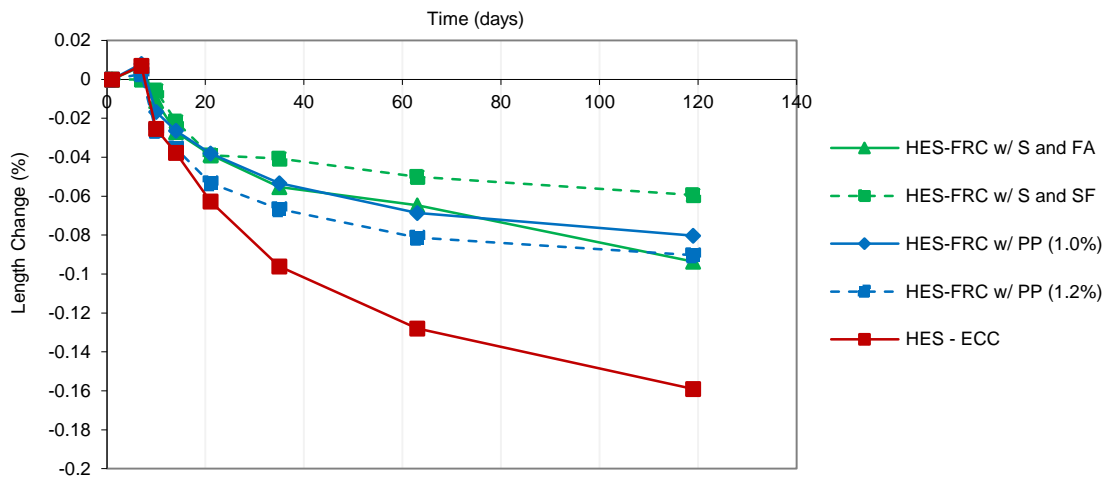


**Figure 5.7: HES-FRCs Drying Shrinkage Results**

The drying shrinkage values need to stay under 0.07% in 4 months to prevent shrinkage cracking (Babaei and Fouladgar 1997). Whereas, the paste content values need to stay under 0.27 to control cracking density (Darwin et al. 2004). Nevertheless, all three HES-FRCs systems had tight cracks in the direction of traffic, but also had gaps in the transverse direction between the closure pour and overlays. A visual survey several months after placement revealed multiple tight cracks (crack widths of 0.1 – 0.2 mm) in the HES-ECC system, and very few tight (0.1 mm) or no cracks for HES-FRCs with PP and S fibers. Potentially, a combination of primary reinforcement and fibers working together facilitated the control of cracking.

### **5.2 Stage II - VHES-FRCs Results**

This section covers the results of the VHES-FRC mixtures with PP and S fibers. In this case, the compressive strength requirement was 3,000 psi within 10 hours. The work done with the exploratory VHES concrete mixtures without fibers, VHES mixtures with fibers, and the final laboratory VHES mixtures with PP and S fibers is presented in this section. Influence of the fresh

concrete and curing temperatures on the early-age strength gain were examined. Toughness and residual strengths were determined and compared for PP and S fiber 28-day specimens. Furthermore, drying shrinkage data was presented and evaluated based on the suggested limits.

## 5.2.1 VHES Exploratory Plain Concrete Lab Mixtures

### 5.2.1.1 *VHES with Silica Fume*

The preliminary laboratory batches with *VHES-800 w/ SF* and *VHES-850 w/ SF* were made at different fresh concrete and curing temperatures. Table 5.9 shows the fresh concrete properties for the three *VHES-800 w/ SF* batches at 72, 84 and 90°F and the *VHES-850 w/ SF* at 75 °F. The air content was within the VDOT specifications for all mixtures (VDOT 2007).

**Table 5.9: VHES-800 w/ SF and VHES-850 w/ SF fresh concrete properties**

<b>Properties</b>	<b>VHES-800 w/ SF</b>			<b>VHES-850 w/ SF</b>
Air Content [%]	5.1	5	5	5.7
Unit Weight [lbs/ft <sup>3</sup> ]	148	149	148	149
Slump [in.]	6.75	5.5	8.5	3.25
<b><i>Temperature [°F]</i></b>	<b><i>72</i></b>	<b><i>84</i></b>	<b><i>90</i></b>	<b><i>75</i></b>

All samples were covered with plastic and insulating material, and kept in the styrofoam containers for the first 24 hours. For the two batches at 84 and 90 °F, the water temperature was increased to 120-130 °F in order to increase the overall fresh concrete mix temperature to above 82 °F (see Equation 4.1 for reference). Figure 5.8 shows the concrete temperature developments over the first 24 hours for the three *VHES-800 w/ SF* batches at three different temperatures, 72 °F (room temperature), 84 °F and 90 °F, and one *VHES-850 w/ SF* at 75 °F. The three *VHES-800 w/ SF* mixtures reached 3,000 psi compressive strength in over 11 hours, 8 hours and 7 hours for 72, 84 and 90 °F mixtures, respectively (indicated by black, solid circles in Figure 5.8). ASTM C918 and C1074 maturity methods using the Nurse-Saul function were utilized to determine the time it

took for the batch at 72 °F to reach the required strength. The time of set varied for mixtures depending on the temperature as well.

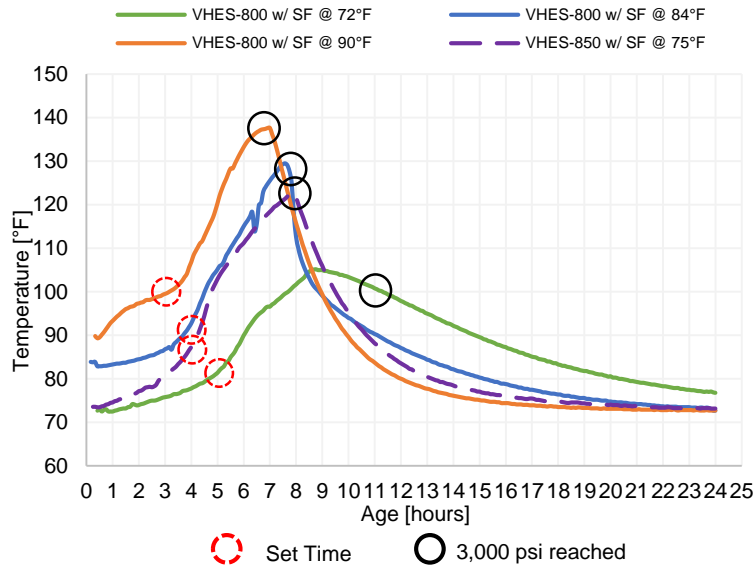


**Figure 5.8: Temperature Development for preliminary VHES w/ SF mixtures**

The set time was about 5 hours, 4 hours and 3 hours for 72, 84, and 90 °F mixtures, respectively (indicated by red, dashed circles in Figure 5.8). The temperature rise after the set was greater for the mixtures with higher initial fresh concrete temperatures, which indicates faster strength development.

The *VHES-850 w/ SF* displayed similar performance to the *VHES-800 w/ SF* at 84 °F, reaching 3,000 psi compressive strength within 8 hours. Higher cement content facilitated the early strength gain. Table 5.10 shows the compressive strength results for the exploratory *VHES w/ SF* batches.

**Table 5.10: Compressive strength results for exploratory VHES w/ SF mixtures**

Age	VHES-800 w/ SF			VHES-850 w/ SF
	72°F	84°F	90°F	75°F
5 hours	-	-	830	1,020
6 hours	510	1,240	2,220	1,920
7 hours	1,180	2,330	<b>3,190</b>	2,860
8 hours	1,800	<b>3,510</b>	-	<b>3,280</b>
Maturity Prediction (11 hours)	<b>3,000</b>			-
24 hours	5,280	5,960	5,940	5,280
7 Days	7,680	8,340	8,000	6,880
28 Days	9,030	9,780	9,350	8,090

### 5.2.1.2 VHES with Fly Ash

As it was indicated in the methods chapter, the *VHES w/ FA* mixtures were adopted from the existing VDOT pavement repair patches. Table 5.11 shows the results of the fresh concrete properties. The air contents were within the VDOT standards (VDOT 2007). The slump values were on the lower side due to the high heat generation, but mixtures were workable enough for sample casting. The same curing procedures as for the *VHES w/ SF* batches were followed.

**Table 5.11: VHES-882 w/ FA fresh concrete properties**

Properties	VHES-882 w/ FA	
Air Content [%]	6	6.1
Unit Weight [lb/ft <sup>3</sup> ]	148	147
Slump [in]	3.5	4.5
Mix Temperature [°F]	75	85
Air Temperature [°F]	75	75
Relative Humidity [%]	40	40

The mixtures reached 2,000 psi compressive strength within 7 hours (Table 5.12). Therefore, it was expected for the *VHES w/ FA* mixtures to gain the desired 3,000 psi compressive strength within 10 hours.

**Table 5.12: VHES-882 w/ FA Compressive Strength Results**

<b>Age</b>	<b>VHES-882 w/ FA @ 75 °F</b>	<b>VHES-882 w/ FA @ 85 °F</b>
6 hours	1,540	1,960
7 hours	2,810	2,360
24 hours	6,490	5,880
7 Days	8,430	7,190
28 Days	9,530	8,750
28-Day Elastic Modulus [ $10^6$ psi]	5.36	4.65

### 5.2.2 VHES-FRC Preliminary Lab Mixtures

Exploratory *VHES-800 w/ SF* and *VHES-850 w/ SF* mixtures with polypropylene or steel fibers were made. The fresh concrete mixture temperatures for the *VHES-800 w/ SF* were around 80° F, a little higher compare to the *VHES-850 w/ SF*. Air content and slump values were within the VDOT specifications and similar for both *VHES-FRCs w/ SF* types. The results of fresh concrete properties for VHES-800 and VHES-850 mixtures are presented in Table 5.13 and Table 5.14, respectively.

**Table 5.13: Fresh concrete properties of VHES-800 w/ SF and fibers**

<b>Properties</b>	<b>VHES-800 w/ SF</b>		
	<b>Plain Concrete</b>	<b>PP fibers (1.00%)</b>	<b>Steel Fibers (0.50%)</b>
Air Content [%]	5.7	4.5	5
Unit Weight [lbs/ft <sup>3</sup> ]	147	147	148
Slump [in.]	5	6	6
Mix Temperature [°F]	80	81	80
Air Temperature [°F]	72	72	72

**Table 5.14: Fresh concrete properties of VHES-850 w/ SF and fibers**

<b>Properties</b>	<b>VHES-850 w/ SF</b>		
	<b>Plain Concrete</b>	<b>PP fibers (1.00%)</b>	<b>Steel Fibers (0.50%)</b>
Air Content [%]	5.3	5.9	5.5
Unit Weight [lbs/ft <sup>3</sup> ]	147	145	149
Slump [in.]	7	6	7.5
Mix Temperature [°F]	76	80	79
Air Temperature [°F]	77	75	75
Relative Humidity [%]	56	56	57

For both *VHES-FRCs w/ SF* mix designs, all batches reached 3,000 psi compressive strength within 7-7.5 hours. Table 5.15 displays the compressive strength results. The temperature development was monitored and recorded (Figure 5.9).

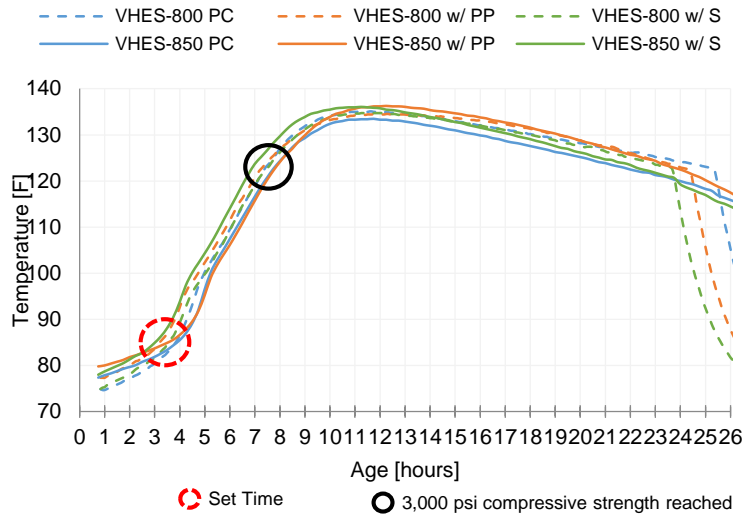


**Figure 5.9: VHES w/ SF (800 and 850) temperature developments**

All batches followed the similar temperature development, which explains similar compressive and flexural strength developments. The permeability values for both *VHES-FRCs w/ SF* types for plain concrete and concrete with PP fibers were satisfactory and significantly below the 1500 C limit. As in previous work, the permeability of samples with S fibers was not tested.

**Table 5.15: Compressive strength results for VHES-FRC w/ SF**

Age	VHES-800 w/ SF			Age	VHES-850 w/ SF		
	Plain Concrete	w/ PP	w/ S		Plain Concrete	w/ PP	w/ S
6.5 hours	-	2,800	2,640	6 hours	1,490	1,220	2,220
<b>7 hours</b>	-	-	<b>3,350</b>	<b>7 hours</b>	2,760	2,370	<b>3,810</b>
<b>7.5 hours</b>	<b>3,490</b>	<b>3,640</b>	-	<b>7.5 hours</b>	<b>3,590</b>	<b>2,970</b>	-
24 hours	8,190	8,760	8,790	24 hours	8,330	7,740	8,760
7 Days	9,100	9,180	9,630	7 Days	9,330	9,160	10,090
28 Days	9,910	9,930	10,850	28 Days	10,530	9,400	10,500

The 28-day flexural load-deflection graphs for specimens with plain concrete, PP fibers, and S fibers are presented in Figure 5.10. The first-peak 28-day flexural strength was about 1,000 psi on average for all specimens, and the percent difference was less than 10% between the plain concrete and fiber reinforced concrete specimens. Nevertheless, it is evident that the addition of fibers significantly improved the post-cracking performance of the concrete. The respective samples for both *VHES-FRCs w/ SF* types followed similar trends.

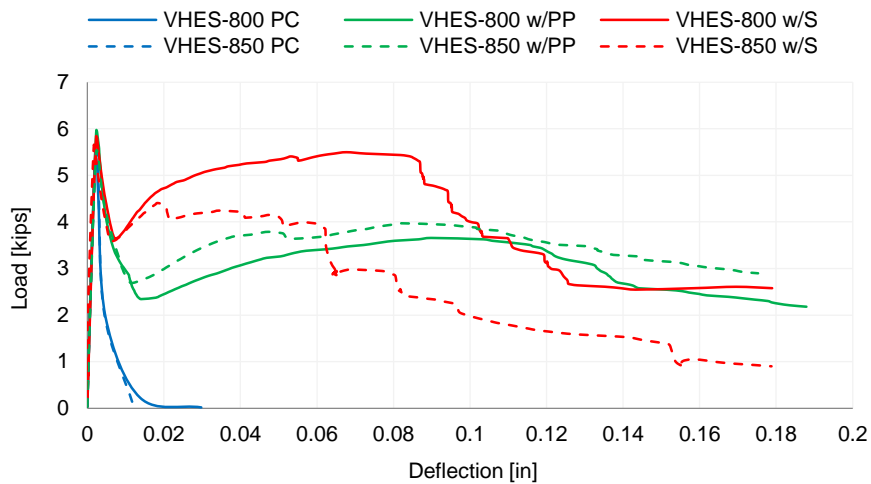


**Figure 5.10: Flexural test results for VHES w/ SF plain and FR concretes**

True deflection hardening behavior was not observed, however the samples w/ S fibers exhibited higher toughness and residual strengths than the samples w/ PP fibers (Table 5.16 and Table 5.17). The *VHES-800 w/ SF* and *S fibers* specimens had on average 65% higher toughness and residual strength values than the samples with *VHES-800 w/ SF* and *PP fibers*. However, the PP and S fibers from the *VHES-850 w/ SF* batch performed similarly, with only 8% difference on average. This could potentially be attributed to an ineffective S fiber distribution and alignment in the beam.

**Table 5.16: 28-Day Trial VHES-800 w/ SF Hardened Properties**

Test	Age	VHES-800 w/ SF		
		Plain Concrete	w/ PP	w/ S
Elastic Modulus [ $10^6$ psi]	28 days	4.12	4.08	4.49
Permeability [C]	28 days	922	598	-
First-Peak / Peak flexural strength [psi]	7 - 7.5 hours	460	420 / 460	400 / 500
	7 days	905	1,040	990
	28 days	1,030	1,120	1,095
Toughness, $T_{150}^D$ [in.-lb]	28 days	0	250	410
Residual Strength, $f_{600}^D / f_{150}^D$ [psi]	28 days	0	455 / 675	890 / 1020
Equivalent Flexural Strength Ratio, $R_{T, 150}^D$ [%]	28 days	0	53	88

**Table 5.17: 28-Day Trial VHES-850 w/ SF Hardened Properties**

Test	Age	VHES-850 w/ SF		
		Plain Concrete	w/ PP	w/ S
Elastic Modulus [ $10^6$ psi]	28 days	4.04	3.85	4.16
Permeability [C]	28 days	848	913	-
First-Peak / Peak flexural strength [psi]	24 hours	555	625	735 / 835
	7 days	915	990	1,010
	28 days	1,030	1,040	1,060
Toughness, $T_{150}^D$ [in.-lb]	28 days	0	280	310
Residual Strength, $f_{600}^D / f_{150}^D$ [psi]	28 days	0	560 / 740	820 / 535
Equivalent Flexural Strength Ratio, $R_{T, 150}^D$ [%]	28 days	0	64	68

Furthermore, the drying shrinkage tests were performed. No significant difference in shrinkage results was observed. The plain concrete samples exhibited about 0.064% of length change in 4 months, whereas the samples with PP and S fibers in 4 months displayed on average 0.060% of length change.

### 5.2.3 Final VHES-FRC w/ SF and VHES-FRC w/ FA Lab Batches

The last step of this stage after the exploratory work was to select optimal plain concrete mixtures, and add PP and S fibers. As it was indicated in the methods section, the amount of steel fibers was increased to 0.60% by volume to improve the post-cracking performance. No significant

difference in flexural results was observed between the PP fiber volume contents of 1.20% and 1.00%. Hence, 1.00% by volume of PP fibers was used to facilitate mixing procedures and better fiber dispersion. In addition, the amount of hardening accelerating admixture was reduced from 30 oz/cwt to 20 oz/cwt to save on the total mixture cost. Hence, some acceptable reduction of the early age strength was expected. The fresh concrete properties are presented in Table 5.18. Higher fresh concrete mix temperatures of 85-95°F on average were used. The air contents of 5.7% on average were within the specifications. Due to high heat generation, the slump values were low, ranging from 2 in. to 5 in. However, the mixes were still workable enough to be placed in the molds.

**Table 5.18: Final Lab VHES-FRCs Fresh Concrete Properties**

Properties	VHES-FRC w/ SF		VHES-FRC w/ FA	
	w/ PP	w/ S	w/ PP	w/ S
Air Content [%]	5.5	5.9	5	6.4
Unit Weight [lbs/ft <sup>3</sup> ]	145	148	148	149
Slump [in]	4	5	2	3
Mix Temperature [°F]	85	90	97	94
Air Temperature [°F]	75	75	75	75
Relative Humidity [%]	37	37	45	50

The temperature developments of four batches: *VHES-FRC w/ SF* and PP or S fibers and *VHES-FRC w/ FA* and PP or S fibers are shown in Figure 5.11. The graphs display that the set time and strength gain of the *VHES-FRC w/ SF* mixtures was about one hour slower than of the *VHES-FRC w/ FA* mixtures due to the difference in initial fresh concrete temperatures. These results were confirmed by the compressive strength testing (Table 5.19). The *VHES-FRC w/ SF* specimens reached 3,000 psi compressive strength within 8-8.5 hours, whereas the *VHES-FC w/ FA* specimens reached 3,000 psi within 7.5-8 hours.

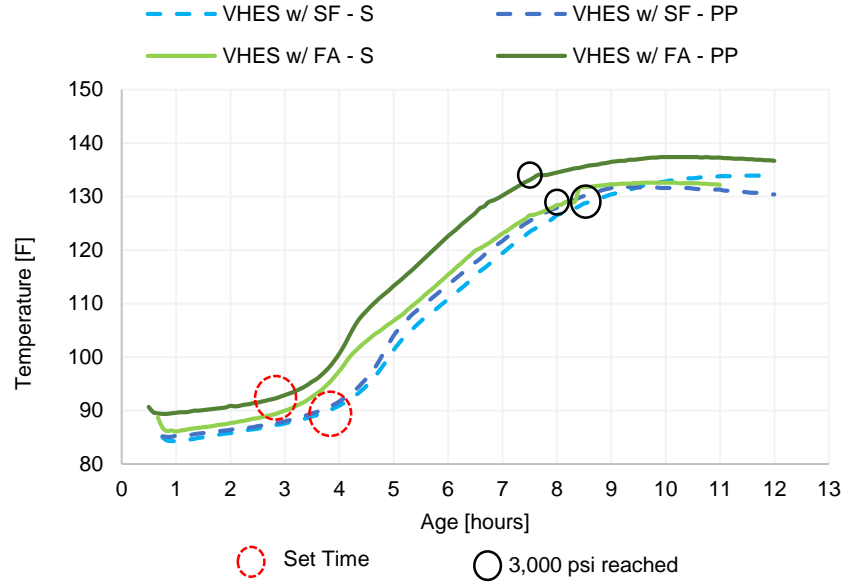


**Figure 5.11: Temperature developments of the final lab VHES-FRCs with PP and S fibers**

Flexural load-deflection plots of the final lab VHES-FRCs mixtures are presented in Figure 5.12 and Figure 5.13. The increase in first-peak and residual flexural strengths with age can be observed. The first flexural specimens were tested at the time 3,000 psi compressive strength was reached. The *VHES-FRCs w/ SF* beams were tested at 8.5 hours and reached a first-peak flexural strength of 490 and 460 psi for PP and S fiber samples, respectively. The *VHES-FRC w/ FA* beam specimens were tested at 7.5 and 8 hours, resulting in first-peak flexural strength of 375 and 465 psi for PP and S fiber samples, respectively. These values exceed the flexural strength requirement of 350 psi from the NJDOT study on VES concretes, previously discussed in the literature review (Punurai et al. 2007). Furthermore, the obtained flexural strength values meet the strength requirements of 260 to 400 psi reported in the NCHRP study (Van Dam et al. 2005) for the 6 to 8-hour concrete repair materials. Table 5.20 contains flexural strength values for all test ages.

**Table 5.19: Final Lab VHES-FRCs Compressive Strength Results**

Age	VHES-FRC w/ SF		VHES-FRC w/ FA	
	w/ PP	w/ S	w/ PP	w/ S
6.5 hours	1,890	950	2,930	2,540
7.5 hours	2,530	2,780	<b>3,860</b>	2,840
8 hours	-	-	-	<b>3,160</b>
8.5 hours	<b>4,150</b>	<b>3,220</b>	-	-
24 hours	6,700	7,540	5,240	4,380
7 Days	7,730	7,880	7,260	5,690
28 Days	8,780	8,880	8,860	8,890
28-day Elastic Modulus [ $10^6$ psi]	4.82	5.17	4.13	3.92

**Table 5.20: Final Lab VHES-FRCs Flexural Results versus Age**

Age	VHES-FRC w/ SF		VHES-FRC w/ FA	
	w/ PP	w/ S	w/ PP	w/ S
7.5-8.5 hours	490	460 / 620	375	465 / 475
24 hours	690	715 / 1,030	660	665 / 1,135
7 Days	985	1,000	985	1,010 / 1,090
28 Days	1,075	1,100 / 1,380	1,095	1,115 / 1,290

For both, SF and FA VHES-FRCs mixtures, *VHES-FRCs w/ S* fibers exhibited significantly better post-cracking performance than the *VHES-FRCs w/ PP* fibers, with displayed deflection hardening behavior and higher residual strength and toughness values.

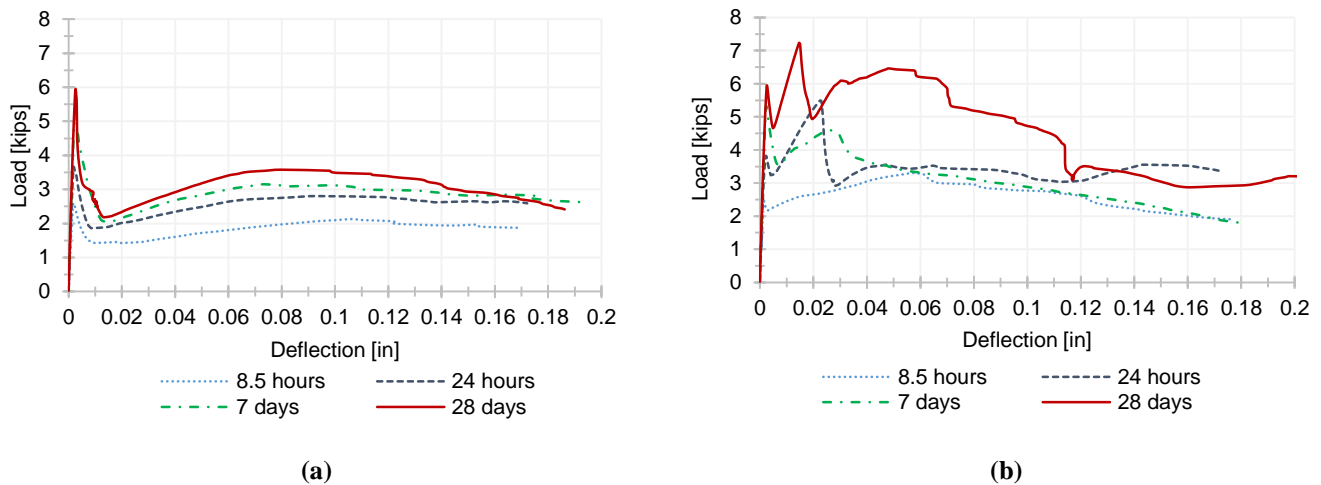


**Figure 5.12: VHES-FRCs w/ SF (a) w/ PP Fibers (b) w/ S fibers**

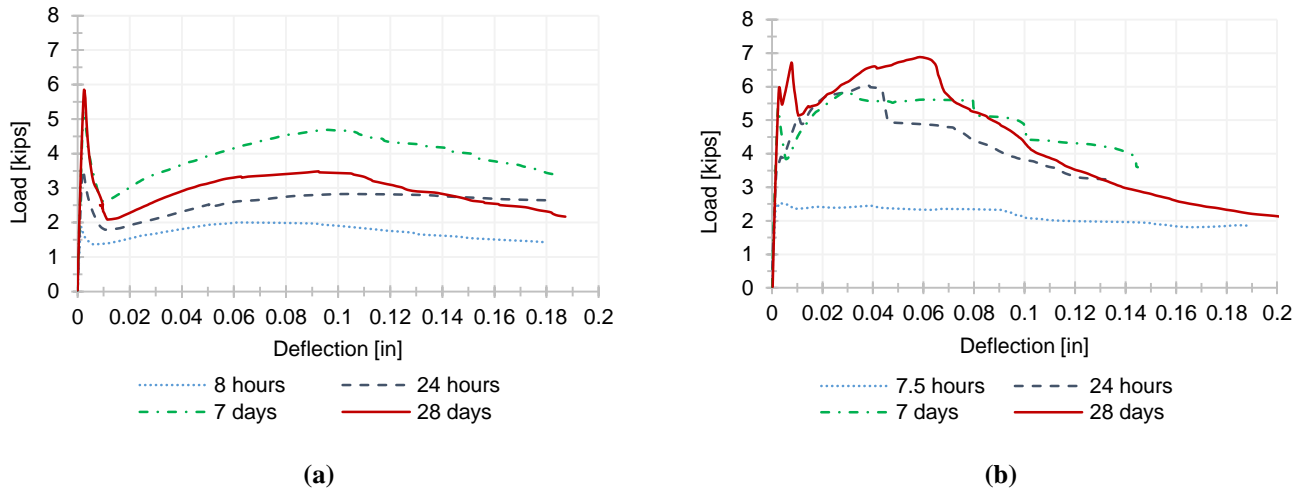


**Figure 5.13: VHES-FRCs w/ FA (a) w/ PP Fibers (b) w/ S fibers**

The beam specimens with S fibers displayed deflection hardening behavior and high residual strengths. Whereas the samples with PP fibers exhibited no deflection hardening, but still produced substantial residual strengths. Toughness at L/150 deflection value was almost doubled for the S fiber samples compared to the samples with PP fibers (Table 5.21).

**Table 5.21: Final Lab VHES-FRCs 28-day Flexural Results**

Test	VHES-FRC w/ SF		VHES-FRC w/ FA	
	w/ PP	w/ S	w/ PP	w/ S
First-Peak / Peak flexural strength [psi]	1075	1100 / 1380	1095	1115 / 1290
Toughness, $T_{150}^D$ [in.-lb]	230	450	220	430
Residual Strength, $f_{600}^D / f_{150}^D$ [psi]	430 / 640	1160 / 860	405 / 570	1040 / 910
Equivalent Flexural Strength Ratio, $R_{T, 150}^D$ [%]	51	96	46	90
$I_5$	3	4	3	4
$I_{10}$	5	8	5	8
$I_{20}$	9	17	8	17
$R_{5,10}$	36	87	42	74
$R_{10,20}$	38	89	27	88

Similar trends can be observed for the residual strength, equivalent flexural strength ratio and toughness indices values. The flexural capacity of the *VHES-FRCs* w/ S fibers was 93% on average

after the first-peak crack, whereas the capacity of *VHES-FRCs w/ PP* fibers was about 49% on average.

Figure 5.14 demonstrates the drying shrinkage values for both *VHES-FRCs* types. At 4 months, *VHES-FRCs w/ FA* exhibited length change values up to 0.074% on average and *VHES-FRCs w/ SF* – 0.065% on average. The values are close to the suggested limit of 0.07% at 4 months. However, the paste contents of 0.32 and 0.33 for *VHES-FRCs w/ SF* and *w/ FA*, respectively, exceed the recommended 0.27 paste content limit (Darwin et al. 2004). High cement contents of 750 lb/yd<sup>3</sup> for both batches and increased fresh concrete temperatures detrimentally affected the shrinkage performance of the concrete.

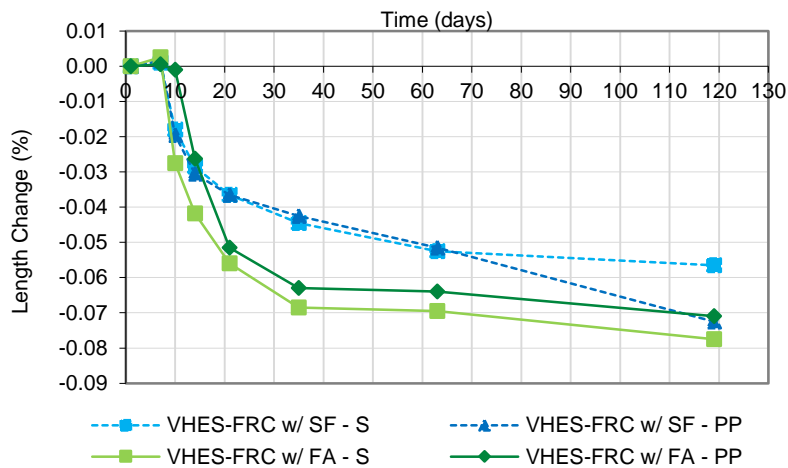


**Figure 5.14: Final Lab VHES-FRCs Drying Shrinkage Results**

### 5.3 Stage III – Permeability of Cracked Samples

The third stage of this research was focused on the permeability testing of the cracked FRC samples. Crack widths of 0.1 to 0.7 mm were formed, and falling head permeability test was performed. In this section, the results of the used methods are explained and analyzed. Comparison

between the collected laser and magnifier data was performed. The crack relaxation after unloading is presented for the HES-FRC w/ PP or S fiber and for the VHES-FRC w/ PP or S fiber systems. Average coefficients of water permeability were calculated for each crack width. The comparison of the obtained and standard values for solid specimens was performed.

### 5.3.1 Splitting Tensile Testing and Crack Formation Analysis

A total of 66 samples was tested to analyze the permeability of cracked FRC samples. The crack widths of 0.1 mm to 0.7 mm (0.004 in. to 0.027 in.) under load were formed. As it was indicated in the methods chapter, the samples were loaded about 0.1 - 0.2 mm of additional crack width displacement in order to achieve the desired crack width after unloading and crack relaxation. In this section the crack dimensions will be discussed in the metric system for convenience. Figure 5.15 displays the load vs laser displacement plots for different crack widths under load.

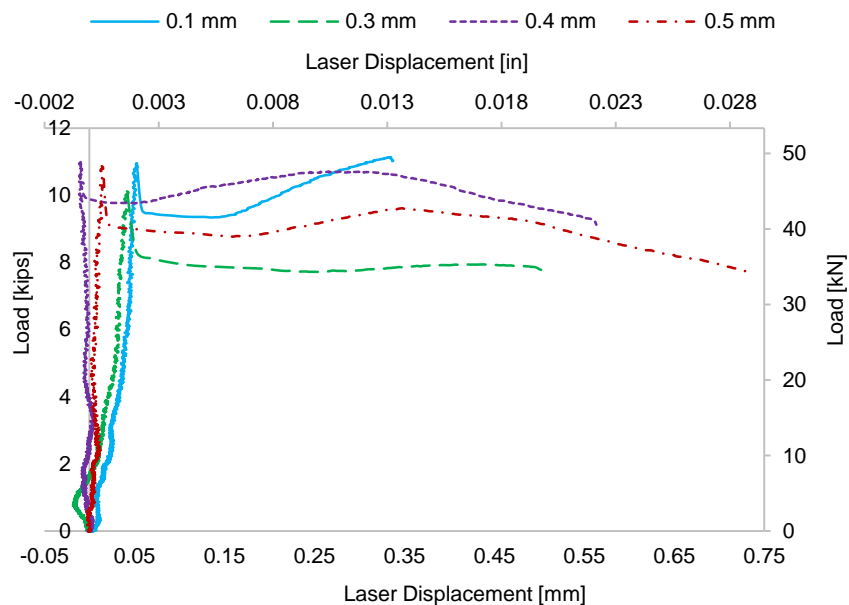


**Figure 5.15: Load versus Laser Displacement Plots for Various Crack Widths (Example)**

The laser displacement indicates the change in distance between the two reflective tapes at the center of the specimen (see Figure 4.9 (a) for reference). The plots demonstrate the laser displacement (crack widths) under load, whereas the legend shows the final crack width after unloading and relaxation. Prior to the first crack the laser was registering a *noise* displacement and did not correspond to the crack width. After the first crack, the laser displacement was representative of the crack width displacement. Hence, the true laser displacement was calculated starting from the first crack peak. After the load was released at maximum laser displacement, and the crack had relaxed, the crack width indicated by the legend in Figure 5.15 occurred. For example, when the maximum displacement was 0.75 mm (indicating a crack width of 0.75 mm at the center of the specimen), upon unloading and crack relaxation the crack width of 0.5 mm was obtained for that specific sample. During the splitting tensile testing the crack would start forming in the center of the sample, extending to the edges with further load applied. The crack widths were measured at the top, middle and bottom section on both sides of the sample. The crack width that was observed the most was used as a final crack width of that sample.

The laser system and magnifier with a scale were utilized for crack measurements. Figure 5.16 shows the correlation between the two measurement methods, with the difference just a little over 10% on average. This difference was deemed to be acceptable due to the irregularity of the crack width and crack patterns.

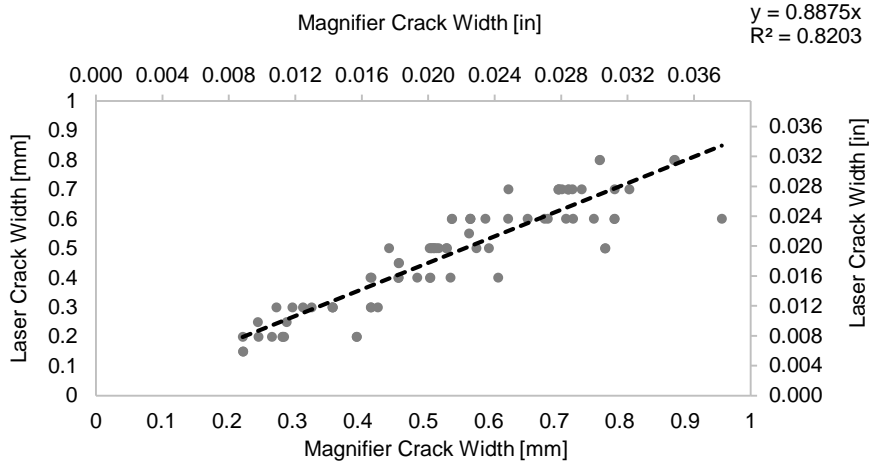


**Figure 5.16: Laser Crack Width versus Magnifier Crack Width Under Load**

Figure 5.17 displays the crack width recovery after unloading. The solid black line represents theoretical no recovery values. The HES-FRCs and VHES-FRCs followed the same trend of recovery, and on average all samples recovered over 43% of the crack width.

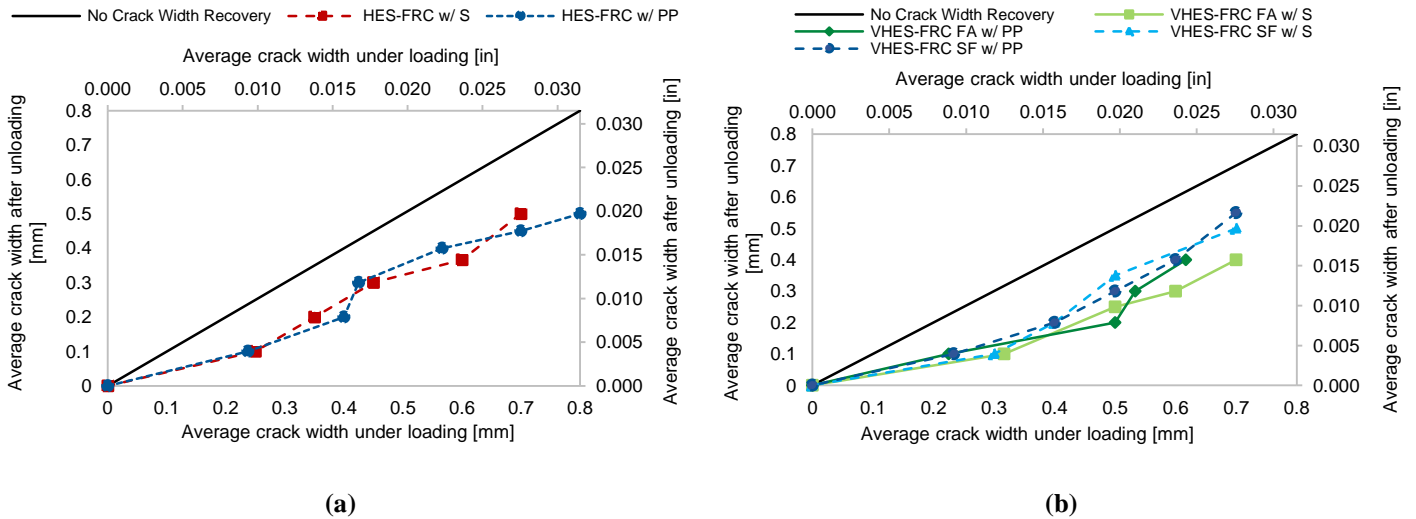


**Figure 5.17: Average Crack Width Recovery After Unloading (a) HES-FRCs (b) VHES-FRCs**

### 5.3.2 Coefficient of Water Permeability

The coefficient of water permeability (CWP) was calculated using the Equation 4.6, defined in the methods chapter. Figure 5.18 (a) and (b) show the permeability results for HES-FRCs and VHES-FRCs, respectively. The CWP values approximately follow the same trend for all samples, and the observed variation could be due to the irregularity of crack size and pattern.

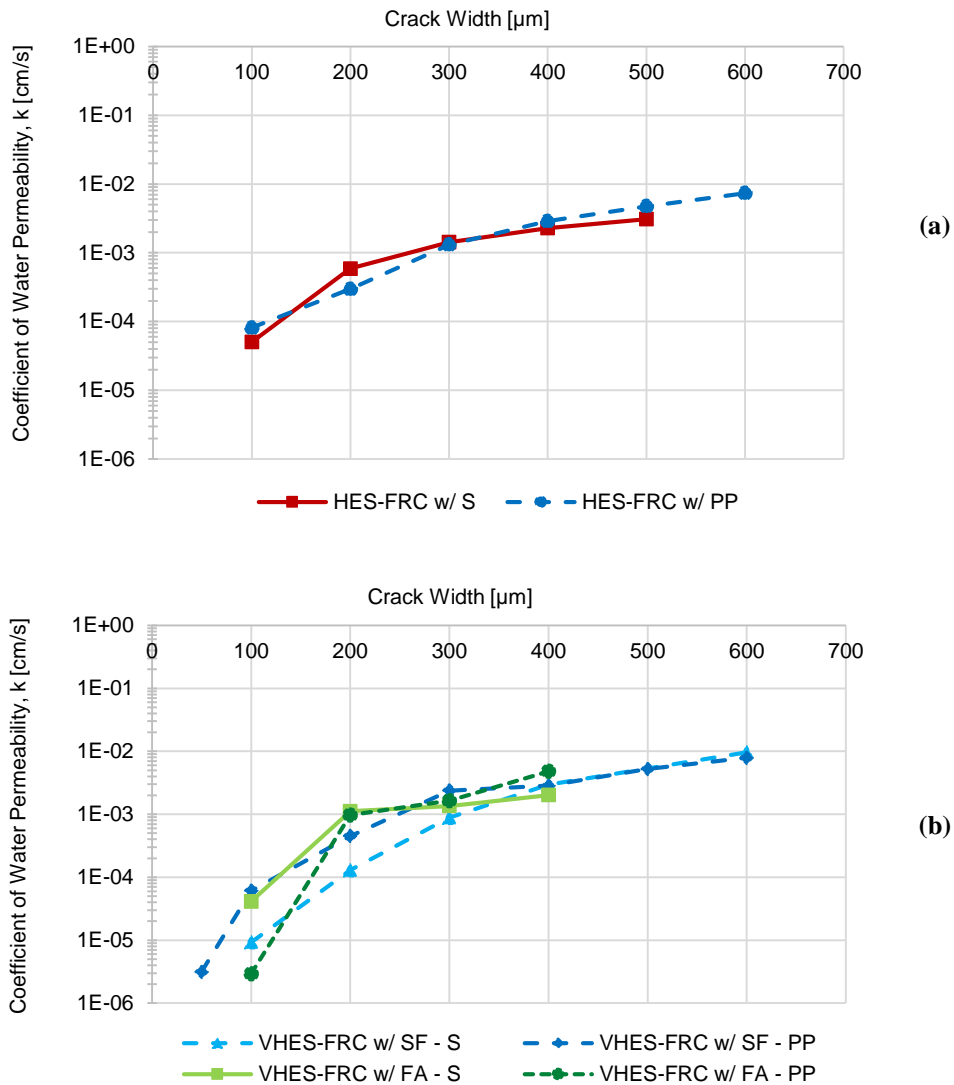


**Figure 5.18: Coefficient of Water Permeability versus Crack Width (a) HES-FRCs (b) VHES-FRCs**  
 Conversion factors:  $0.1 \text{ mm} = 100 \mu\text{m} = 0.0039 \text{ in}$ .

This means that the crack width was the controlling factor, and not the FRC material or fiber type. A significant increase in the CWP for smaller crack widths can be observed. For VHES-FRC samples the increase of CWP by 20 times on average was observed for crack widths increasing from 100  $\mu\text{m}$  to 200  $\mu\text{m}$ . The sample VHES-FRC w/ FA and PP fibers exhibited an increase of over 300 times. CWP growth of HES-FRC was less pronounced. For crack widths larger than 300  $\mu\text{m}$  the CWP growth was significantly less rapid.

Typical values of the CWP for normal strength and high strength concretes are about  $10^{-10}$  cm/s and less than  $10^{-14}$  cm/s, respectively (Nawy, 2001). The obtained CWP values were on the order of  $10^{-10}$  cm/s for the solid specimens without cracks, above  $10^{-6}$  to  $10^{-5}$  cm/s for crack widths greater than 100  $\mu\text{m}$ , and above  $10^{-3}$  cm/s for cracks greater than 200  $\mu\text{m}$ . In this case, the corrosion of primary reinforcement due to leakage through cracks widths greater than 100  $\mu\text{m}$  is highly probable.

In addition, the comparison of results with the literature review was performed. The threshold of 50-100  $\mu\text{m}$  crack widths was not observed in this case. However, the data comparison between the different literature review studies showed similar trends, but did not have an adequate correlation. The crack formation process, and highly irregular crack widths were most likely the cause. Additional testing with slower loading rates, forming crack widths less than 100  $\mu\text{m}$  is recommended.

#### 5.4 Stage IV – Fiber Distribution Analysis

The last stage of the project was focused on the analysis of fiber distribution. Fiber density (number of fibers per unit area) and spatial fiber dispersion were examined. Two cutting methods were utilized for the steel fiber samples, *HTH* and *THTHT*, where *H* is a cross-section cut in the horizontal direction along the length of the beam, and *T* is a transverse direction cut perpendicular to length of the beam (see Figure 4.14 for reference). The two cutting methods allowed for a more complete fiber distribution analysis. As it was indicated in the methods chapter, only fibers oriented up to  $45^\circ$  were included in the fiber count. MATLAB was used for the image analysis processing. If improper objects (aggregates, voids and etc.) were included in the count by the code, their coordinates were removed manually from the data file. On the other hand, if the fibers were missed by the MATLAB code, then the coordinates were entered manually to ensure a proper fiber count.

Figure 5.19 displays the step outputs of the MATLAB image analysis processing code and the final image with overlaid fiber coordinates. The brief code summary was presented previously in the methods chapter, and the full code is included in the Appendix.



**Figure 5.19: Steel Fiber Cross-Section Image Analysis**

Figure 5.20 displays the average steel fiber density for transverse and horizontal cross-sections for two cutting methods. It can be observed that the steel fibers had a tendency to align parallel

along the length of the beam in transverse direction. This alignment is beneficial to the flexural and tensile capacities of the specimens, due to greater number of fibers at the beam crack face effectively resisting the applied stresses. The fiber preferential alignment could be due to the beam size and the casting methods.

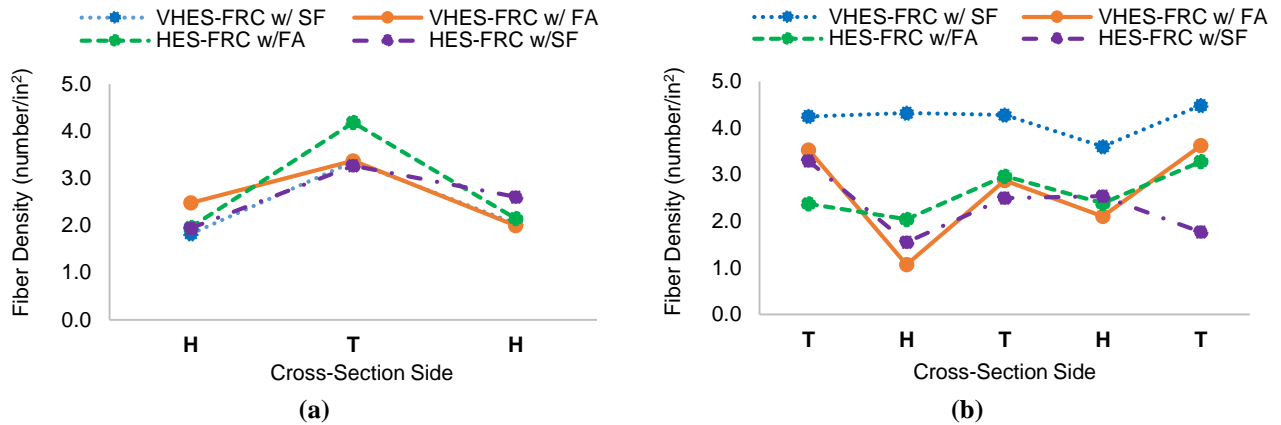
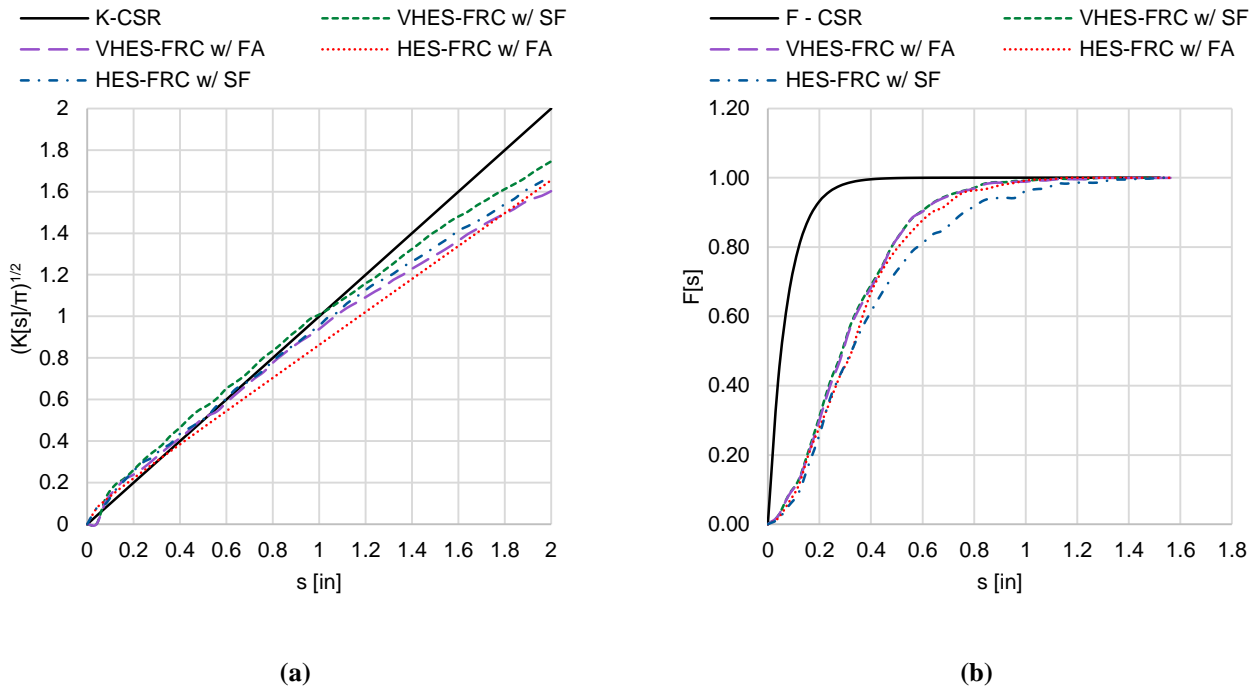


Figure 5.20: Steel Fiber Density per Cross-Section Side (a) HTH (b) THTHT

In addition, statistical spatial point pattern analysis was performed to examine fiber distribution. Spatial dispersion of steel fibers was analyzed on both sides of the crack and average results are presented. The calculated K-function and F-function values were compared to the theoretical CSR values. Figure 5.21 (a) displays average  $\left(\frac{K[s]}{\pi}\right)^{1/2}$  results for the cross-sections at the crack location for the FRC samples with S fibers. The results of the F-function are presented in Figure 5.21 (b). The closer the calculated values to the theoretical  $\left(\frac{K[s]}{\pi}\right)^{1/2}$  under the CSR condition (solid, black line), the more random the distribution. The *VHES-FRC w/ SF* samples displayed the most fiber clumping compared to the rest of the samples at small  $s$  distances up to about 1 in. Whereas, the *HES-FRC w/ FA* samples exhibited the least tendency of fiber clumping.

The *VHES-FRC w/ FA* and *HES-FRC w/ SF* samples at smaller  $s$  distances displayed values close to the CSR values, indicating more of a random distribution.



**Figure 5.21: Spatial Steel Fiber Distribution Analysis (a)  $(K[s]/\pi)^{1/2}$  (b) F - function**

The closer the slopes of the calculated F-functions to the slope under the CSR condition (solid, black line), the more random the distribution of fibers. Hence, from the graphs it is apparent that all samples displayed some degree of fiber clumping and more empty areas without fibers, with the slopes less steep than the F-CSR slope. The specimen with HES-FRC w/ SF and 0.50% of S fibers by volume displayed more fiber-free areas compare to the rest of the samples with 0.60% of S fibers by volume.

#### 5.4.1 FRC Cross-Sections with Polypropylene Fibers

The image processing of the cross-sections with PP fibers was more complicated and time consuming due to fiber size, form and appearance. Hence, only one beam, cut with *HTH* configuration, from each batch was studied (see Figure 4.13 and Figure 4.14 for reference). Figure 5.22 shows the step outputs of the MATLAB image analysis processing code for the cross-sections with PP fibers.

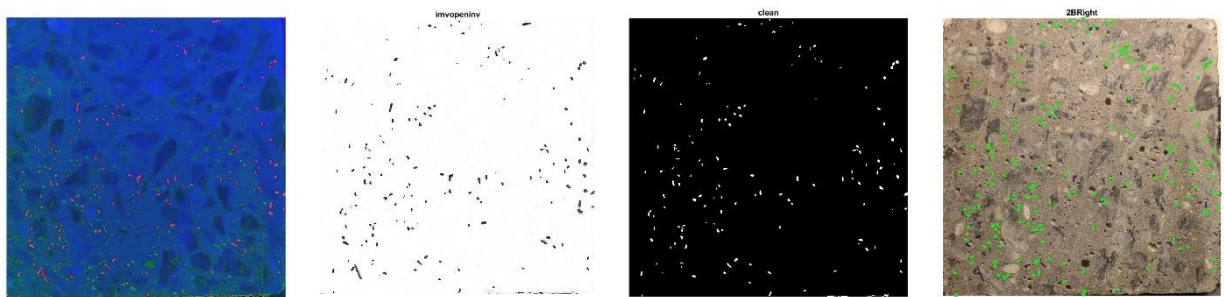


**Figure 5.22: PP Fiber Cross-Section Image Analysis Processing**

Fiber density of samples with PP fibers is shown in Figure 5.23. It can be observed that the alignment in transverse direction is less pronounced compare to the S fiber samples. In this case, the fibers were more evenly aligned and equally distributed in both, transverse and horizontal directions. This could be due to the smaller fiber length of 2 in. and the flexibility of the synthetic fibers. Figure 5.24 displays the results of  $\left(\frac{K[S]}{\pi}\right)^{1/2}$  function (a) and F-function (b). The HES-FRC w/ 1.0% of PP fibers by volume indicated more fiber clumping tendency and more fiber-free areas compare to the other samples. This could be explained by observed mixing issues and balling during the placement of the first field batch with PP fibers.

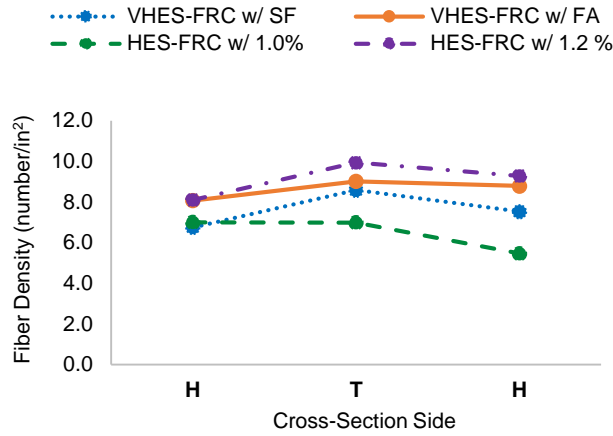


**Figure 5.23: PP Fiber Density per Cross-Section Side (HTH)**

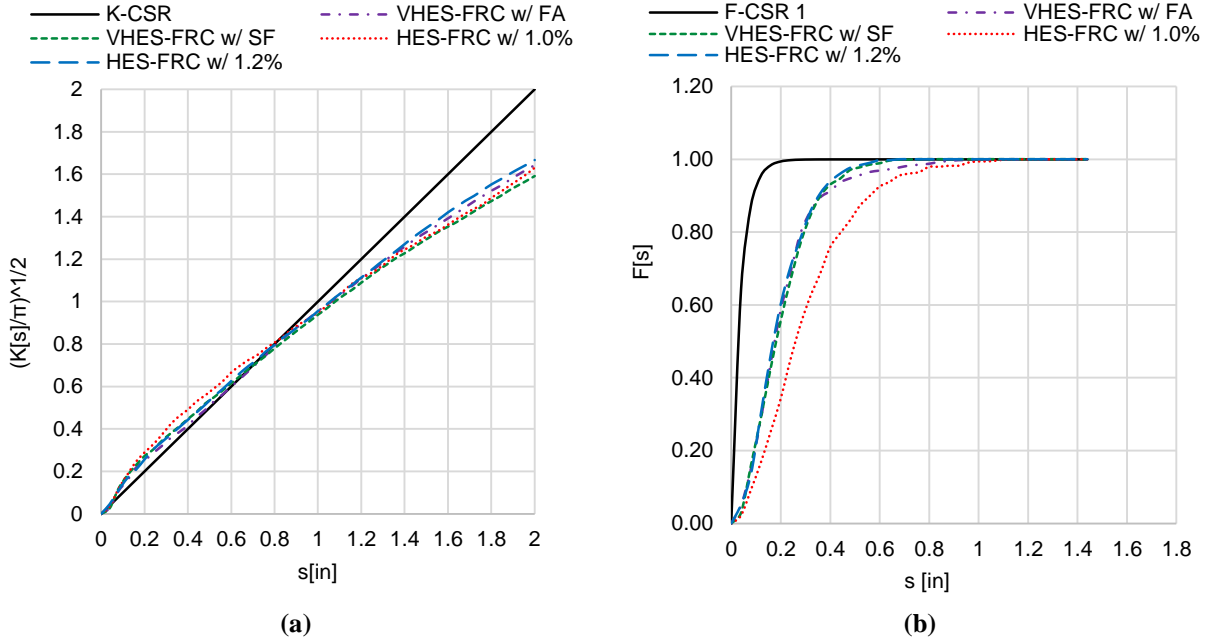


**Figure 5.24: Spatial PP Fiber Distribution Analysis (a)  $(K[s]/\pi)^{1/2}$  (b) F – function**

The improvement in fiber dispersion for the second HES-FRC batch and VHES-FRCs batches after the modification of the mixing procedure can be observed. For the specimens with VHES-FRCs and HES-FRC w/ 1.2% of PP fibers by volume, the fibers were added in the beginning of the mixing with aggregates and water to facilitate better fiber distribution.

A comparison between specimens with S and PP fibers was performed for the two VHES-FRC batches with SF and FA (Figure 5.25). The base concrete mixture designs were the same, except for the fiber type and volume content. The K-function displayed the same degree of clumping tendency for both systems.

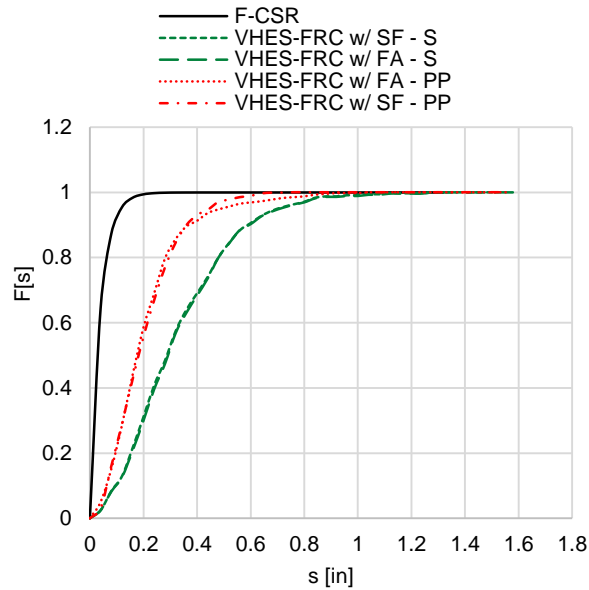


**Figure 5.25: F-function comparison between S and PP fiber cross-sections**

The F-function demonstrated a more pronounced difference, with samples with PP fibers having a significantly steeper slope compare to the S fiber samples. This indicates that there are less fiber-free areas in PP specimens than in the S fiber specimens. This could be explained by a greater volume content of PP fibers and the flexibility of synthetic fibers. In addition, due to a smaller diameter size of PP fibers, the calculated function values were less impacted by the edge effects.

## **6.0 - CONCLUSIONS**

The research objectives for this project were to develop durable, high early strength concretes with controlled cracking that would facilitate rapid and effective repairs, reducing traffic interruptions and decreasing long-term maintenance costs. This project focused on the concretes that can achieve high early compressive and flexural strengths within 24 and 10 hours. The addition of different types of SCMs contributed to the durability enhancement. In addition to high early strength, various amounts and types of fibers were considered to evaluate the post-cracking performance and cracking resistance of the developed FRCs. Furthermore, other concrete characteristics as toughness, residual strengths, permeability of cracked concrete and fiber distribution were examined. The results of this study showed that the HES-FRCs and VHES-FRCs are promising technologies that may satisfy the rapid construction and durability requirements for improvement of service life of structures.

### ***6.1 Stage I***

The designed HES-FRCs mixtures reached the required compressive strength of 3,000 psi within the desired time of 24 hours. The increased cement amounts, low w/cm ratios, increased fresh concrete temperatures above 80 °F and addition of accelerating admixtures facilitated the strength gain at early ages. All systems displayed low permeability values below the 1500 C limit. The HES-FRCs exhibited improved post-cracking performance, with high ductility, toughness and residual strengths. The HES-ECC and HES-FRC w/ S fibers at 0.60% by volume exhibited deflection hardening behavior, beneficial to maintaining tight cracks widths.

- HES-ECC

The HES-ECC demonstrated self-consolidating characteristics, facilitating mixing and placing. The mix is highly suitable for placement in narrow or congested sections of structural elements. The HES-ECC exhibited significant deflection hardening behavior, with the average increase in peak flexural strength by over 60% after the first-peak. Average toughness values of 400 in.-lb and equivalent flexural strength ratios of over 120 % were determined. Due to high paste content of 0.83 and water content of 570 lb/yd<sup>3</sup>, the HES-ECC displayed significant shrinkage of over 0.16% in 4 months, a double of the suggested limit. Hence, the visual survey in the field revealed gaps between the closure pours and overlays. Still, due to high volume dosage of PVA fibers the HES-ECC closure pour exhibited multiple tight cracks of 0.1 mm in width, with few cracks up to 0.2 mm.

- HES-FRCs w/ PP Fibers

Two batches were made for the HES-FRC w/ PP fibers with 1.0% and 1.2% of PP fibers by volume, respectively. The mixtures were significantly less workable than the HES-ECC, and displayed mixing issues and fiber balling. No significant difference in compressive or flexural strength results was observed between the two batches. A 0.2% increase of PP fibers by volume did not influence the post-cracking performance of the second batch. Both batches did not exhibit deflection hardening behavior, but had residual flexural strength capacity of about 59% on average after the first-peak. Similar to the other HES-FRCs systems, the visual survey indicated gaps between the HES-FRC w/ PP fiber closure pours and overlays due to increased shrinkage.

However, the closure pours exhibited very few tight (up to 0.1 mm in width) or no cracks due to high fiber dosages and the presence of primary reinforcement.

- HES-FRCs w/ S Fibers

Two batches were made with the HES-FRC w/ S fibers: one with 20% of fly ash and 0.60% of S fibers by volume, and one with 7% silica fume and 0.50% of S fibers by volume. The mixtures were less workable than the HES-ECC mixture, however no mixing or placing issues were observed. The first batch exhibited deflection hardening behavior followed by deflection softening, with the increase in flexural strength by 20% on average after the first-peak. Whereas, the second batch did not display deflection hardening behavior. In addition, higher toughness and residual capacity values were observed for the first mix with 0.60% of fibers by volume compared to the second batch. The batch with silica fume exhibited overall higher compressive and first-peak flexural strengths compared to the first batch with fly ash, by about 3% and 12%, respectively. The addition of silica fume had a more substantial impact on the early- and long-term strength developments. Gaps were observed for all closure pours with HES-FRCs w/ S fibers. Higher paste content contributed to the increased shrinkage. The mixture with fly ash exhibited shrinkage of 0.09% in 4 months, whereas the batch with silica fume displayed lower shrinkage values of 0.06% at 4 months. Visual survey of closure pours revealed minor cracking, with both batches displaying very few tight (up to 0.1 mm in width) or no cracks.

For all HES-FRCs systems the combination of primary reinforcement and fibers contributed to the improved cracking control, despite of the values of paste content and drying shrinkage being above the suggested limits.

## 6.2 Stage II

The VHES-FRCs mixtures reached the required compressive strength of 3,000 psi within 8.5 hours. The increased cement amounts, reduced w/cm ratios, increased fresh concrete temperature of 85-95°F, increased amounts of accelerating admixtures and the use of insulated curing significantly contributed to the early-age strength development. In addition, the type of accelerating admixtures was important. Accelerating admixtures that reduce concrete setting time and increase the strength gain after the set are necessary for achieving high concrete strengths at early age. The *VHES-FRCs w/ S fibers* post-cracking performance was substantially superior to the *VHES-FRCs w/ PP fibers*, exhibiting toughness and residual strength values almost double of the samples with PP fibers.

- VHES-FRCs w/ S fibers

Due to lower fresh concrete temperature and higher w/cm ratio the batch with silica fume reached the 3,000 psi compressive strength about half an hour later (at 8.5 hours) than the batch with fly ash. However, both batches exhibited similar flexural strength development, with deflection hardening behavior after the first-peak, followed by deflection softening. The values of toughness and flexural capacity after the first-peak were comparable, with less than 6% difference between the two batches. The silica fume batch displayed the least shrinkage, with a value of 0.06% at 4 months compared to the fly ash batch with a value of 0.08% at 4 months. The lower water and paste contents contributed to the improved shrinkage performance over the *Stage I HES* mixtures.

- VHES-FRCs w/ PP fibers

The batches with PP fibers exhibited higher compressive strength development compare to the batches with S fibers. The batch with silica fume reached over 4,000 psi compressive strength in 8.5 hours, whereas the batch with fly ash reached over 3,800 psi in compression in 7.5 hours. Both batches exhibited no deflection hardening behavior, with the residual flexural strength capacity after the first-peak of about 49% on average. The values of drying shrinkage in 4 months were about 0.07% for both batches, at the suggested limit of 0.07%.

The benefits and drawbacks of the addition of silica fume or fly ash materials to the concrete mixture are summarized in Table 6.1. Whereas, Table 6.2 presents a summary of the advantages and disadvantages of the final developed HES-FRCs and VHES-FRCs mixtures for each fiber type. Depending on the project needs and the importance of specific mixture properties, the tables could be used to select a suitable material.

**Table 6.1: Advantages and Disadvantages of the SCMs addition**

SCMs	Advantages	Disadvantages
Silica Fume	<ul style="list-style-type: none"> <li>• Small substitution amounts (7%)</li> <li>• Does not retard early strength development</li> </ul>	<ul style="list-style-type: none"> <li>• Increases water demand</li> <li>• Reduces workability</li> <li>• Expensive</li> </ul>
Fly Ash	<ul style="list-style-type: none"> <li>• Reduces water demand</li> <li>• Facilitates workability</li> <li>• Cost-effective</li> </ul>	<ul style="list-style-type: none"> <li>• Large substitution amounts (15-20%)</li> <li>• Retards early strength development</li> </ul>

**Table 6.2: Advantages and Disadvantages of the HES-FRCs and VHES-FRCs**

Mixture Type	Fiber Type and Dosage	Advantages	Disadvantages
<i>High early strength 24-hour FRC mixtures</i>			
HES-ECC	<b>Polyvinyl Alcohol:</b> 44 lb/yd <sup>3</sup> (2.0% by vol.)	<ul style="list-style-type: none"> <li>• Self-consolidating</li> <li>• Deflection hardening</li> <li>• High toughness and residual flexural capacity</li> <li>• Multiple tight cracks</li> <li>• Non-corrosive</li> </ul>	<ul style="list-style-type: none"> <li>• Displayed the highest shrinkage (~ 0.16%)</li> <li>• Most expensive out of all developed systems</li> </ul>
HES-FRCs	<b>Polypropylene:</b> 15 - 18 lb/yd <sup>3</sup> (1.0-1.2% by vol.)	<ul style="list-style-type: none"> <li>• Non-corrosive</li> <li>• Provides residual strength and toughness</li> <li>• Least expensive</li> </ul>	<ul style="list-style-type: none"> <li>• No deflection hardening</li> <li>• Displayed high shrinkage (~ 0.09%)</li> <li>• Workability and balling issues</li> </ul>
HES-FRCs	<b>Steel:</b> 80 lb/yd <sup>3</sup> (0.6% by vol.)	<ul style="list-style-type: none"> <li>• Deflection hardening</li> <li>• High toughness and residual flexural capacity</li> <li>• No workability or balling issues</li> </ul>	<ul style="list-style-type: none"> <li>• Surface fiber corrosion</li> <li>• Displayed high shrinkage (~ 0.09%)</li> <li>• Second most expensive</li> </ul>
	<b>Steel:</b> 66 lb/yd <sup>3</sup> (0.5% by vol.)	<ul style="list-style-type: none"> <li>• Provides residual strength and toughness</li> <li>• No workability or balling issues</li> <li>• Displayed the least shrinkage (~ 0.06%)</li> </ul>	<ul style="list-style-type: none"> <li>• No deflection hardening</li> <li>• Surface fiber corrosion</li> <li>• Second most expensive</li> </ul>
<i>Very high early strength 10-hour FRC mixtures</i>			
VHES-FRCs	<b>Polypropylene:</b> 15 lb/yd <sup>3</sup> (1.0% by vol.)	<ul style="list-style-type: none"> <li>• Non-corrosive</li> <li>• Provides residual strength and toughness</li> <li>• Least expensive</li> <li>• Displayed shrinkage (~ 0.07%)</li> </ul>	<ul style="list-style-type: none"> <li>• No deflection hardening</li> <li>• Workability and balling issues</li> </ul>
VHES-FRCs	<b>Steel:</b> 80 lb/yd <sup>3</sup> (0.6% by vol.)	<ul style="list-style-type: none"> <li>• Deflection hardening</li> <li>• High toughness and residual flexural capacity</li> <li>• No workability or balling issues</li> <li>• Displayed the least shrinkage (SF ~ 0.06%; FA ~ 0.08%)</li> </ul>	<ul style="list-style-type: none"> <li>• Surface fiber corrosion</li> <li>• Second most expensive</li> </ul>

### ***6.3 Stage III***

The results of the permeability of cracked VHES-FRC specimens demonstrated an increase of CWP by 20 times on average for crack widths increasing from 100  $\mu\text{m}$  to 200  $\mu\text{m}$ . The CWP growth of HES-FRC was less pronounced. For crack widths larger than 300  $\mu\text{m}$  the CWP rise was high but significantly less rapid. The CWP values for solid specimens without cracks were on the same order as that given in the literature for solid specimens of conventional concrete, about  $10^{-10}$  cm/s. However, the calculated CWP values were above  $10^{-6}$  cm/s for crack widths between 100 and 200  $\mu\text{m}$ , which are significantly higher than the typical values for solid samples for normal strength and high strength concretes. Thus, there is a high risk of corrosion of primary reinforcement and steel fibers due to leakage through crack widths above 100  $\mu\text{m}$ .

### ***6.4 Stage IV***

The fiber distribution analysis demonstrated that the steel fibers had a tendency to align parallel along the length of the beam, which is beneficial to the flexural and tensile capacities of the specimens. The PP fibers were more evenly aligned and equally distributed in transverse and horizontal directions. The statistical analysis of spatial fiber patterns showed that all FRC systems had a tendency for fiber clumping to various degrees.

## 7.0 - RECOMMENDATIONS AND FUTURE WORK

The following recommendations are suggested for future research:

- The HES-FRC and VHES-FRC mixtures can be further optimized to improve the early-age strength development for even faster repairs and construction. In addition, the mixtures need to be more user friendly and cost effective for potential implementation in the field.
- Additional testing to further evaluate the durability of the FRC systems is recommended.
- Improvement of the shrinkage performance of the mixtures is necessary. Reduction of the shrinkage through mixture proportions and ingredients, use of shrinkage reducing and other admixtures, and lightweight aggregates should be explored.
- The workability of the systems needs to be improved to enable easier placement of the mixtures and better fiber dispersion.
- The FRCs with PP fibers did not display deflection hardening behavior. However, in the field application the HES-FRC w/ PP fibers performed as well as the HES-FRC w/ S fibers, with very few tight or no cracks observed. Hence, research into the behavior of the FRC systems with existing primary reinforcement needs to be performed, and necessity of deflection hardening behavior evaluated.
- Investigation of the behavior of FRCs through numerical analysis is recommended.
- Further testing of the permeability of cracked FRC samples is recommended. Formation of the smaller crack widths up to 200  $\mu\text{m}$  at lower loading rates should be more closely investigated.

- The fiber distribution analysis shows the dependence of fiber alignment on the sample size. Hence, additional large scale specimens should be cast to examine more true random distribution of the fibers, independent of the sample size. Furthermore, the MATLAB code could be further optimized for more precise and automated fiber detection.

## 8.0 - REFERENCES

- American Concrete Institute (ACI), "Report on Fiber Reinforced Concrete". ACI 544.1R-96, Farmington Hills, Michigan (2009).
- American Concrete Institute (ACI), "ACI Concrete Terminology". ACI CT-13, Farmington Hills, Michigan (2013).
- American Concrete Institute (ACI), "Report on High-Strength Concrete". ACI 363R-10, Farmington Hills, Michigan (2015).
- Akkaya, Y., Peled, A., and Shah, S. P. (2000a). "Parameters related to fiber length and processing in cementitious composites." *Materials and Structures*, 33(8), 515–524.
- Akkaya, Y., Picka, J., and Shah, S. P. (2000b). "Spatial distribution of aligned short fibers in cement composites." *Journal of Materials in Civil Engineering*, 12(3), 272–279.
- Akkaya, Y., Shah, S. P., and Ankenman, B. (2001). "Effect of Fiber Dispersion on Multiple Cracking of Cement Composites." *Journal of Engineering Mechanics*, 127(4), 311–316.
- Aldea, C.-M., Ghandehari, M., Shah, S. P., and Karr, A. (2000). "Estimation of water flow through cracked concrete under load." *ACI Structural Journal*, 97(5), 567–575.
- Aldea, C.-M., Shah, S. P., and Karr, A. (1999). "Permeability of cracked concrete." *Materials and Structures*, 32(5), 370–376.
- American Society of Civil Engineers (ASCE), "2015 Report Card for Virginia's Infrastructure". (2015)  
Retrieved from [www.infrasturcturereportcard.org/virginia](http://www.infrasturcturereportcard.org/virginia).
- Babaei, K., and Fouladgar, A. M. (1997). "Solutions to Concrete Bridge Deck Cracking." *Concrete International*, 19(7), 34–37.
- Bekaert. (2016). "Dramix 5D steel fibres for concrete reinforcement." <http://www.bekaert.com/>.
- Brown, M. C., Ozyildirim, C., and Duke, W. L. "Investigation of Fiber-Reinforced Self-Consolidating Concrete". VTRC 10-R8, Virginia Transportation Research Council (2010).
- Cangiano, S., Meda, A., and Plizzari, G. A. (2009). "Rapid hardening concrete for the construction of a small span bridge." *Construction and Building Materials*, Elsevier Ltd, 23(3), 1329–1337.
- Van Dam, T. J., Peterson, K. R., Sutter, L. L., Panguluri, A., Sytsma, J., N., B., R., K., and P., D. (2005). "NCHRP Report 540: Guidelines for Early-Opening to Traffic Portland Cement Concrete for Pavement Rehabilitation." Washington, Transportation Research Board, 26.
- Darwin, D., Browning, J., and Lindquist, W. D. (2004). "Control of Cracking in Bridge Decks: Observations from the Field." *Cement, Concrete, and Aggregates*, 26(2), 148–154.
- Diggle, P. J. (2003). "Statistical Analysis of Spatial Point Patterns", London, Hodder Education Publishers.
- Grace. (2016). "Construction Products: STRUX BT50." <https://gcpat.com>.
- Kang, S. T., and Kim, J. K. (2011). "The Relation Between Fiber Orientation and Tensile Behavior in an Ultra-High Performance Fiber Reinforced Cementitious Composites (UHPFRCC)." *Cement and Concrete Research*, Elsevier Ltd, 41(10), 1001–1014.
- Kang, S. T., and Kim, J. K. (2012). "Investigation on the Flexural Behavior of UHPCC Considering the Effect of Fiber Orientation Distribution." *Construction and Building Materials*, Elsevier Ltd, 28(1), 57–65.

- Kang, S. T., Lee, B. Y., Kim, J.-K., and Kim, Y. Y. (2011). "The Effect of Fibre Distribution Characteristics on the Flexural Strength of Steel Fibre-Reinforced Ultra-High Strength Concrete." *Construction and Building Materials*, Elsevier Ltd, 25(5), 2450–2457.
- Klieger, P. (1958). "Effect of Mixing and Curing Temperature on Concrete Strength." *Journal of the American Concrete Institute*, 54(62), 1063–1081.
- Kosmatka, S. H., and Wilson, M. L. (2011). *Design and Control of Concrete Mixtures*. Portland Cement Association, Skokie, Illinois, USA.
- Li, M., and Li, V. C. (2011). "High-Early-Strength Engineered Cementitious Composites for Fast, Durable Concrete Repair-Material Properties." *ACI Materials Journal*, 108(1), 3–12.
- Li, V. C. (2003). "On Engineered Cementitious Composites (ECC). A Review of the Material and its Applications." *Journal of Advanced Concrete Technology*, 1(3), 215–230.
- Mehta, P. K., and Burrows, R. W. (2001). "Building Durable Structures in the 21st Century." *Concrete International*, March, 57–63.
- Naaman, A. E. (2007). "Deflection-Softening and Deflection-Hardening FRC Composites: Characterization and Modeling." *Concrete International*, (SP-248-5), 53–66.
- Naaman, A. E., Alkhairi, F. M., and Hammoud, H. (1993). "Mechanical Behavior of High Performance Concretes (V6), High Early Strength Fiber Reinforced Concrete, ". Strategic Highway Research Program, Washington, National Research Council.
- Naik, T. R., and Ramme, B. W. (1990). "High Early Strength Fly Ash Concrete for Precast/Prestressed Products." *PCI Journal*, December, 72–78.
- Nawy, E. G. "Fundamentals of High-Performance Concrete". New York, John Wiley & Sons (2001).
- National Bridge Inventory (NBI), "Highway Bridges by Superstructure Material 2015." Federal Highway Administration (2015).
- National Cooperative Highway Research Program (NCHRP), "High Performance Concrete Specifications and Practices for Bridges". Synthesis 441, Washington, Transportation Research Board (2013).
- Nycon. (2013). "Nycon-PVA RECS15." <http://nycon.com>
- Ozyildirim, C. (1993). "High-Performance Concrete for Transportation Structures". *Concrete International*, (January), 33–38.
- Ozyildirim, C. (2005). "History of HPC in Virginia." *ACI, SP-228, Seventh International Symposium on the Utilization of High-Strength / High-Performance Concrete*, 2821–832.
- Ozyildirim, C., Moen, C., and Hladky, S., "Investigation of Fiber-Reinforced Concrete for Use in Transportation Structures". VTRC 97-R15, Virginia Transportation Research Council (1997).
- Ozyildirim, C., and Vieira, M., "Exploratory Investigation of High-Performance Fiber-Reinforced Cementitious Composites for Crack Control". VTRC 08-R12, Virginia Transportation Research Council (2008).
- Ozyurt, N., Mason, T. O., and Shah, S. P. (2006). "Non-destructive monitoring of fiber orientation using AC-IS: An industrial-scale application." *Cement and Concrete Research*, 36(9), 1653–1660.
- Parker, F., and Shoemaker, W. L. (1991). "PCC Pavement Patching Materials and Procedures." *Journal of Materials in Civil Engineering*, 3(1), 29–47.
- Portland Cement Association (PCA), "Fiber Reinforced Concrete". Skokie (1991).

- Punurai, S., Punurai, W., and Hsu, C.-T. T. (2007). "A Very Early Strength Concrete for Highway Construction." *Journal of Testing and Evaluation*, 35(6), 1–9.
- Rapoport, J., Aldea, C.-M., Shah, S. P., Bruce, A., and Karr, A., "Permeability of Cracked Steel Fiber-Reinforced Concrete". National Institute of Statistical Sciences (2001).
- Shah, S. P., and Wang, K. (1997). "Microstructure, Microcracking, Permeability, and Mix Design Criteria of Concrete." Fifth International Conference on Structural Failure, Durability and Retrofitting, 260–272.
- Soroushian, P., and Lee, C. (1990). "Distribution and orientation of fibers in steel fiber reinforced concrete." *ACI Materials Journal*, 87(5), 433–439.
- Soroushian, P., and Ravanbakhsh, S. (1999). "High-Early-Strength Concrete: Mixture Proportioning with Processed Cellulose Fibers for Durability." *ACI Materials Journal*, 96(5), 593–600.
- Sounthararajan, V. M., and Sivakumar, A. (2012). "The Effect of Accelerators and Mix Constituents on the High Early Strength Concrete Properties." International Scholarly Research Network, Civil Engineering, 1–7.
- Sprinkel, M. M. (2006). "Very Early Strength Latex-Modified." *Transportation Research NEWS*, 247 (December), 34–35.
- Vanikar, S. N., and Triandafilou, L. N. (2005). "Implementation of High-Performance Concrete Bridge Technology in the USA." *ACI SP-228, Seventh International Symposium on the Utilization of High-Strength / High-Performance Concrete*, 11–12.
- Virginia Department of Transportation (VDOT), "2007 Road and Bridge Specifications". VDOT (2007).
- Virginia Department of Transportation (VDOT), "VDOT Guide Manual for Causes and Repair of Cracks in Bridge Decks". VDOT (2009).
- Virginia Department of Transportation (VDOT), "Virginia Department of Transportation Special Provision for Engineered Cementitious Composite (ECC)". VDOT (2015).
- Wang, K., Jansen, D. C., Shah, S. P., and Karr, A. F. (1997). "Permeability Study of Cracked Concrete." *Cement and Concrete Research*, 27(3), 381–393.
- Wang, S., and Li, V. C. (2006). "High-Early-Strength Engineered Cementitious Composites." *ACI Materials Journal*, 103(2), 97–105.
- Xia, J., and Mackie, K. (2014). "Axisymmetric fiber orientation distribution of short straight fiber in fiber-reinforced concrete." *ACI Materials Journal*, 111(2), 133–142.
- Zia, P., Leming, M. L., Ahmad, S. H., Schemmel, J. J., and Elliott, R. P. (1993). "Mechanical Behavior of Production of High Performance Concrete". Strategic Highway Research Program, Washington, National Research Council.

## APPENDIX

- Matlab Code for Image Analysis Processing

```
%% START

clear all
close all

% Open image
I = imread('5BLeft.jpg');
k = 5;

Img = rgb2hsv(I);

% Use only "saturation" layer of the image for PP Fiber Cross-Sections
imv=(Img(:,:,1));

% Use only "value" layer of the image for Steel Fiber Cross-Sections
imv=(Img(:,:,3));

% Remove difference in lighting in the background
imvopen=imv-imopen(imv,strel('disk',30));

% Inverse the image colors
imvopeninv=1-imvopen;

% Convert to Black and White Image,
% USE level or therhold or value from 0 to 1: Adjust manually
level = graythresh(imvopeninv);
Ibw = im2bw(imvopeninv,level);

% Select only black pixels
It = (Ibw == 0);

% Remove all pixels smaller than LB and greater than UB: Adjust manually
LB = 10;
UB = 500;
Icl = xor(bwareaopen(It,LB), bwareaopen(It,UB));

%%
% Plot centroids
% Adjust manually for noise data or absent fibers

Ilabel = bwlabel(Icl);
stat = regionprops(Ilabel,'centroid');
imshow(I); hold on;
for x = 1: numel(stat)
    plot(stat(x).Centroid(1),stat(x).Centroid(2),'ro');
```

```

end

%% Save Centroid Coordinates

for x = 1: numel(statCL)
    Xc(x) = statCL(x).Centroid(1);
    Yc(x) = statCL(x).Centroid(2);
end

[rows columns depth] = size(imv);

% Numbers of Fibers then equals to the size of statCL array
NF = numel(statCL);

% Count the number of fibers at the top and bottom halves
TopF = 0;
BottomF = 0;

for n = 1:NF
    if statCL(n).Centroid(2) >= rows/2
        TopF = TopF+1;
    else
        BottomF = BottomF+1;
    end
end

% Plot the fiber coordinates over the original image

figure; imshow(I);
hold on;
for x = 1: numel(statCL)
    plotLC = plot(statCL(x).Centroid(1),statCL(x).Centroid(2),'o');
    set(plotLC, 'MarkerEdgeColor', 'g', 'MarkerFaceColor', 'g', 'MarkerSize', 4)
end

%% END

```

- Matlab Code for K-function Calculation

```

%% START

clear all
close all

[num,txt,row] = xlsread('PPCoord.xlsx','HES1.2', 'D:E');
I = imread('5BRight.jpg');
[rows columns depth] = size(I);

% Concrete Samples in inches

```

```

width = 4;
height = 4;

% Convert from pixel to true size in inches
Wf = rows/width;
Hf = columns/height;

for x = 1: numel(num)/2
    Xc(x) = num(x,1)/Wf;
    Yc(x) = num(x,2)/Hf;
end

%% Edge Correction and Buffer Zone

R = 3.9; % Samples with Steel Fibers
AR = R*R;
NFinR =0;
Density = numel(Xc)/AR;

for i=1:numel(Xc)
    if ((Xc(i) <= R) && (Yc(i) <= R)) && ((Xc(i) >= 0.1) && (Yc(i)>= 0.1))
        NFinR = NFinR + 1;
    end
end

%% Calculation of K - function

NFinr(numel(Xc)) = 0;
d(numel(Xc)) = 0;

rK = 0;
rK_count = 1;
nK = 96;

SumNFinr(nK) = 0;
K(nK)=0;

for zK=rK:0.04:R

    for j = 1:numel(Xc)
        for i = 1:(numel(Xc))
            if i==j
            else
                d = sqrt( (( Xc(j)-Xc(i))^2) + (( Yc(j) - Yc(i))^2) );

                if (d <= zK)
                    NFinr(j) = NFinr(j) + 1;
                end
            end
        end
    end
end

```

```

        end

SumNFinr(rK_count) = sum(NFinr);
K(rK_count) = SumNFinr(rK_count)/(NFinR*Density);

rK_count = rK_count + 1;

        for i = 1:(numel(Xc))
            NFinr(i) = 0;
        end
end

Kinv = K';

%% END

```

- Matlab Code for F-function Calculation

```

%% START

clear all
close all

[num,txt,row] = xlsread('PPCoord.xlsx','HES1.2','D:E');
I = imread('5BRight.jpg');
[rows columns depth] = size(I);

% Concrete Samples in inches
width = 4;
height = 4;

% Convert from pixel to true size in inches
Wf = rows/width;
Hf = columns/height;

for x = 1: numel(num)/2
    Xc(x) = num(x,1)/Wf;
    Yc(x) = num(x,2)/Hf;
end

%% Edge Correction and Buffer Zone

R = 3.9;
AR = R*R;
NFinR =0;

```

```

for i=1:numel(Xc)
    if ((Xc(i) <= R) && (Yc(i) <= R)) && ((Xc(i) >= 0.1) && (Yc(i)>= 0.1))
        NFinR = NFinR + 1;
    end
end

% Density Calculation
Density = NFinR/AR;

%% Creating a k x k Grid

k = 2*sqrt(NFinR);
grid_step = round(R/k,1);

xgrid = 0.1:grid_step:R;
ygrid = 0.1:grid_step:R;
[xg,yg]=meshgrid(xgrid,ygrid);

plot(xg,yg,'go');
hold on;
for x = 1: numel(num)/2
    plot(num(x,1)/Wf,num(x,2)/Hf,'ro');
end

% Total Number of Grid Points
TotalNGridP = numel(xg);

%% Calculation of F - function

dgrid=0;
nF = 98;
rF = 0;
rF_count = 1;

NGP(numel(xgrid),numel(xgrid)) = 0;
NGridP(nF) = 0;
F(nF) = 0;

for z=rF:0.04:R
    for j=1:1:numel(xgrid)
        for i=1:1:numel(ygrid)
            for jf=1:1:numel(Xc)
                %Distance b/w fibers and grid point
                dgrid = sqrt( (( xg(i,j)- Xc(jf))^2) + (( yg(i,j) - Yc(jf))^2)
            );
                if (dgrid <= z)

%Count how many fibers for each i,j Grid Point within distance rF
                    NGP(i,j) = NGP(i,j) + 1;
                end
            end
        end
    end
end

```

```

%IN Grid Loop. If Grid Point i,j has fibers within rF
    if (NGP(i,j) >= 1)
        NGridP(rF_count) = NGridP(rF_count) + 1;           %Add a NGridP
    end
end
end
F(rF_count) = NGridP(rF_count)/TotalNGridP;
rF_count=rF_count+1;

for i=1:1:numel(xgrid)
    for j=1:1:numel(ygrid)
        NGP(i,j)=0;
    end
end
end

Finv = F';

%% END

```